energies

MDPI

Review

Comprehensive Review Comparing the Development and Challenges in the Energy Performance of Pneumatic and Hydropneumatic Suspension Systems

Ryszard Dindorf

Faculty of Mechatronics and Mechanical Engineering, Kielce University of Technology, 25-314 Kielce, Poland; dindorf@tu.kielce.pl

Abstract: The purpose of this review is to comprehensively compare the developments and challenges in the energy performance of unconventional pneumatic suspension (PS) and hydropneumatic suspension (HPS), which have special applications in passenger cars, trucks, military vehicles and agricultural equipment. The main differences between PS and HPS, as well as their advantages and disadvantages, are presented. The PS system is discussed along with its principle of operation, advances in development, principle of operation of air springs, their models, characteristics, vibration isolation, and simulation models. The HPS system is discussed, along with its operational principles, progress in development, models, and characteristics. This review also discusses new trends in HPS development, such as the effect of a pressure fluctuation damper (PFD) placed in a hydraulic cylinder on the damping performance index (DPI) of an HPS under off-road driving conditions. It highlights innovative solutions that can be expected in the future in PS and HPS systems, with the expectations of drivers and passengers. The review focused on trends and challenges in PS and HPS development, such as integration with electronics, smart solutions, customized solutions, emphasis on compliance with ecological and environmental requirements, and applications in electric vehicles (EVs) and autonomous vehicles (AVs).

Keywords: vehicle suspension system; pneumatic suspension system; hydropneumatic suspension system; air spring; hydropneumatic accumulator; energy performance

Academic Editor: Adolfo Dannier

Received: 1 January 2025
Revised: 16 January 2025
Accepted: 17 January 2025
Published: 19 January 2025

Citation: Dindorf, R. Comprehensive Review Comparing the Development and Challenges in the Energy Performance of Pneumatic and Hydropneumatic Suspension Systems. *Energies* **2025**, *18*, 427. https://doi.org/10.3390/en18020427

1. Introduction

The suspension system of a vehicle is attached to both the wheels and the body and is an integral part of its structural design [1]. The suspension system ensures that the body is properly suspended on the wheels and is responsible for keeping the tire in contact with the ground and supporting the brake and steering mechanisms of the vehicle [2]. When a vehicle encounters a pothole or bump on the road, the suspension is responsible for absorbing the vibration energy and preventing the car body from reacting to shocks. A suspension system was used to improve vehicle ride and handling, passenger safety, and comfort. In the field of automobiles, ride comfort can be defined as the ability of a vehicle suspension system to protect passengers and cargo from vibrations and jolts caused by uneven road conditions. In [3], the effects of vehicle vibrations on humans were investigated considering the physical model of the investigated system, which consists of a vehicle model and a driver. The limits of vibration to which humans can be exposed over time are specified in the ISO 2631 standard [4], and the frequency weighting that is applicable in the frequency range of 1 Hz to 80 Hz is defined. However, safe and comfortable driving conditions depend on the dynamic properties of the suspension systems [5]. The suspension system of a vehicle contains

mechanical components that connect wheels to a frame or body. There are three main types of mechanical suspension components: linkages, springs, and shock absorbers [6]. Linkages consist of bars and brackets that support the wheels, springs, and shock absorbers. Different shaped linkages have been used in different types of suspension systems. The simplest linkage is a straight bar that connects one wheel to the other on the opposite side of the vehicle and is designed to support springs, shocks, and wheels on vehicle frames or body structures. Suspension springs ensure optimal performance and work with other suspension components, such as shock absorbers, sway bars, and control arms. The primary functions of the suspension springs include supporting vehicle weight, absorbing shocks and vibrations, and maintaining tire contact. Springs help cushion vehicles by reducing the impact of bumps and holes on the roads. Three different types of springs are used in mechanical suspension systems: coils, leaves, and torsion bars. Shock absorbers use hydraulic elements to cushion a vehicle under shock loads and damping spring oscillations. Shock absorbers use a hydraulic cylinder in conjunction with adjustable valves to control the flow of the hydraulic fluid, which sets the damping force, absorbs road bump forces, and dampens spring oscillations. Shock absorbers improve vehicle performance and restore original positions after encountering obstacles on the road. A vehicle suspension system must be durable and capable of supporting a heavy vehicle body. The conventional MacPherson suspension system is generally used as the front suspension system in passenger cars because it requires less space and provides more space for the engine compartment [7]. Independent suspension systems such as McPherson with coil springs are predominantly used in passenger cars. This suspension system is inexpensive and reliable in terms of frequency of failure. In [8], a model was developed based on the application of the fundamentals of static and dynamic behavior of a bus suspension system.

This review applies pneumatic suspension (PS), also called air suspension (AS), and hydropneumatic suspension (HPS), also known as hydraulic suspension (HS), which are used in various vehicles. This review identifies different types of PS and HPS systems, modeling techniques, control methods, and vehicle applications. The application of PS and HPS offers distinct benefits that can improve the experience of handling vehicles. This review focuses on highlighting research gaps, evaluating the prospects and challenges of PS and HPS systems, and suggesting future research and development directions to improve ride comfort, efficiency, and safety for vehicle users.

The paper is organized as follows. In Section 2, the vehicle suspension system is compared, and the primary difference between the nonconventional PS and HPS systems is provided. In Section 3, PS systems are discussed, including their principle of operation, advances in development, operating models and characteristics, vibration isolation, and simulation models for air springs. In Section 4, HPS systems are discussed, including their operating principles, development progress, models, characteristics, simulation, dynamics, and impedance modeling. HPA–DT modeling is presented with contended RLC lumped parameters (R is the hydraulic resistance, L is the hydraulic inductance, C is the hydraulic conductance), which are critical for the simulation and control of the HPS strut. In Section 5, the impedance modeling of an HPS with a PFD is discussed. In Section 6, the conclusions are summarized, and advances in the effectiveness of PS and HPA systems are reviewed. HPS models were evaluated using the DPI.

2. Materials and Methods

Although both the shock absorber and the suspension struts contribute to the way the vehicle rides and handles, they have different designs and positions in the suspension system. The shocks are individual parts that are installed between the frame and the suspension, whereas the struts are integral to the suspension assembly. The upper control arm and the upper ball joint used in conventional suspension are replaced by

suspension struts [9]. Suspension struts have a lighter design that saves space compared to shock absorbers in conventional suspension systems. The suspension struts of a vehicle suspension system are responsible for cushioning and minimizing excessive bouncing caused by uneven roads. The purpose of the suspension strut is to improve the driving experience by guaranteeing a smoother and more comfortable ride. Struts work together with leaf springs, coil springs, and stabilizer bars to increase the tension and support of the suspension system. Suspension struts can evenly distribute the vehicle's body weight while being driven. The great advantage of mechanical suspension is its robustness and ease of maintenance, making it a great option for vehicles operating in extreme conditions. The MacPherson strut is widely used in the front suspension of modern vehicles, using the top of a telescopic damper as the upper steering pivot. Figure 1 shows diagrams of the mechanical design of the automotive suspension system with the trailing arm and McPherson strut.

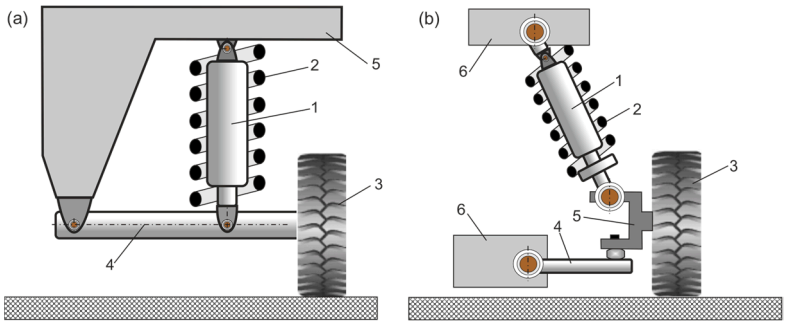

Figure 1. Diagrams of mechanically designed automotive suspension systems: (**a**) traditional trailing arm: 1—shock absorber, 2—coil spring, 3—wheel, 4—linkage, rotation arm, 5—frame, (**b**) McPherson strut: 1—strut (shock absorber), 2—coil spring, 3—wheel, 4—wishbone arm, 5—wheel hub, 6—frame.

An overview of the different types of shock absorbers is extensively discussed in the latest developments in the field of vehicle suspension [10]. Suspension systems can be classified on the basis of how they interact with the vehicle to reduce vibration and improve driving comfort. This classification takes into account whether an active force can be generated, whether energy can be added to the system and whether electronic control is used. Depending on the type of suspension system integrated into the vehicle chassis, there are three basic concepts for mechanical suspension: passive, semi-active, and active [11]. Figure 2 compares passive, semi-active, and active mechanical vehicle suspension systems.

Passive suspension systems, which are commonly used in many vehicles, are based on mechanical parts such as springs, dampers, and bushings [12]. These systems have the objective of achieving an equilibrium between providing a smooth ride and maintaining control by minimizing the impact of bumps and vibrations on the road. Springs support vehicle weight and absorb vertical movements caused by road irregularities. Dampers, also known as shock absorbers, control the speed at which the suspension compresses and retracts, affecting both the comfort of the ride and the stability. The bushings are used to connect the suspension components to the vehicle frame or axle. They help reduce noise, vibration, and harshness while also allowing controlled movement. When the wheel encounters bumps, potholes, or uneven surfaces, the springs absorb energy, and the dampers dampen the resulting oscillations. Passive suspension systems, which lack electronic sensors or control mechanisms to adjust damping levels in real-time, respond consistently to road conditions, regardless of where or how they are driving. The structure approach is commonly used to design passive suspensions based on passive elements (springs, dampers, and bushings) connected in parallel or in series [13]. Table 1 compares passive mechanical, pneumatic, and hydraulic suspension systems. When comparing pneumatic and hydropneumatic suspension systems, additional

factors include the dependence of the degree of damping on the ambient temperature and operating medium.

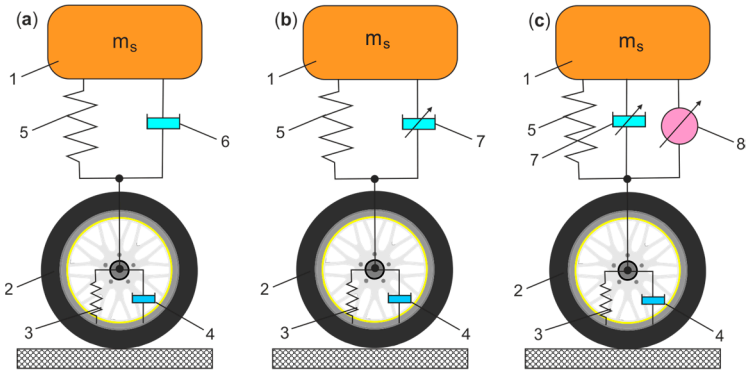

Figure 2. Comparison of mechanical vehicle suspension systems: (**a**) passive, (**b**) semi-active, (**c**) active: 1—body mass of the vehicle, sprung mass, 2—mass of the wheel assembly, unsprung mass, 3—stiffness of the tire, 4—damping of the tire, 5—suspension spring, 6—fixed suspension damper, 7—controllable suspension damper, 8—active-controlled force actuator.

Table 1. Comparison of passive suspension systems [14].

Mechanical Suspension	Pneumatic Suspension	Hydraulic Suspension
Friction between linkages. No inherent damping, extra damping is needed. Less space is required.	No friction between linkages. Inherent damping, less the need for additional damping. Bulky in nature.	No friction between linkages. Inherent damping, less the need for additional damping. Moderate space requirement.

Semi-active suspension refers to a suspension system in vehicles that adjusts the damping force of the shock absorber based on changing conditions of the road surface. In a semi-active suspension, the viscous damping coefficient of the shock absorber changes, but no energy is added to the suspension system. A semi-active suspension can change the damping of the suspension system using a semi-active damper. One of the semi-active dampers is a hydraulic damper that adjusts its damping effect by altering the size of the orifice opening. Another commonly used and popular type of semi-active damper is a magnetorheological damper (MR) [15]. In an MR damper, the damping can be adjusted by altering the magnetic field, thus altering the viscosity of the magnetorheological fluid and ultimately changing the damping value of the system. A semi-active suspension system is less complex than an active suspension and, therefore, more cost-effective and simpler to manage while still enabling the reduction of the compromise between performance and ride comfort. A semi-active suspension is widely used in heavy vehicles due to its low cost, simple manufacturing process, and favorable damping effect [16]. In [17], a semi-active suspension system was shown to suppress vibration and improve ride handling compared to a conventional passive suspension system. In another study [18], it was discussed that a semi-active suspension also helps with brake performance when used with an anti-brake lock system (ABS). Semi-active suspension can adjust the suspension parameters according to the control strategy to achieve satisfactory performance under different driving and road conditions [19]. The skyhook control suspension is a semi-active suspension that can be implemented without extensive information on the state of the road [20]. In [21], the Skyhook control strategy was improved by incorporating sliding mode control and internal model theory. Skyhook control is a strategy applied to semi-active suspension systems in which a skyhook damper is connected to an inertial reference in the stationary sky. Skyhook control can eliminate the trade-off between resonance control and

high-frequency isolation, which is a common situation in passive suspension systems. In turn, the ground hook control strategy uses an imaginary damper fixed to the ground and an unsprung mass. A suspension system with sky-hook control offers better ride comfort and handling than ground-hook control.

The active suspension system actively adapts to driving conditions to improve the smoothness and comfort of travel or carrying cargo [22,23]. The active suspension system uses electronic sensors, special shock absorbers, and actuators that are controlled by computers. Sensors constantly monitor the road surface and rider's style while also recording data to the computer. The computer controls the actuator and shock absorber in real time to counteract any bumps or dips on the road. Shock absorbers have the ability to change the viscosity of the fluid as the electric current passes through them. Changes in shock absorption damping characteristics can be achieved in three ways: by using magneto-rheological fluid (MR), electro-rheological fluid (ER), and controlled valves [24]. The damping characteristics of the shock absorbers can be precisely controlled, resulting in a smoother ride. The active suspension system continuously controls the force actuator placed on the suspension axis. There are three active-controlled force actuators: electromechanical (electromagnetic), electrohydraulic, and electro-pneumatic. Active suspension systems sense the forces that are applied to the wheels and constantly adjust the mechanical connections between the chassis and wheel assemblies to keep the chassis level and/or optimally absorb the energy associated with the vertical motion of the wheels. The active suspension system can adjust the suspension to maintain level and stability in a tight corner. In reality, active suspension systems can be compared to having an intelligent assistant that continuously adjusts your car's ride to ensure maximum smoothness and comfort. They are specifically designed for luxury vehicles or high-performance cars where comfort and handling are considered the most important factors. Although active suspension has strong adaptability and an obvious improvement in ride comfort and stability, it requires an external energy supply that is more complex and costly than semi-active suspension [25]. The current use of adaptive suspension is difficult due to its elaborate and costly components, as well as its high energy consumption. The energy effectiveness of an adaptive suspension strut depends on the mass, stroke, and frequency of the suspension, as well as the speed of travel and the condition of the road surface.

Passive suspension systems can only achieve limited performance for both ride comfort and vehicle handling under stable operating conditions and specific classes of vehicles due to physical constraints. The dynamic performance of active suspension systems can be improved by controlling them on the basis of online information provided by sensors in appropriate positions in the vehicle. Passive, semi-active, and active suspension systems can be compared according to different classifications on the basis of their descriptions and discussion. Table 2 compares passive, semi-active, and AS and HPS active suspension systems [26,27].

The main vibration frequency ranges of a car's body are the result of the vehicle bouncing, rocking, and rolling over uneven surfaces. Common suspension vibration frequencies: 1.0 Hz for passenger cars, 1.25 to 1.75 Hz for sports cars, 2.0 to 2.5 Hz for low-downforce autocross and race cars, and more than 2.5 Hz for high-downforce racecars. To improve vehicle ride comfort, one alternative is to minimize the vibration transfer function from the rough road to the vehicle's body over the range of frequencies 0.1 to 100 Hz. Excitation frequencies of 0.1 to 0.5 Hz are important for assessing motion sickness, and excitation frequencies of 0.5 to 100 Hz are recommended for assessing ride comfort.

Semi-active suspensions have better damping characteristics under closed-loop control compared to passive suspensions. Consequently, the car body's roll and pitch motions are greatly reduced. Semi-active suspensions are characterized by easy control, small volume, low weight, and adequate cost. The disadvantages of semi-active suspension are that the roll and pitch motions cannot be fully eliminated. Active PS and HPS systems have the ability to achieve high force density, active force control, and efficient elimination of

vehicle rolling motions. Active suspension PS and HPS systems are controlled by electric drives, and the source power is provided by a battery or a conventional internal combustion engine (ICE). Hydraulic systems are typically used for body control systems because of their simplicity and reliability in operation, as well as the availability of various commercial parts. Examples include hydraulic solutions in BMW and Mercedes. However, hydraulic systems have disadvantages, such as high supply pressure, increased response time constants resulting from the elasticity of the hydraulic hose, harmful effects of hydraulic fluids, and increased total sprung mass.

Table 2. Comparison of various automotive suspension systems.

Rating Parameters	Passive	Semi-Active	Active AS/HPS
Structure	Simplest	Complex	Most complex
Weight/volume	Lowest	Low	Hight
Cost	Lowest	Low	Highest
Ride comfort	Bad	Medium	Good
Handling	Bad	Medium	Good
Reliability	Highest	High	Medium
Dynamic	Passive	Passive	Medium
Switching frequency	No	Medium	High
Power requirement	No	Low	High
Energy regeneration	No	No	No
Commercialization	Yes	Yes	Yes

The basic characteristics of different automotive suspension systems are studied using theoretically simplified vehicle models such as passive, semi-active, or active under realistic conditions, such as different types of road surfaces. Several models can be used to investigate the behavior and operation of suspension systems: the quarter vehicle model, in which only one suspension system is on one of the four wheels; half vehicle model with two suspension systems on two wheels; and the full vehicle model with four suspension systems on each wheel. In [28], a robust control scheme for a quarter-car suspension system was presented under a road disturbance profile. In [29], the design and development of a semi-active suspension system were presented using a quarter-car model using a proportional-integral (PI) controller to control the damper properties. In [30], the objective was to design an efficient control scheme for the active suspension system of the quarter car, in which particle swarm optimization (PSO) is used to design a fuzzy controller for the active suspension system. In [31], active vibration control of a quarter-vehicle suspension system was discussed, and damping control methods were analyzed: higher-order sliding mode control (HOSMC), first-order sliding mode control (FOSMC), integral sliding mode control (ISMC), use of proportional integral derivative (PID) and linear quadratic regulator (LQR).

In [32], in the suspension system, an electromechanical device (EM) was proposed, actuated by the ball screw nut, which is driven by an electric motor through a planetary gear. An alternative is a mechanical drive that uses a rack and pinion. The obvious advantage of an EM system is controllability. The damping force depends on the electric generator and its electrical load. No external power supply is needed because the damper can generate its own electrical supply. The design methodology for the EM system with height adjustment and performance optimization was presented in [33]. EM systems represent the next trend for future vehicles due to their high reliability and relatively low cost. AUDI AG has patented an EM height adjustment system with an ad hoc electric motor and a screw mechanism [34]. In [35], a solution of a height adjustment system using EM, actuated by a differential gear, was presented. The vehicles' Electronic Control Suspension (ECS) was patented [36]. This system consists of a strut assembly that is connected to the

vehicle body, and its lower part is inserted through the housing to absorb wheel vibrations. The vehicle height control module transforms the rotational force of a motor into a linear movement of the strut assembly. This occurs when the rotational force is transmitted to the screw section surrounding the strut assembly. This enables the strut assembly to change its vertical position with respect to the housing, thereby regulating the vehicle's height. Direct-drive electromagnetic systems are a variation of the EM system and are more appropriate for parallel suspensions where the actuator's inertia is minimized. In [37], a study on electromagnetic dampers (EMDs) with nonlinear damping force characteristics was presented for automobiles and their road tests. In [38], an active electromagnetic suspension system with a tubular permanent magnet actuator (TPMA) was proposed that provides additional stability and maneuverability by performing active roll and pitch control during cornering and braking, as well as eliminating road irregularities, thus improving vehicle and passenger safety and driving comfort.

The concept is an interesting alternative to EM, which is electrorheological (ER) dampers and magnetorheological (MR) dampers, but it remains to demonstrate its useful life and manufacturing economics. The MR damper is an innovative technology that utilizes dampers filled with an electromagnetic fluid and is controlled by electromagnetic forces. The density of the electromagnetic fluid changes when an electric current is used, allowing quick and accurate modifications to the damping rate. The unmatched combination of comfort and performance makes this technology highly sought-after in both high-performance and luxury vehicles. Major car manufacturers, such as General Motors and VW Group, use suspension systems equipped with MR dampers. The usual design of an MR damper involves a single tube filled with magnetorheological fluid. Synthetic oil contains small iron particles that are only a few micrometers thick (equivalent to a few thousandths of a millimeter). When exposed to a magnetic field created by one or more magnetic coils in the damper, the particles become arranged in a certain order. The MR damper is an intelligent damper that is utilized for vibration control of semi-active suspension systems [39]. In [40], the response characteristics of a magnetorheological suspension with a modified skyhook control scheme, focusing directly on the command current, were analyzed considering the nonlinearity of the hysteresis. In [41], a combination of the magnetorheological damper lookup table based on the control of the skyhook and the groundhook, based on a technique called hybrid control for a quarter car, is developed using measured data for vertical acceleration, the absolute velocity of the vehicle (sprung mass) and its relative velocity. In [42], theoretical and experimental research was carried out on the control of vehicle suspension systems using a quarter-car suspension equipped with an MR damper using fuzzy logic and the control of the Skyhook technique as system controllers. In [43], a robust controller for a semi-active suspension system with MR dampers addresses the problem of vibration attenuation in a vehicle without a fault MR damper and with oil leakage in the MR damper.

Nonconventional PS and HPS systems are alternatives to mechanical and electromechanical suspension systems. PS and HPS systems offer many more advantages than mechanical suspension. From a safety perspective, PS and HPS systems are much superior to mechanical suspension and are currently the preferred choice for vehicle suspension systems. The PS system uses gas springs with constant volume controlled by regulating gas pressure and additional dampers [44]. The HPS strut uses a constant mass gas spring, controlled pressure, and flow rate of hydraulic fluid, damping element, and hydraulic cylinder [45]. Figure 3 shows a comparison of the PS and HPS systems used in the quarter-vehicle suspension.

PS and HPS systems are becoming increasingly popular in both the high-end and mainstream automotive sectors. These systems allow drivers to modify the height of the vehicle's suspension, providing a personalized driving experience depending on road

conditions or individual choices. Furthermore, these suspensions are better suited for heavy loads, making them a highly suitable option for SUVs and trucks. Compared to PS, HPS is complex and often requires specialist knowledge for maintenance and repair, contributing to higher costs, and is associated with greater weight and the potential for more intensive maintenance.

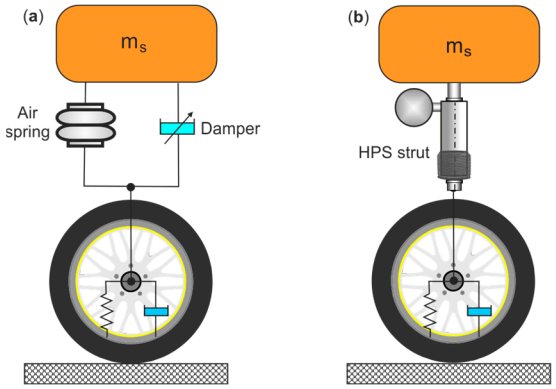

Figure 3. Comparison of the PS (**a**) and HPS (**b**) systems used in the suspension models of the quarter vehicle.

The passenger ride comfort indicator of the PS and HPS system can be determined based on ISO 2631-1 [46], in which the vibration evaluation is based on the weighted root mean square acceleration, calculated as follows:

$$A_w = \sqrt{\frac{1}{T}\int_0^T a^2(t)\,dt} \tag{1}$$

where $a(t)$ is the weighted acceleration as a function of time; T is the duration of the measurements.

The Dynamic Load Coefficient (DLC) is often used to characterize the dynamic load on an axle of a vehicle for a specific combination of unevenness and speed on the road [47]. The DLC value is close to zero when the axle of a truck wheel moves on a perfectly smooth road. The DLC is calculated by comparing the standard deviation of the fluctuation of the dynamic load with the static load as follows:

$$DLC = \frac{F_{rms}}{F_s} \tag{2}$$

where F_{rms} is the standard deviation of the dynamic wheel load, and F_s is the average or nominal static wheel load.

In [48], the performance of the PS and HPS systems was compared using two objective functions defined in (1) and (2). The evaluation results showed that the A_w and DLC values for the PS system, respectively, are reduced by 11.87% and 41.46% compared to the HPS system.

The latest trends in the development of PS and HPS systems demonstrate how innovative technologies have changed the comfort of road travel and vehicle driving. Vehicle manufacturers continuously strive to improve driving comfort, stability, and driving experience using technological innovations in PS and HPS systems. When comparing PS and HPA systems, it is important to consider not only the suspension medium and mechanics but also factors such as ride quality, cost, and longevity.

Primary differences between PS and HPS systems:

Medium: The HPS system is based on the use of a hydraulic fluid, while the PS system is based on a pressurized air spring. PS and HPS require continuous operation under pressure.

Responsiveness: HPS offers instantaneous responses, while the PS system may have slight delays. Fluid systems such as PS and HPS have higher response time constants due to the elasticity of the gas and the flexibility of the hoses.

Complexity: HPS systems typically have a larger number of components, making them more complex.

Maintenance: The complexity of HPS systems often leads to more expensive and frequent maintenance compared to PS systems.

When comparing PS and HPS system modifications, different paths are considered:

Customization: The PS modification is simpler than the HPS and allows for a more direct height adjustment of the ride.

Ride quality enhancement: Compared to PS, the HPS system offers a more significant improvement in ride quality and performance.

Installation: Compared to PS, the HPS system usually requires professional installation due to its complexity. PS and HPS require more space for installation in the vehicle body, although they do not contribute to increasing the overall sprung mass.

Cost: Long-term installation and maintenance costs for the HPS system tend to be higher than those for PS systems.

The PS and HPS systems allow for lift and lowering of the vehicles:

Lifting: These systems can significantly raise the body of the vehicle, which is advisable for off-road riding or for a standout look.

Lowering: These systems can lower vehicles to hug the ground for a sleek low-rider effect that also improves handling at high speeds.

The choice between the PS system and the HPS system depends on the specific needs and preferences, while the following factors are taken into account: ride comfort, performance, payload capacity, and budget. The PS system provides a comfortable ride and adaptable performance, while the HPS system prioritizes precision control and durability. Table 3 compares the advantages and drawbacks of PS and HPS systems.

Some common problems with PS systems can be encountered: air leaks can lead to suspension failure, compressor failure can lead to a compromise of the entire system, and damaged air springs lead to a loss of pressure and ride quality. Although HPS systems are powerful, they have potential complications, such as hydraulic fluid leaks, leading to reduced performance and potential damage to the system or vehicle. The complexity of HPS maintenance requires a deeper understanding of its maintenance and repair. Wear of HPS components, such as those in hydraulic cylinders and pumps, requires repair or replacement.

Adaptive damping systems in suspension technology have become increasingly popular and widely adopted [49]. These advanced systems use sensors to observe and track various factors, such as wheel speed, steering input, and road conditions. Subsequently, they modify the damping rates in real-time to improve both the comfort of the ride and the way the vehicle is handled. This technology enables a smooth transition between relaxed and agile driving, providing a truly adaptable driving experience. In [50], an adaptive suspension damping control was proposed that adjusts to the frequency of a sinusoidal kinematic input. The control system is based on an adaptive algorithm that uses the relationship between the gain function of the frequency response of the suspension system, the damping factor, and the input frequency. In [51], the LQR and the multiobjective optimization algorithm for an adaptive control suspension were proposed to automatically adjust the controller parameters based on vehicle speed and road roughness grade while maintaining the optimal control effect of the suspension. In [52], the idea of an adaptive suspension

system is explained, which is designed to neutralize jerks due to speed breaks and uneven surfaces on the road by actuating the suspension system. In [53], a semi-active suspension control method was developed, in which vehicle-to-cloud-to-vehicle (V2C2V) technology served as the basis for road adaptation capabilities to the future of the suspension system, and the operation of the proposed system was validated by simulation of real data in the TruckSim and CarSim simulation environment. TruckSim software offers the most precise, comprehensive, and effective ways to model the performance of multi-axle commercial and military vehicles. CarSim software provides the most precise, comprehensive, and effective simulation methods for the performance of passenger vehicles and light-duty trucks.

Table 3. Comparison of the advantages and drawbacks of the PS and HPS systems.

Characteristics	PS System	HPS System
Complexity	Simple control system	Moderately complex control system
Power	Moderate	Very high
Control	Solenoid valves	Servo valves
Position accuracy	It is difficult to achieve accurate positioning	Achieving positioning requires additional support
Speed	High	Moderate
Payload capacity	High	Very high
Lifetime	Moderate	Long
Acceleration	Very high	Very high
Shock loads	Capable of handling shock loads	Shock-proof
Environmental	High noise levels	Hydraulic fluid leaks and disposal
Components	Compressor, air springs, storage tank, valves, lines	Pump, cylinders, accumulators, valves, lines
Efficiency	Low	Low
Reliability	Excellent	Good
Maintenance	High user-maintenance	High user-maintenance
Purchase cost	Low	High
Operating cost	Moderate	High
Maintenance cost	Low	High

Predictive suspension systems enhance suspension technology by using complex algorithms and artificial intelligence (AI) driven predictive analytics. These systems analyze information collected from various sources, such as cameras, sensors, and GPS, to predict road conditions. Predictive suspension systems improve overall comfort and control of the ride by adjusting suspension settings in real-time, especially when navigating rough or difficult terrain. In [54], a novel method was proposed to design a robust multivariate nonlinear predictive control for nonlinear active suspension systems using the fuzzy Takagi-Sugeno approach. In [55], a new predictive control approach was used for nonlinear multi-input multi-output (MIMO) control of a vehicle suspension with four degrees of freedom, including pitch and bounce motions. In [56], a Model Predictive Control (MPC) was proposed based on linear parameter variation to improve damping control of the suspension system based on vehicle speed. In [57], the latest advances in road profile sensors made the implementation of predictive suspension control a viable option in vehicles; therefore, an explicit model predictive controller (e-MPC) was proposed for an active suspension system with a preview. In [58], the design of an MPC optimized with a particle swarm was proposed for a half-car nonlinear electrohydraulic suspension system that performs deterministic road disturbances.

The shift towards electronically controlled suspension systems is a prominent trend in the automotive suspension system market. These systems use sensors, actuators, and electronic control units to continuously adjust the damping rate and suspension stiffness based on driving conditions and road surfaces. Controllable suspension systems typically involve the operation of shock absorbers with adjustable characteristics (shock absorbers that feature a control valve that adjusts fluid flow through the bypass or those that use a magnetorheological fluid). Examples of such controllable suspension system solutions are as follows:

- Sachs Continuous Damping Control (CDC), also known as Skyhook or IDS, is a feature found in various car brands, including WV, BMW, GM, Opel, Fiat, Porsche, Ferrari, and Maserati [59]. This solution is based on an electronic system that uses shock absorbers with two solenoid valves that can be adjusted to control vibration damping in both compression and tension.
- Mercedes-Benz used the Bilstein Adaptive Damping Control (ADC) system in various models, including S, E, CLS, SL, CL, and SLK [60]. This system, which is dependent on the solenoid valves within the shock absorber, allows for adjustable vibration damping through the electronic system.
- Monroe Continuously Controlled Electronic (CCE), also known as Four-C, is used in Volvo S60R/V70R and S80 [61]. An electronic system of adjustable vibration damping with shock absorbers and solenoid valves is the basis of this solution.
- The Kayaba Dynamic Ride Control (DRC) solution is used in the Audi RS6 Quattro [62]. This system is based on a hydraulic connection between the shock absorbers of each wheel and the valves that regulate the fluid movement.
- Delphi MagnetiRide is a common solution known as Magnetic Ride Control, which is used in vehicles produced by GM corporations, including the Chevrolet Corvette [63]. This system operates using the characteristics of a magnetorheological fluid.
- Jaguar XJ Computer Active Technology System (CATS) was used in Mercedes-Benz models E and S, equipped with the AIRmatic suspension system [64].
- The Pneumatic Damping Control (PDC) of the shock absorbers is used in Audi Allroad. The pressure in the air springs is adjusted by the settings of the PDC valve installed on the PS shock absorber [65].
- Citroen uses hydroactive solutions with HPS in models such as BX, XM, and Xantia and optionally in C5 and C6. The third-generation Hydractive system automatically, instantly, and continuously adopts both the driving style and the state of the road [66].
- WABCO Electronically Controlled Air Suspension (ECAS) controls all components of cars, vans, and trucks; provides optimal traction, pressure ratio control and pressure equality, axle load indication, and passenger detection; has an anti-tilt function; improves vehicle handling; increases off-road clearance; and improves driver comfort on a variety of terrains [67].

The automotive industry is always striving to improve car suspension technology. The improvement of PS and HPS with adaptive damping and electromagnetic systems is revolutionizing ride comfort and vehicle handling. The latest trends in suspension development are centered on comfort, performance, and sustainability. The future of automobile design is being shaped by their efforts to provide safer, more comfortable, and more efficient journeys for both drivers and passengers. The Hübner Group presented an HPS in electric buses [68]. In electric buses, instead of compressed air as the real energy drain, a better alternative is to use hydraulic fluid in suspension and damping. The HPS system provides a high degree of comfort and stability even on uneven road surfaces. Also, there is a significantly higher energy efficiency than with compressed air.

3. PS Systems

In 1959, the German BPW company introduced the first PS, often called air suspension (AS), for its automotive chassis, and since then, it has gone through a lot of innovation. The AS of BPW can be used for axle loads up to 14 tons, and its application is suitable for on- and off-road conditions that transport general and sensitive cargo. The AS system is a type of suspension in which air springs are used as the primary or only means of vibration isolation [69]. Air springs maintain a consistent height and provide a more comfortable ride due to their low natural frequency. An air spring can be used as a spring element to

raise and lower the vehicle body. The deflection of the air springs depends on whether the load vehicle AS is compatible with any damper, such as magnetorheological, adaptive, and variable damping. The PS can be used without dampers and is considered the most comfortable suspension to ride on. A vehicle equipped with a pneumatic suspension has mechanisms to adjust the height by inflating the air spring and has the ability to maintain a consistent level above the ground regardless of the amount of weight it is carrying. The vehicle (urban bus example) can be tilted slightly around its main axis to facilitate passenger entry or exit. Additionally, this solution allows for a smooth handling vehicle by providing control over the selection of air spring stiffness based on road conditions and driver preferences. PS in trucks and trailers has huge advantages, such as reducing noise and vibration and improving fuel consumption and tire life, but there are some disadvantages, such as lower durability compared to leaf spring suspension and the need for professional service.

3.1. Principle of Operation of a PS System

PS systems are composed of air springs such as air compressors, compressed air storage tanks, air preparation units (to eliminate moisture), and control systems, including control valves, height, and pressure sensors [70,71]. Conventional PS systems use a variety of flexible rubber air springs (typically a textile-reinforced rubber sleeve/bag filled with pressurized air), such as airbags, double convoluted air bellows, rolling lobe bags and tapered sleeve bags, which are used to transfer chassis load to wheels. The new PS utilizes two airbags that allow independent adjustment of ride height and stiffness and can adapt to different riding conditions by controlling air pressure. Figure 4 shows the main components of the PS system diagram with the air spring of the airbag and the air bellows.

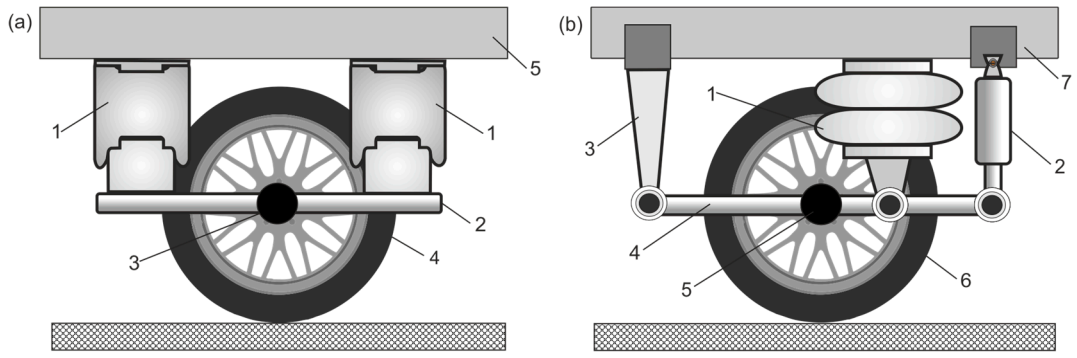

Figure 4. Diagrams of PS system: (**a**) air spring bag: 1—airbag, 2—twig rotation arm, 3—wheel hub, 4—wheel, 5—frame; (**b**) air spring bellows: 1—double convoluted air bellows, 2—damper, 3—rotation arm hinge bracket, 4—twin rotation arm, 5—wheel hub, 6—wheel, 7—frame (body).

Few scientific and academic publications are dedicated to PS systems, while most of the available data on construction, operation, and maintenance can be found in service books [72–76] and company catalogs [77–85].

Figure 5 shows diagrams of the pneumatic control circuits of the PS system, distinguishing its main components: air compressor, compressed air storage tanks, air preparation unit and supply line, control valve blocks, and air springs such as airbags and air bellows (polyurethane or rubber flexible elements). In PS circuits, it is possible to control air spring lifting and leveling, equalize the pressure, and compensate for air leaks. If high requirements are applied to the leveling of the PS or bellows are used for vibration isolation, automatic control valves should be used. Complete PS systems that include air springs, level controls, and all accessories are available from dealers.

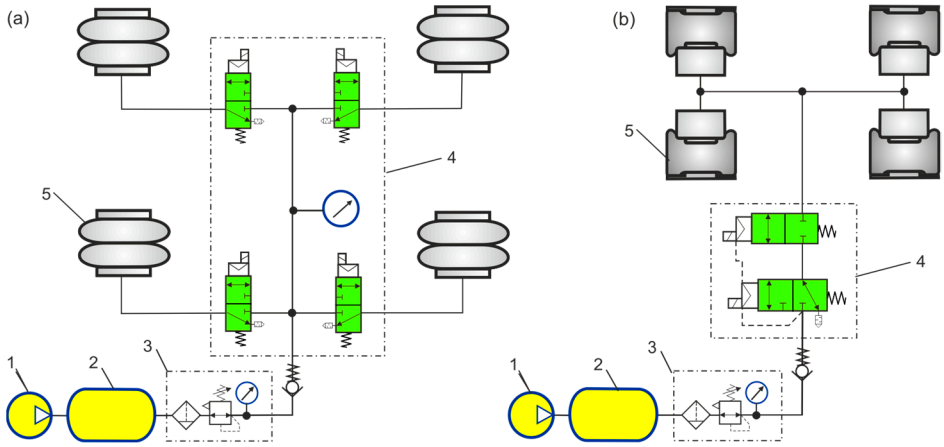

Figure 5. Diagram of the pneumatic control circuit of the PS system: (**a**) two-axle vehicle, (**b**) semi-trailer: 1—compressor, 2—compressed air storage tank, 3—air preparation unit, 4—control valve block, 5—air springs (air bellows, airbag).

The PS system improves comfort and quality while driving, providing the ability to effectively handle obstacles.

Advantages of PS systems:

Comfort ride: One of the primary advantages of air suspension-equipped cars is the increased comfort experienced while driving, which makes them suitable for everyday use. The ability to adjust the air suspension enhances comfort when driving on rough roads and enhances control when driving off-road. Using airbags instead of springs in the wheel area improves passenger ride comfort.

Reduced noise and vibration: PS systems offer the additional benefit of minimizing damage and deterioration to both the suspension system and the parts of the vehicle. This is achieved by reducing the impact and vibrations, particularly during intense driving situations. The incorporation of air suspension allows the vehicle to navigate rough roads smoothly, even in conditions such as potholes, uneven surfaces, and speed bumps, ensuring a comfortable ride experience.

Versatility on the road: The PS system enables the driver to customize the car according to their preferences for a comfortable ride and optimal handling. When faced with different terrains, the driver has the option of choosing to drive in highway conditions or having a more comfortable experience on challenging roads, ensuring continuous control over the vehicle. Air suspension allows for increased speeds while taking corners and offers improved control because the vehicle is more compatible with road conditions. A suspension system that can be adjusted to lower the vehicle to the ground has the potential to decrease drag at faster speeds. Furthermore, the practicality of being able to raise the vehicle for daily activities proves to be very advantageous for navigating rough terrain.

Versatility of load: Another benefit of an air suspension is its ability to adapt to different loads. The height of the car can be altered based on the load it carries, allowing for easier loading with the “kneel” or “raise” features. The purpose of air suspension is to provide uniformity among all wheels, as well as to reduce the chances that the vehicle rolls when turning corners. Additionally, it reduces the possibility of damage, such as breakage and load shift, by decreasing the frequency of vibrations transmitted through the suspension system. Additionally, the enhanced vehicle firmness allows better control, resulting in better towing capacity, especially for larger vehicles.

Fuel economy: Vehicles equipped with air suspension have the advantage of being able to tailor their ride to different road conditions, which contributes to improved fuel efficiency. To illustrate, having a lower ride height when driving on a motorway results

in improved aerodynamics and decreased wind resistance. However, if a suspension is designed to match a specific road surface and provide superior control, it can result in faster speeds when cornering and ultimately save time on routes that have numerous turns.

Disadvantages of PS systems:

Cost: A drawback of an air spring system is its higher purchase cost than that of a conventional spring suspension system. Typically, only high-end vehicles are equipped with an integrated air suspension system as a standard feature. However, the cost of installation might be balanced by the higher price of purchase, which is typically higher than that of vehicles equipped with a steel spring suspension.

Maintenance: Another disadvantage of air suspension is the cost of maintenance. In the immediate period, air suspension is dependable; however, it is more likely to require frequent repairs due to long travel distances and the time spent on the road. Choosing not to fix your suspension is not a viable option, as it will cause your car to lean toward one side when you drive. If you choose to replace the air spring system with a more affordable steel spring, you will forfeit the advantages typically associated with air suspension vehicles. Therefore, it is understood that expense is, unfortunately, an essential trade-off.

Mechanical issues: Air suspension systems are susceptible to mechanical problems. Your suspension may experience failure due to rust or damage caused by moisture in the interior or a malfunctioning air fitting in the air tube that connects to the air system. Air springs are commonly developed leaks that can potentially cause the compressor to overheat and fail.

3.2. Advances in PS Systems Development

The PS are used with great success in road and railway vehicles because of their reliable, functional, and solid design. PS systems are mainly applied in heavy-duty vehicles and high-end automobiles, as well as in buses used for public transportation, where the priority is to improve the comfort level of passengers. In [86], an analysis of the uncertainty of AS systems in buses was proposed. In the initial stage, the influence of the sprung mass of the bus on the operation of the PS system was examined. Data from bus road tests were used to train a deep neural network model whose objective was to accurately identify the spring mass. In [87], a general analytical model for an air spring is created that represents the main characteristics of stiffness and hysteresis. The analytical model of an air spring can be used effectively in the design of PS systems in vehicles to provide better ride and handling characteristics, as well as various functions for the convenience of passengers. In [88], pneumatic elastic elements were presented, which are widely used in the secondary suspension of modern railway vehicles due to their important advantages compared to conventional ones. An analysis was carried out to determine the influence of individual parameters of pneumatic elastic elements on the stiffness of the rail suspension and its dynamic response. In [89], the optimization of an air suspension design was discussed with adjustment of the height and stiffness of the ride. An analytical formulation was developed to obtain the optimal design of the new air suspension system. The new air suspension system has advantages, and the experimental results confirm the mathematical modeling. The suspension height change is simple and can be achieved by compressing or expanding the air in pneumatic cushions. PS systems lose efficiency when there is a significant change in ride conditions or frequent fast vehicle height; adjustments are required, especially when the compressed air storage in the tank is depleted. In [90], the operation of the Toyota Electronic Modulated Suspension (TEMS) was explained. It consisted of four independent shock absorbers mounted on all four wheels and could be used in an automatic or driver-selected mode based on the technology of the Precision Engineered Geometrically Advanced Suspension (PEGASUS). TEMS manages

the suspension spring rate, damping force, and height of the vehicle by regulating the air volume in the air spring according to vehicle travel conditions. The spring rate and damping force are heightened during braking and cornering to diminish the occurrence of pitch (the forward or backward movement of a vehicle's weight) and roll (the side-to-side tilt of a vehicle). At high speeds, the vehicle height is reduced to enhance stability. When driving on uneven roads, the vehicle height is raised to prevent it from hitting any bumps. The complexity and cost of the TEMS system are elevated due to the incorporation of sensors (such as height, steering, and throttle position) and actuators that regulate the spring rate. This is in addition to the already expensive pneumatic elements. In [91], the implementation of a PS on the McPherson strut was presented. A variable rate rolling lobe air spring is used in conjunction with a hydraulic damper to strike a balance between ride comfort and handling performance. This system offers three settings, namely, track, sport, and touring, allowing for different ride levels. To enhance vehicle handling capabilities, it is possible to reduce vehicle height by adjusting the air volume in the rubber bag. Due to the high cost of the components used in PS systems, they are mainly used in vehicle models of the E- and F-segment, such as the Grand Cherokee with the quadra lift air suspension system and the self-leveling PS system in BMW models. In [92], to improve vehicle ride comfort, a mathematical and simulation analysis of a nonlinear model for air spring suspension is performed. The simulation findings indicate that as the transient impact load increases, the stiffness of the air spring also increases. In addition, the peak of the transfer function increases and shifts to higher frequencies, approaching the natural frequency of the body. The maximum value and frequency of the transfer function vary only slightly around the natural frequency of the wheel. In [93], a new air suspension configuration with active, interconnected air suspension and outsourced air pressure was presented. When developing this system, the focus was on reducing the energy consumed by the compressor by the interconnected air springs. In the optimized PS version, the system can run in mode without using the compressor; then, the energy consumption is reduced by 46%. In [94], a new interconnected air spring with quasi-zero stiffness is presented to improve the vibration isolation performance of commercial vehicle suspension systems under frequent load changes. In this new structure, negative stiffness air chambers are added to the traditional PS system to reduce the natural frequency of the suspension. The solenoid valves between the negative stiffness air chambers can control the PS system and adjust to different loads and road conditions. In [95], the predicted vehicle states by the model predictive controller (MPC) for a semi-active suspension system with air springs and a continuous damping controller (CDC) were presented.

3.3. Principle of Air Spring Operation

In [96], the importance of rubber bellows in PS systems was explored, and the mechanical properties of air springs were examined, using amplitude and frequency correlation to describe their mechanical features. Simulation results show that the rubber bellows have a certain impact on the suspension's sprung mass displacement and on the performance of the active suspension. In [97], the forces versus deformation characteristics of an air spring were analyzed, including the dynamic rigidity of the spring during compression and expansion, the dissipation of energy by the spring, and the damping coefficient.

The operating conditions of the air springs (bellows or bags) are as follows:

- The bellows can only operate under load; therefore, they cannot be filled (connected to a power supply) without load.
- The bellows should be equipped with end-of-stroke limiters (with maximum and minimum heights); otherwise, they may be damaged.

- The pressing force required to press the bellows to the minimum height is derived from the mass load.
- The entire supporting surfaces of the upper and lower plates of the bellows should be used to transfer the loading force.
- The bellows do not require lubrication or maintenance.
- The bellows do not require sealing; therefore, they operate without friction loss.
- The bellows must be vented before disassembly (assembly, disassembly, and replacement of the bellows are easy and quick).
- During operation, the bellows must not come into contact with other elements; therefore, a suitable assembly clearance must be maintained (with sufficient space around the bellows).
- The bellows operate without maintenance under difficult working conditions, such as in an aggressive environment with dust, dirt, or underwater.
- When operating below ambient temperatures below +2 °C, attention should be paid to air humidity.

Depending on the construction and operation principles, the bellows are divided into bellows, bellows with threaded studs, rolling lobes, and air springs in the sleeves. On the basis of the number of bellows, they are divided into single--, double-, and triple-convolution bellows. Figure 6 shows the diagrams of air springs (including double convolution bellows and rolling lobe bellows).

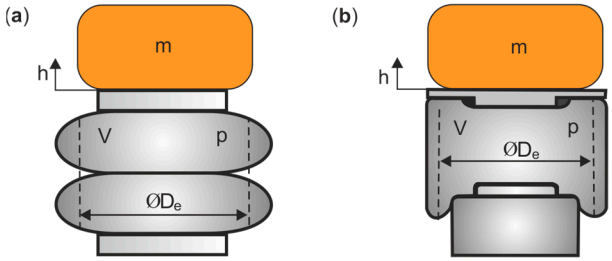

Figure 6. Diagram of air springs: (**a**) double convolution bellow; (**b**) rolling lobe bellow.

The load force on the air spring is defined as follows:

$$F_m = m\,g = A_e(h)\;p \Rightarrow\; A_e(h) = \frac{m\,g}{p} \tag{3}$$

where F is the load, $F = m\,g$, m is the load mass, g is the acceleration of gravity, p is the absolute pressure of the air spring, h is the stroke (deflection) of the air spring, and A_e is the effective area of the air spring,

$$A_e = \frac{\pi\,D_e^2}{4} \tag{4}$$

where D_e is the effective diameter of the air spring.

The effective area A_e corresponds to the load-carrying capacity of an air spring at a given point in the stroke since the mass load is divided by the air pressure in the bellows. The effective area of the air spring is hard to define directly but can instead be estimated by measuring the force exerted on the bellows depending on the height and pressure. In convolution bellows, the effective area of a flexible air spring can fluctuate greatly during its stroke, but in rolling lobe bellows, the effective area stays constant. The convolution below is stiff in the axial direction and elastic in the radial direction because of the extensibility of its rubber-textile coating.

The static characteristics of the air spring are determined experimentally and then approximated by the fitting function.

In [98], for the air convolution of the bellows of type Rubena 340/3, the dependence of the effective area A_e on the stroke h was defined as a polynomial function,

$$A_e = 0.0726 - 0.0564\,h - 0.6436\,h^2 \tag{5}$$

In [99], the effective area with respect to the height of the convolution bellows was found by applying the least squares method (LSM), which describes the mass load of the bellow relative to the pressure and then fits it to a polynomial function of the fourth degree.

$$A_e = -0.0289 + 0.08362\,h - 3.0689\,h^2 + 4.9616\,h^3 - 2.9041\,h^4 \tag{6}$$

As the single convolution bellow expands, its outer diameter changes from its maximum D_{max} to its minimum D_{min}, as shown in Figure 7.

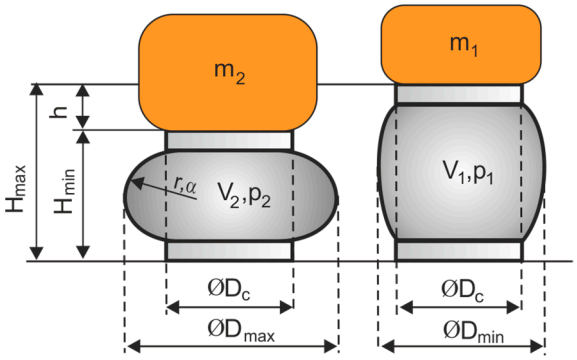

Figure 7. Diagram of the deflection of the single convolution bellow the air spring.

For the case shown in Figure 7, the adiabatic compression of the gas is considered,

$$p_1\,V_1^{\kappa} = p_2\,V_2^{\kappa} \quad \Rightarrow\; p_2 = p_1\left(\frac{V_1}{V_2}\right)^{\kappa} = p_1\left(\frac{V_1}{V_1 - \Delta V}\right)^{\kappa} \tag{7}$$

After considering the pressure and incremental volume $\Delta V = Vg\,h$ in 2 states, the mass force can be determined as follows:

$$F_{m_2} = m_2\,g = A_{e2}(h)\,p_2 = A_{e2}(h)\,p_1\left(\frac{V_1}{V_1 - Vg\,h}\right)^{\kappa} \tag{8}$$

where κ is the adiabatic exponent, Vg is the volume gradient, $Vg = \Delta V/\Delta h$.

For the air spring, the equation of mechanical work dWm is as follows

$$dW_m = F_{m_2}\,dh \tag{9}$$

The energy stored in the air spring is equal to the mechanical work dW_m performed as follows:

$$E_{S2} = \int_0^{h_2} F_{m_2}\,dh = p_1\int_0^{h_2} A_{e2}(h)\,\left(\frac{V_1}{V_1 - Vg\,h}\right)^{\kappa} dh \tag{10}$$

From the equation for the equilibrium of the mechanical work dW_m and the pressure-volume work dW_p,

$$dW_m = dW_p \Rightarrow\; F_{m_2}\,dh = p_2\,dV \tag{11}$$

The volume gradient is as follows.

$$\frac{dV}{dh} = \frac{F_{m_2}}{p_2} = \frac{m_2\,g}{p_2} \tag{12}$$

The volume increment ΔV of convolution bellow is the sum of the volume of the cylinder with diameter D_c and the volume of the coating segment in the circumferential (longitudinal) radius r and angle α [100], as follows:

$$\Delta V = \frac{\pi D_c^2}{4} h + r^3[1 + \sin(2\alpha)] \tag{13}$$

In [101], the increase in the volume of the bellows is due to the displacement of the bellows coating in the transverse direction.

$$\Delta V = \frac{\pi D_c^2}{4} h + 2\pi\left[-\frac{4}{9} h r^2 + h^2\left(\frac{28 r}{90} + \frac{\pi D_c}{4}\right)\right] \tag{14}$$

In [102], the spring volume was determined from the expansion of the Taylor series around the volume gradient that depends on the stroke,

$$V(h) = V_0 + \sum_{n=1}^{\infty} \frac{1}{n!} \frac{d^n V}{dh^n} h^n \tag{15}$$

In [103], the volume V in m^3 was determined based on the stroke h in mm of the bellows based on the approximate polynomial function,

$$V = \left(0.2077 - 0.0033\, h - 0.0001\, h^2\right) 10^{-3} \tag{16}$$

The stiffness of the air spring is affected by the enclosed air volume, resulting in a conflict between the available installation space and the optimal stiffness. In [104], to reduce the stiffness of the air spring while maintaining the same design space, adsorbents such as activated carbon were used in the enclosed air volume of the air spring. The volume of the enclosed air spring can be filled with more air molecules by binding them to the adsorbent despite the size and pressure of the air spring remaining the same.

Rolling-lobe air springs incorporate a piston that allows the flexible member to roll along the surface of the piston. Depending on the shape of the piston of the rolling lobe bellows, there may be three cases of effective area A_e depending on the stroke h, which are shown in Figure 8.

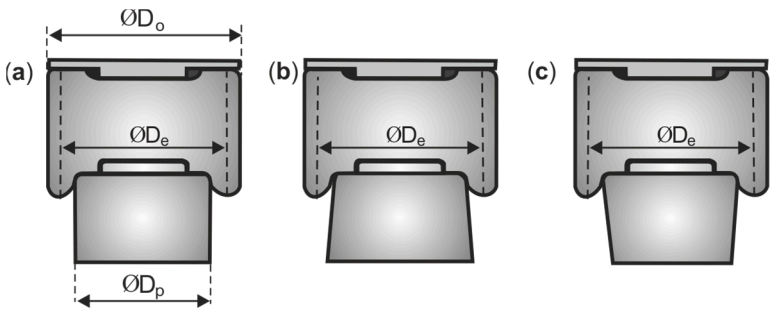

Figure 8. Diagram of the rolling lobe bellows: (**a**) constant effective area, $dA_e/dh = 0$, (**b**) increasing effective area, $dA_e/dh > 0$, (**c**) decreasing effective area, $dA_e/dh < 0$.

For a constant effective area (A_e = const) of the rolling lobe bellows, the volume gradient depends on the outer diameter D_o and the diameter D_p of the piston as follows [105],

$$V_g = \frac{\Delta V}{\Delta h} = \frac{\pi}{4}\left(0.4\, D_o^2 - 0.6\, D_p^2\right) \tag{17}$$

3.4. Model and Characteristics of Air Springs

Air springs are common in automotive applications, where low spring rate (stiffness) and low natural frequencies are beneficial. The compressibility of gas gives air springs a desirable isolation performance. Frequency analysis of air springs can help reduce the sprung mass, relieve suspension systems, and filter out specific unwanted frequencies. The sealed air spring maintains a constant mass of air; therefore, the mass load causes the spring to deflect, resulting in the stiffness of the gas spring. The natural frequency of the sealed air spring also depends on this relationship. Figure 9 shows diagrams of the basic model of sealed air springs.

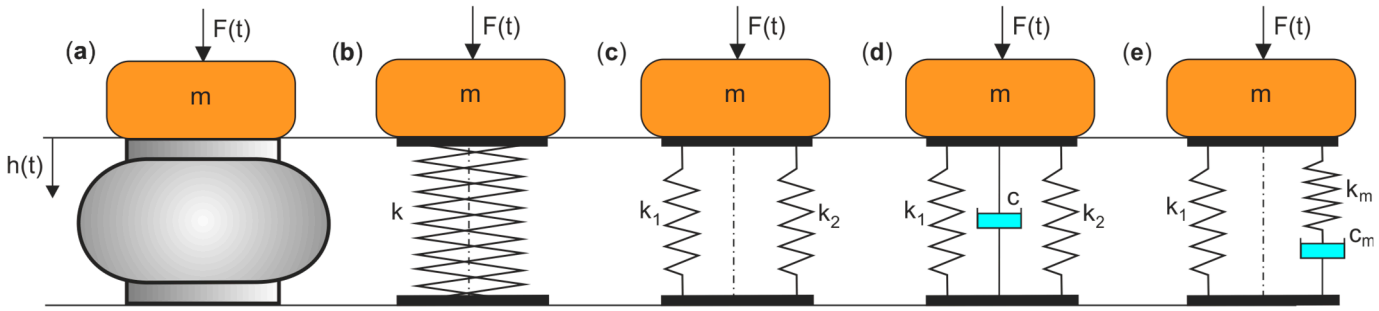

Figure 9. Diagrams of the sealed air spring model: (**a**) air spring calculation diagram, (**b**) simple dynamic model for $dA_e/dh = 0$, (**c**) classical dynamic model for dA_e/dh 0, (**d**) classical dynamic model with viscous damping, (**e**) dynamic model with Maxwell elements.

Air is a compressible medium because the stiffness of the air spring is low, which is why air bellows are used in systems with, i.e., "soft damping". The main manufacturers in the car air suspension market are Continental AG, Firestone, Wabco, ZF Friedrichshafen AG, Tenneco, BWI Group, AccuAir Suspension, Hitachi, Dunlop, and ThyssenKrupp Bilstein.

Figure 10 shows a trailer wheel suspension with an air spring in the rolling-lobe.

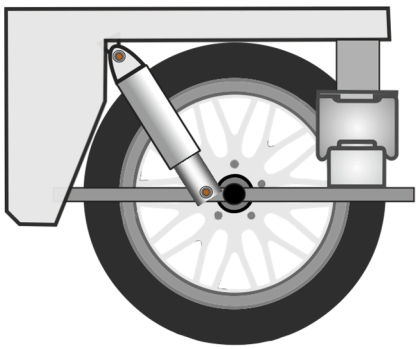

Figure 10. Diagram of the air suspension of a wheel for a trailer with a rolling lobe air spring.

The stiffness k of the rolling lobe air spring, according to the simple dynamic model in Figure 9a, as defined by the following parameters: effective area A_e = constant, volumes $V_H \approx A_e\, H$, $V_h \approx A_e\, h$, and $V = V_H - V_h$,

$$k(h) = \frac{dF_m}{dh} = A_e^2 \frac{dp}{dV} = A_e^2\, \kappa\, p_i \frac{V_H^\kappa}{V^{\kappa+1}} = \kappa\, p_i\, A_e\, \frac{H^\kappa}{(H-h)^{\kappa+1}} = \frac{\kappa\, p_i\, A_e}{H} \left(\frac{H}{H-h}\right)^{\kappa+1} \tag{18}$$

where F_m is the mass load, H is the height of the air spring, p_i is the initial pressure inside the bellows, κ is the adiabatic exponent.

In the case of a small rolling lobe bellow deflection $h << H$, the stiffness k of the air spring from (18) is simplified to the generally accepted form,

$$k = \frac{dF}{dh} = A_e^2 \frac{dp}{dV} = \frac{\kappa\, p_i\, A_e^2}{V} \approx \frac{\kappa\, p_i\, A_e}{H} \tag{19}$$

The force of the rolling lobe air spring is as follows:

$$F_m = k\,(H-h) = \kappa\, p_i\, A_e \left(\frac{H-h}{H}\right)\left(\frac{H}{H-h}\right)^{\kappa+1} \tag{20}$$

In the case of a Goodyear rolling lobe air spring with technical specifications: effective diameter D_e = 250 mm, $H_{\max}$ = 300 mm, $H_{\min}$ = 180 mm, and stroke h = 120 mm, the adiabatic curves of stiffness k according to (19) and force F_m according to (20) versus spring stroke h were calculated for different pressures p and are presented in Figure 11.

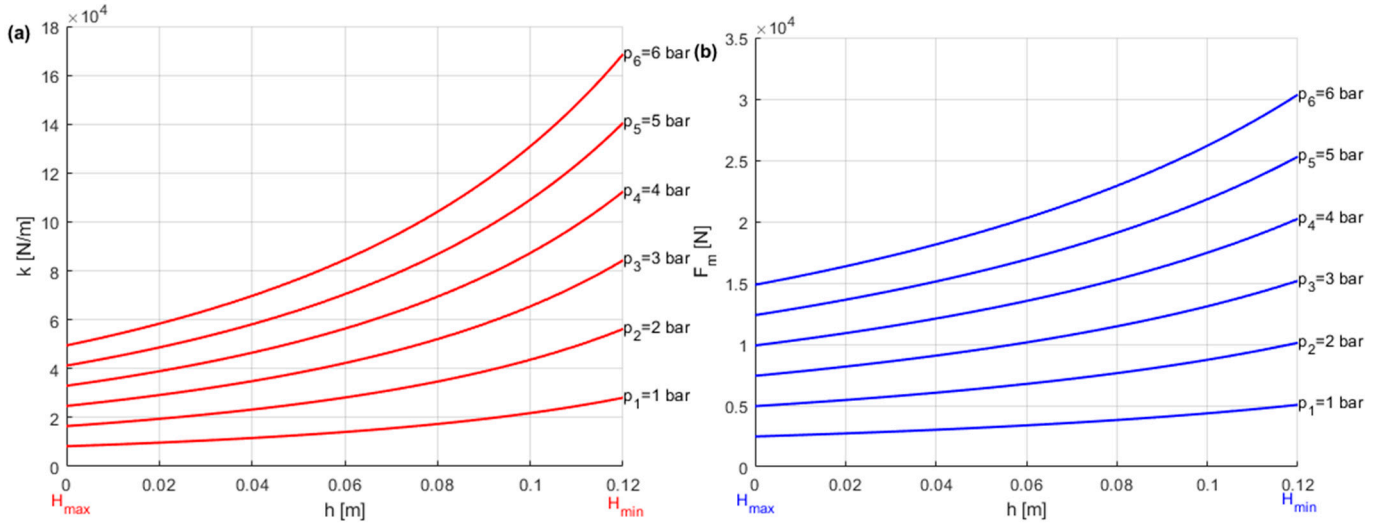

Figure 11. Adiabatic curves for the rolling lobe air spring of a trailer for different pressures: (**a**) air spring stiffness versus stroke, (**b**) air spring force versus stroke.

According to the classical dynamic model in Figure 9c, the stiffness of the convolution air spring for an effective A_e = var is defined as follows:

$$k = \frac{dF}{dh} = \frac{d(p, A_e)}{dh} = A_e \frac{dp}{dh} + p \frac{dA_e}{dh} = k_1 + k_2 \tag{21}$$

where k_1 is the stiffness of the air spring due to adiabatic air compression in the convolution air spring, k_2 is the stiffness of the air spring due to changes in its effective area during compression or expansion of the convolution air spring,

$$k_1 = A_e \frac{dp}{dh} \tag{22}$$

$$k_2 = p \frac{dA_e}{dh} \tag{23}$$

where p is the instantaneous pressure inside the convolution air spring.

The thermodynamic state equation results in the expression for pressure change,

$$\frac{d(p\, V^\kappa)}{dh} = p\, \kappa\, V^{\kappa-1} \frac{dV}{dh} + V^\kappa \frac{dp}{dh} = 0 \Rightarrow \frac{dp}{dh} = -\frac{\kappa\, p}{V} \frac{dV}{dh} \approx \frac{\kappa\, p\, A_e}{V} \tag{24}$$

where V is the instantaneous volume of the convolution air spring.

The stiffness of the convolution air spring after taking into account the dependencies (22)–(24) is written as follows:

$$k = k_1 + k_2 = \frac{\kappa\, p\, A_e^2}{V} + p\,\frac{dA_e}{dh} \tag{25}$$

instantaneous pressure inside the convolution air spring,

$$p\, V^{\kappa} = p_i\, V_i^{\kappa} \Rightarrow \quad p = p_i \left(\frac{V_i}{V}\right)^{\kappa} = p_i \left(\frac{V_i}{V_i - \Delta V}\right)^{\kappa} \tag{26}$$

where ΔV is the reduction of the volume of the convolution air spring as a function of h, $\Delta V = A_e\, h$.

$$k(h) = k_1 + k_2 = p_i \frac{\kappa\ V_i^{\kappa}\ A_e^2}{(V_i - A_e\, h)^{\kappa+1}} + p_i\, \frac{V_i^{\kappa}}{(V_i - A_e\, h)^{\kappa}}\, \frac{\Delta A_e}{\Delta h} \tag{27}$$

The force of the convolution air spring is as follows:

$$F_m = k\,(H - h) \tag{28}$$

Based on experimental studies [106], for an Aventics single convolution air spring 0822419002 in the height range of $H_{\max}$ = 100 mm, $H_{\min}$ = 50 mm, and h = 50 mm, the approximation function of the effective surface A_e as a function of H of the air spring in the range $[H_{\min}, H_{\max}]$ was determined as follows:

$$A_e(H) = -0.0155\, H^2 + 1.06\, H + 118\ \text{cm}^2 \tag{29}$$

Figure 12 shows the effective area A_e as a function of the stroke (deflection) h of the single convolution air spring.

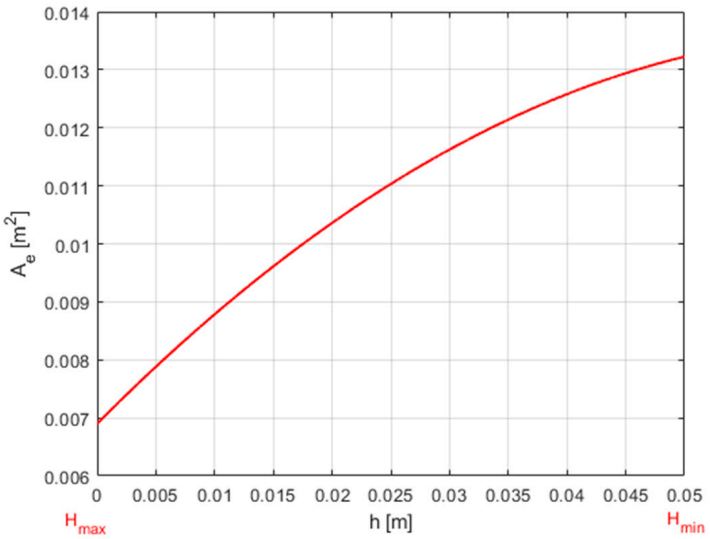

Figure 12. The effective area is a function of the stroke (deflection) of the single convolution air spring.

Figure 13 shows the suspension of the wheels of a passenger car with a convolution air spring.

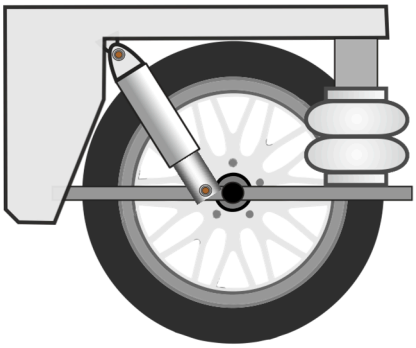

Figure 13. Diagram of a wheel air suspension for a passenger car with convolution air spring.

For a single convolution air spring of Aventics, the adiabatic curves of stiffness k according to (27) and force F_m according to (28) versus the spring stroke h were calculated for different pressures p and are presented in Figure 14.

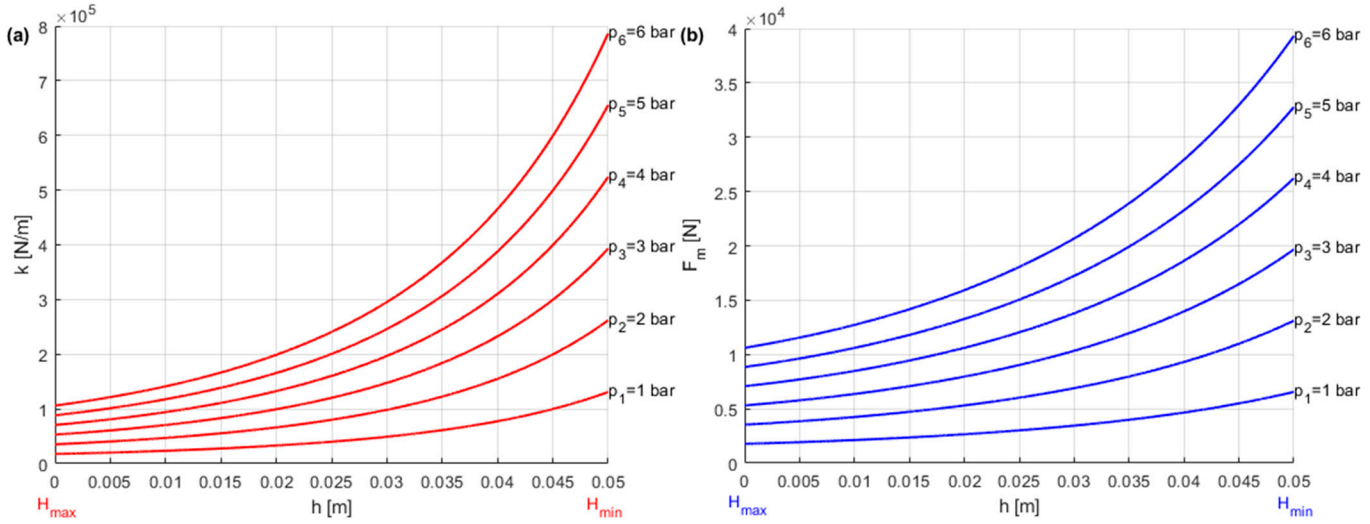

Figure 14. Adiabatic curves for the single convolution air spring of a passenger car for different pressures: (**a**) air spring stiffness versus stroke, (**b**) air spring force versus stroke.

In [106], after applying the regression analysis, the coefficient of the approximation function of the single convolution air spring force F_m was determined as a function of pressure p and stroke (deflection) h as follows.

$$F_m(p,h) = 0.016\ p^2 - 0.0003\ h^2 + 1.727\ p + 0.04\ h + 0.01\ p\ h - 1.04 \quad (30)$$

Based on the approximation function (30), a 3D graph of the force $F_m(p,h)$ is presented in Figure 15 as a function of the pressure p and the stroke h of a single convolutional air spring.

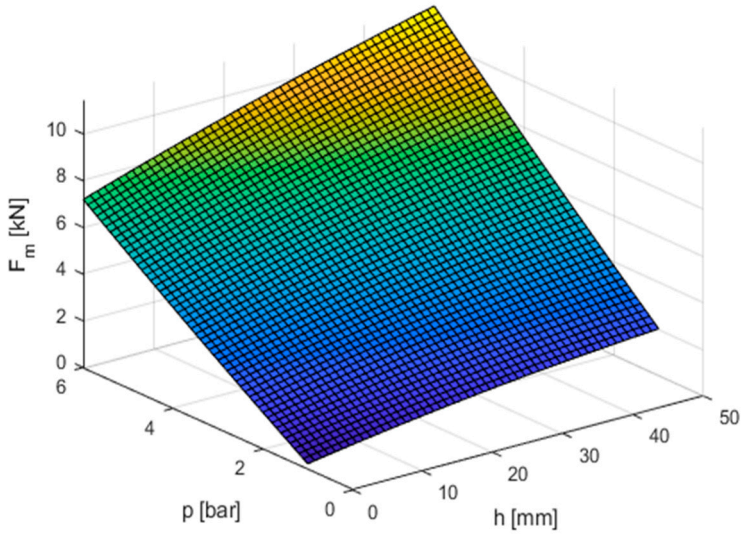

Figure 15. A 3D graph of the force $F(p,h)$ as a function of the pressure p and the stroke h of the single convolution air spring.

3.5. Vibro-Isolation of Air Springs

The bellows, which are used as air springs, are loaded with mass and excited by an external force, creating a vibration system. In the case of forced undamped vibrations (the bellows have a small damping coefficient), the equation of motion for the mass–air spring stiffness system according to the simplified model of the air bellows in Figure 9b can be written as follows:

$$m\,\ddot{h} + k\,h = F_m + F \Rightarrow\ \ddot{h} + \omega_n^2\,h = \frac{F_m + F}{m} \tag{31}$$

where F is the external exciting force, ω_n is the natural angular frequency vibration of the bellows according to (31),

$$\omega_n = \sqrt{\frac{k}{m}} \tag{32}$$

The natural frequency of the bellow vibrations is as follows:

$$f_n = \frac{\omega_n}{2\,\pi} = \frac{1}{2\,\pi}\,\sqrt{\frac{k}{m}} \tag{33}$$

Figure 16 shows the natural frequency f_n of the rolling lobe air spring and the single convolution air spring for the stiffnesses k according to (19) and (27) versus the spring stroke h for different pressures p.

In the case of harmonic excitation, the excitation force of the air bellows is expressed as follows:

$$F = F_e\ \sin(\omega_e\,t) = F_e\ \sin(2\pi f_e\,t) \tag{34}$$

where F_e is the amplitude of the excitation force, ω_e is the natural undamped angular frequency, f_e is the natural undamped frequency,

$$f_e = \frac{\omega_e}{2\,\pi} \tag{35}$$

After considering the harmonic forcing, the equation of motion of the bellows is as follows:

$$\ddot{h} + \omega_n^2\,h = \frac{F_m}{m} + a_e\ \sin(\omega_e\,t) \tag{36}$$

where a_e is the constant coefficient,

$$a_e = \frac{F_e}{m} \tag{37}$$

In the analytical solution of the differential Equation (36), the response of the mass–air spring system is as follows:

$$h(t) = h_0 \ \sin(\omega_e \, t + \varphi) = \frac{a_e}{\omega_e^2 - \omega_n^2} \ \sin(\omega_e \, t + \varphi) \tag{38}$$

where φ is the phase shift.

For a phase shift of $\varphi = 0$, the forced vibrations are in phase with the exciting force in the range of the frequency ratio $\omega_e/\omega_n < 1$.

For a phase shift of $\varphi = -\pi$, the forced vibrations are in phase opposite to the exciting force in the range of the frequency ratio $\omega_e/\omega_n > 1$.

Knowing the natural frequency f_n is essential to predict the efficiency of isolating vibrations. The excitation frequency to be isolated depends on the system's natural frequency. This relationship can be calculated using the vibration transmissibility T [107],

$$T = \frac{1}{\left(\frac{f_e}{f_n}\right)^2 - 1} \tag{39}$$

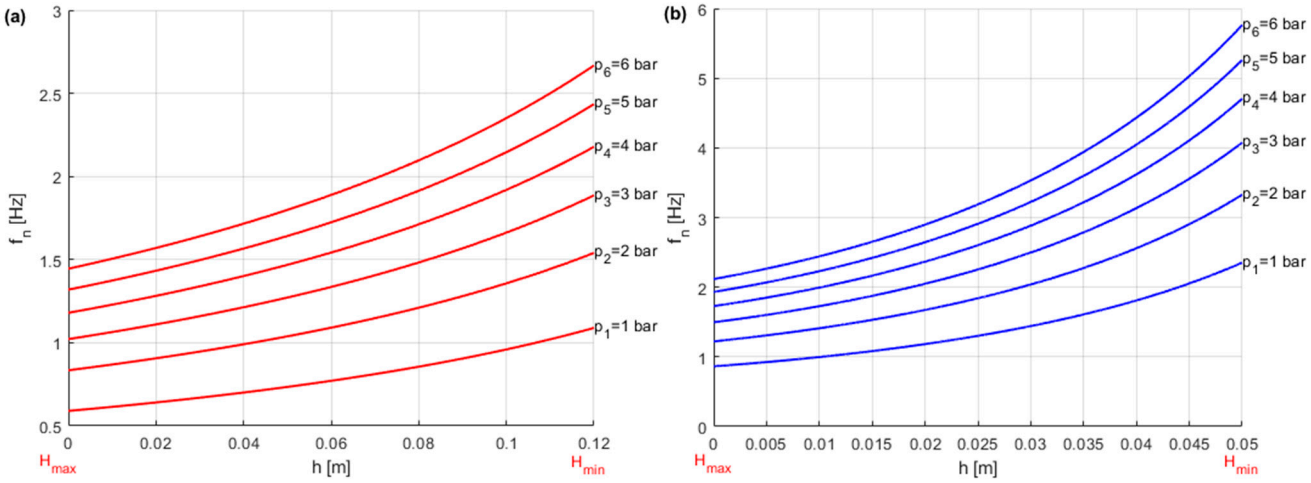

Figure 16. Natural frequency f_n for the stiffnesses k versus the spring stroke h for different pressures p: (**a**) rolling lobe air spring, (**b**) single convolution air spring.

For air bellows used as air springs, the proper degree of vibration isolation occurs for the frequency $f_e > \sqrt{2}\, f_n = 1.4142\, f_n$, i.e., in the range of excitation vibration frequencies higher than the resonance vibration frequency when $f_e = f_n$. A high degree of vibration isolation occurs in the frequency range $f_e >> f_n$.

The isolation rate IR for air-spring bellows is calculated using the formula,

$$IR = 1 - T = 1 - \frac{1}{\left(\frac{f_e}{f_n}\right)^2 - 1} \tag{40}$$

Figure 17 shows the isolation rate curves for the air spring bellows.

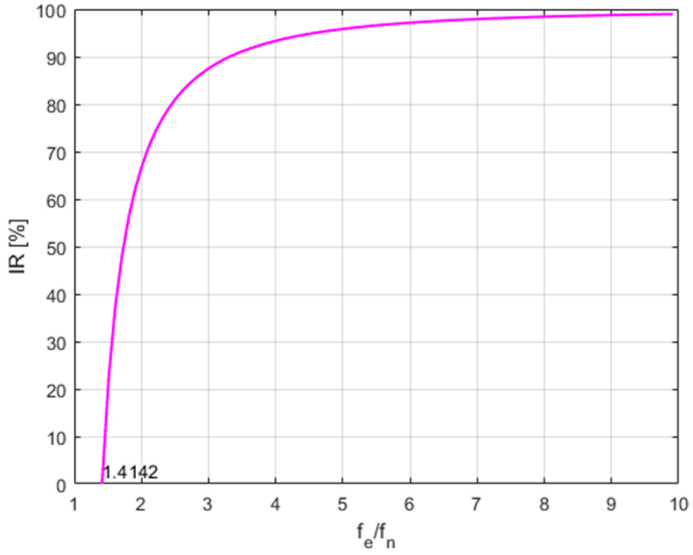

Figure 17. The isolation rate curve for the air-spring bellows.

According to the classical dynamic model with viscous damping of the air bellows in Figure 9d, the dynamic equation of the mass–air spring–damping system can be written as follows:

$$m\,\ddot{h} + c\,\dot{h} + k\,h = \Delta F_m + F \Rightarrow\ \ddot{h} + 2\,\xi\,\omega_n\,\dot{h} + \omega_n^2\,h = \frac{\Delta F_m + F}{m} \tag{41}$$

where c is a viscous damping constant that primarily describes the damping of the material of the air spring, ξ is the damping ratio,

$$\xi = \frac{c}{2\,m\,\omega_n} \tag{42}$$

Taking into account the damping ratio, the vibration transmissibility T is presented in the form [108]

$$T = \sqrt{\frac{1 + \left(2\,\xi\,\frac{f_e}{f_n}\right)^2}{\left[1 - \left(\frac{f_e}{f_n}\right)^2\right] + \left(2\,\xi\,\frac{f_e}{f_n}\right)^2}} \tag{43}$$

At a frequency ratio of $f_e/f_m = 1$ (resonance), the transmissibility depends only on the damping ratio ξ is as follows:

$$T = \sqrt{1 + \frac{1}{4\,\xi^2}} \tag{44}$$

3.6. Simulation Model of Air Spring

In air spring modeling and tests, the material properties and certain creep characteristics of rubber bellows are generally taken into account. The air spring rubber bellows consist of an elastomer matrix complemented by in-line reinforcement yarns. Deformations of the yarn in the cross-layered air spring bellows cause shears in the elastomer, leading to complex stress and deformation conditions. This leads to friction between the inner material and the rubber bellows of the air spring [109]. In [110], a new, fully dynamically defined experimental model of the friction force of an air spring was presented, which was used to determine the air spring hysteresis curve with greater precision. In the air bellows, the friction force is generated mainly by the incorporated rubber components and the relative motion of the rubber bellow and its surface. Rubber air springs also have

the viscoelastic properties of rubber materials, such as Zener, Maxwell, Kelvin-Voigt, and fractional models [111]. Friction is a factor that contributes to the force hysteresis behavior of a rubber air spring. In [103], the friction force was generated by filling the rubber components and the relative motion between the rolling lobe and the surface of the piston. A Berg model of the frictional hysteresis air spring was considered [112].

The simulation block for the sealed air spring to isolate shock and vibrations is available in Simscape tools from Matlab Simulink R2021a software. Figure 18 shows a simulation model using the Simscape block for the sealed air spring.

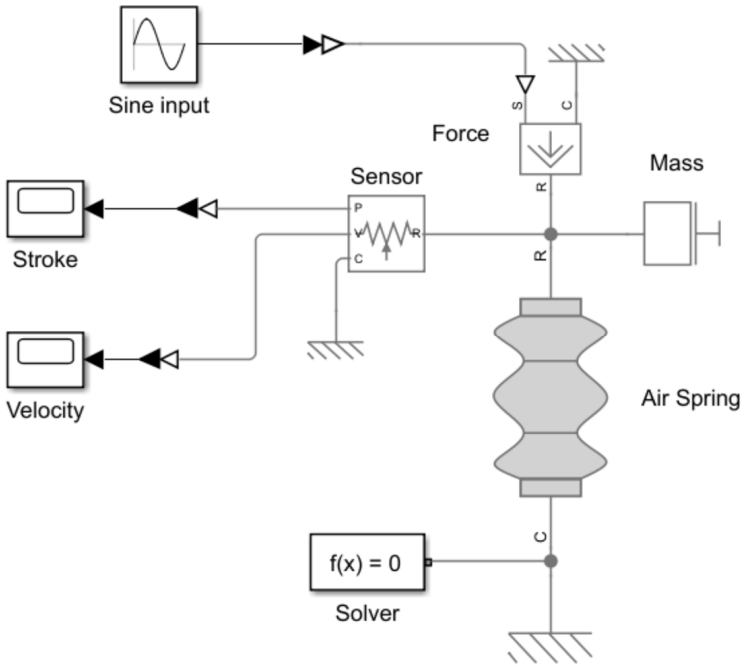

Figure 18. Diagram of the Simulink dynamic model of the Simscape block of the sealed suspension air spring.

The air spring block takes into account the relative translational movement between ports R and C to estimate its height and speed using the information entered. The simulation block computes the non-linear responses of the air spring to the external load by utilizing the force dynamic equation.

$$m\,\ddot{h} + c(h)\,\dot{h} + k(h,p)\,h = F_{ex} \tag{45}$$

where m is the mass of the load, $h(t)$ is the stroke of the air spring, $\dot{h}(t)$ is the deflection velocity of the air spring, $c(h)$ is the viscous damping coefficient, $k(h,p)$ is the stiffness of the air spring, F_{ex} is the external force.

Three dynamic stroke and velocity responses were obtained from the simulation of the suspension air spring in the Simscape environment. Figure 19 shows the results for k = constant and $F_e = 0$, Figure 20 shows the results for $k(p,h)$ and $F_e = 0$, and Figure 21 shows the results for $k(p,h)$ and $F_e(t)$.

The dynamic air suspension model with the Maxwell transformed element consists of a serial connection of a spring element with coefficient k_m and a linear dashpot element with coefficient c_m, as shown in Figure 9d, and was the subject of research in [105,113–115]. In [116], various air-spring suspension models are discussed, such as Nishimura, Vampire, Gensys, and Simpac.

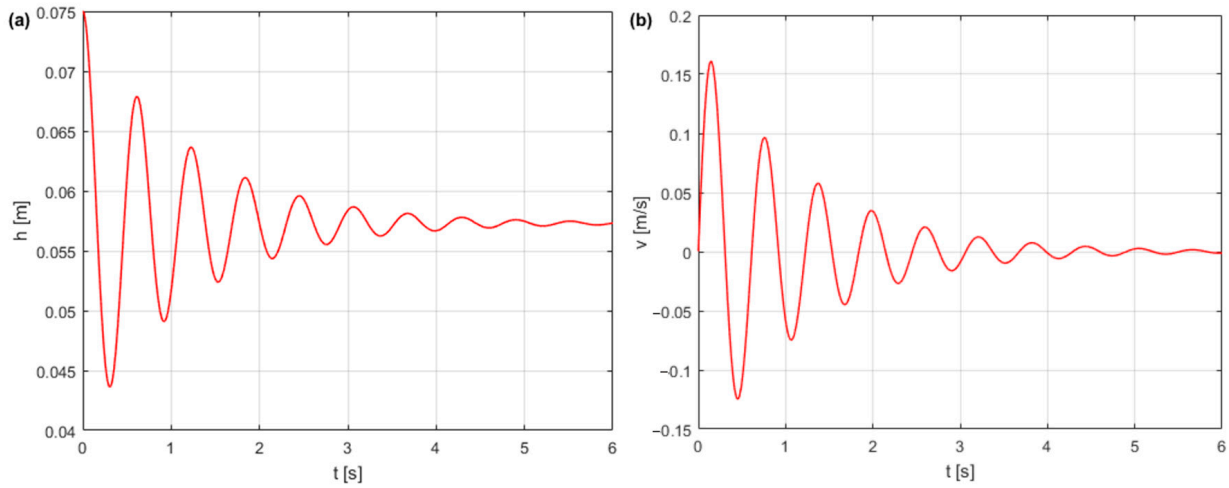

Figure 19. Dynamic responses of the stroke (**a**) and velocity (**b**) of the suspension air spring for k = constant and $F_e = 0$.

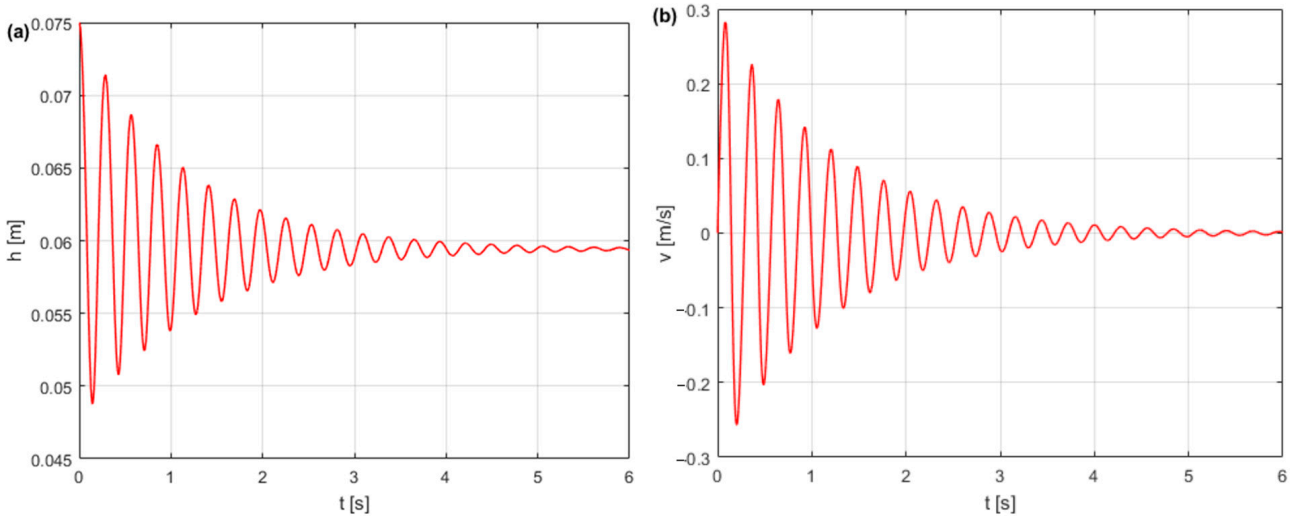

Figure 20. Dynamic responses of the stroke (**a**) and velocity (**b**) of the suspension air spring for $k(p,h)$ and $F_e = 0$.

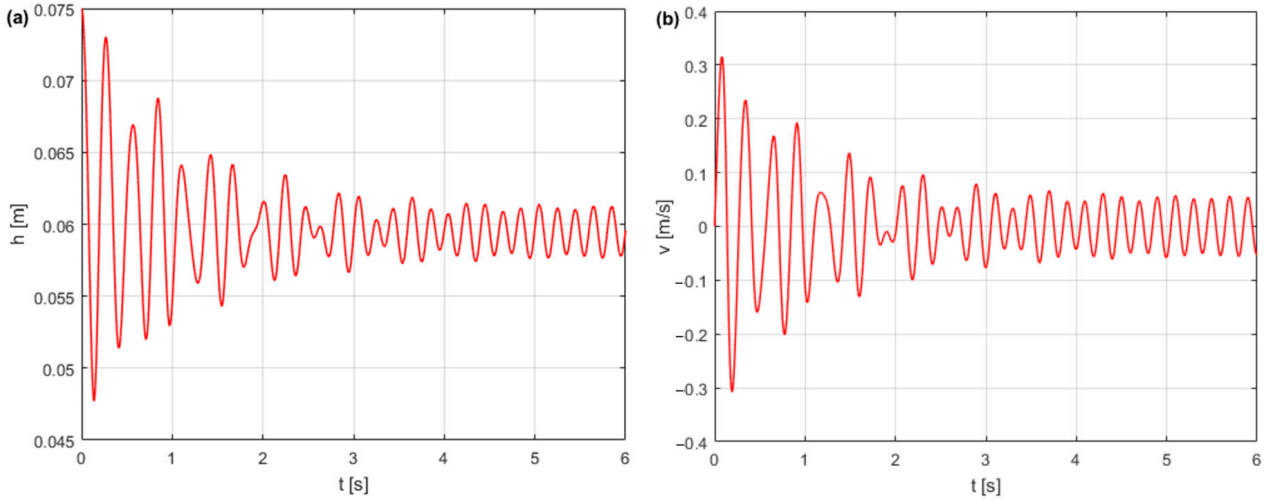

Figure 21. Dynamic responses of the stroke (**a**) and velocity (**b**) of the suspension air spring for $k(p,h)$ and $F_e(t)$.

In [117], using Matlab/Simulink software, the control model of an active automotive pneumatic system was modeled with a quarter-passenger car, in which an air spring with almost linear characteristics between force and displacement and volume and displacement were used. In [118], the spring stiffness of the airbag is calculated using its model in a Matlab environment. In [119], the dynamic responses of a mass-spring-damper system were studied and the dynamic equations of which were modeled using Simscape Multibody models. In [120], Simulink simulation was used together with the objective optimization function of OptiY to obtain an air spring suspension model equivalent to a passive suspension system. In [121], to address the large height error and attitude destabilization phenomenon in regulating the frame height of trucks with electronic control air suspension (ECAS), a dynamic model was designed, consisting of an AEMSim model for ECAS and a Simulink model for the truck. Other software, such as Altair HyperWorks 2023, Automation Studio™, and SimulationX, offer the versatile open design and simulation platforms available, empowering automotive engineers with a comprehensive suite of software for PS systems. Rapid Axle Concept Evolution (RACE) is a software package that uses MBS (multibody simulation)/MBD (multibody dynamics) to develop suspension systems.

3.7. Trends and Challenges in PS Systems

Most air suspension studies consider models consisting of three main parts: an air spring, an auxiliary tank, and a pipe connecting the two as a damping tube [122]. In [123], two air chambers (rubber airbags) were proposed as a new air suspension, which allows independent adjustment of ride height and stiffness. The air pressure in the two air chambers allows for the simultaneous adjustment of the vehicle's stiffness and ride height under different driving conditions in this air suspension system. Using this feature, the natural frequency and height of the vehicle can be adjusted according to load and road conditions. In [124], a complex analytical stiffness model of an air spring system with an auxiliary chamber was developed considering the inertial effects of gas on the connecting tube. The proposed model is particularly suitable for air-spring systems with high gas inertia in large, low-damping pipelines.

The main trends and challenges in the development of PS systems are as follows:

Integration of electronic systems with PS systems has become increasingly common. Electronically controlled PS systems enhance ride quality by automatically modifying suspension settings in response to road conditions and driving dynamics, resulting in smoother and more enjoyable rides. Integrating PS systems with Advanced Driver-Assistance Systems (ADAS) enhances vehicle handling and safety. Using the PS system in combination with ADAS and adaptive cruise control, vehicle dynamics can be adapted to driving conditions and maneuvers, improving overall efficiency and ride safety.

The Adaptive pneumatic suspension (APS), in which the active suspension system has adjustable damping, is integrated with electronic microprocessor control, is used in many luxury cars and is a standard or very expensive option. APS continuously analyzes road conditions (longitudinal and transverse body tilt), driving style, vehicle load, and terrain configuration. Electronically controlled system elements allow the selection of appropriate APS damping characteristics to ensure the highest possible comfort and travel safety.

The development of a hybrid suspension system as a combination of an air spring and a coil spring is very comfortable and has ease of installation. The air spring part gives the best performance, smooth ride, greatest energy dissipation, and variable ride height. The coil spring part of the hybrid suspension helps to avoid the failure of the air spring part and reduces side swing.

The emergence of environmentally friendly PS solutions as sustainable suspension systems is based on reducing the weight of the PS, utilizing recyclable materials, and

reducing the environmental impact. The ecological trend in PS systems not only aligns with global sustainability goals but also contributes to improving the fuel efficiency of vehicles.

PS systems are increasingly being used in vehicle personalization and aftermarket enhancements that allow for personalization in ride height and suspension stiffness, catering to high-performance ride enthusiasts and professional drivers.

Smart PSs with Internet of Things (IoT) connectivity can gather and assess data in real-time, allowing immediate adjustments to suspension systems. This not only extends the lifespan of the suspension components but also enhances overall ride performance.

The use of PS in EVs and AVs is an ideal solution due to its ability to provide improved ride quality and stability, which is desirable given the heavy weight of EV batteries. Additionally, the PS system helps to maintain optimal ground clearance, which is a key factor in the aerodynamic efficiency of EVs and AVs.

4. HPS System

4.1. Principle of Operation of the HPS Strut

Compared to other suspension systems, the HPS strut is advantageous due to its ability to combine the advantages of gas springs and the beneficial damping properties of hydraulic fluids (the suspension fluid LHM+ is compatible with Citroën HPS systems). The hydraulic fluid absorbs and dampens the forces applied to the suspension system of a car while it is in motion and is just as important as the mechanical components of a vehicle suspension. The hydraulic fluid lubricates moving parts to reduce friction and wear and adds a layer of protection against rust and corrosion; however, it must be changed periodically to prevent leaks.

The HPS strut has the significant benefit of being able to adapt to the specific needs and situations on the road after which the vehicle is driving [125]. The HPS strut not only reduces wheel vibrations but is also responsible for the overall operation of the vehicle's suspension and is also used to adjust the vehicle suspension height. HPS struts are especially suitable for automotive applications such as passenger cars, trucks, military vehicles, and agricultural equipment. HPSs are used for axle, cabin, and boom suspension, among others. Different types of HPS struts are used, depending on the specific vehicle model, such as front axle suspension, rear axle suspension, or full suspension. HPS is mainly related to the Citroen, Rolls Royce, Maserati, and Mercedes brands that first used HPS struts. The idea of HPS involves the elimination of conventional suspension components, such as springs, torsion bars, and leaf springs. Instead of these traditional parts, each wheel has an HPS strut. In the tuning community, HPS struts are highly appreciated for their ability to be highly customized to adjust vehicle height and the way it feels while driving.

HPS struts are useful in the following vehicles:

Luxury vehicles: HPS provides an extremely smooth and supple ride.
Performance cars: HPS provides precise and stable ride handling.
Heavy-duty vehicles: HPSs can withstand heavier loads, making them ideal for commercial vehicles.

Figure 22 shows the diagrams of the standard automotive HPS struts, a functional scheme of the HPS strut, and the Citroën HPS struts. The Citroën HPS strut (since 1954) is simple and reliable, providing an unmatched level of comfort and excellent handling and grip [126].

The basic hydraulic components of the HPS strut:

Hydropenumatic accumulators (HPAs) stored pressurized gas and hydraulic fluid and maintained pressure in HPS systems at the same level. Volume, pressure, and thermodynamic processes are important HPA parameters.

The hydraulic cylinder is used to adjust vehicle height and transmit wheel vibrations. The piston rod of the cylinder is connected to the vehicle wheel, and the cylinder barrel is connected to the vehicle body. The load on the hydraulic cylinder is mainly due to the weight of the vehicle body, suspension, and tires.

Damping elements, such as the orifice or throttle, are located in the standard HPS strut between the HPA and the hydraulic cylinder. These damping elements prevent pressure surges in the hydraulic cylinder due to the vibration of the wheel shock.

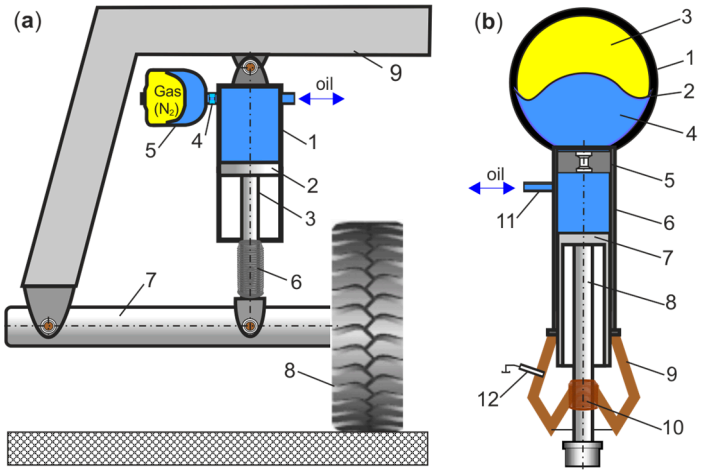

Figure 22. Diagram of standard automotive HPS struts: (**a**) functional scheme of the HPS strut: 1—hydraulic cylinder, 2—piston, 3—piston rod, push rod, 4—orifice damper, 5—hydropneumatic accumulator, 6—dust protector, 7—rotation arm, 8—wheel, 9—frame (body), (**b**) Citroën HPS strut: 1—sphere, 2—diaphragm, 3—the upper half of sphere, 4—lower half of sphere, 5—damper, 6—cylinder, 7—piston, 8—push rod, 9—dust shield, 10—dust bellows, 11—fluid leak tube, 12—high fluid pressure tube.

The displacement of the hydraulic cylinder piston in the HPS strut caused by the movement of the vehicle wheel led to pressure fluctuations and pulsing fluid flow directed to the hydropneumatic accumulator (HPA) through the damper. HPA is adapted to absorb pressure shocks and eliminate pressure pulsations and fluctuations. In standard HPS struts, HPA is called a sphere. However, the HPA is a gas-charged accumulator, which is often referred to as a gas-spring accumulator. HPA contains an N_2 nitrogen gas chamber (upper half of the sphere) and an oil chamber (lower half of the sphere) separated by gas-tight partitions, such as a diaphragm (membrane). A diaphragm-type accumulator is mainly adopted to dampen pressure fluctuations. They are lightweight, have no mechanical moving parts, respond quickly even to small changes in pressure, have high working pressure, and the diaphragm provides a good seal between the gas and oil chambers. The accumulator diaphragm is a separator that balances the pressure in the HPA. When the oil pressure increased, the gas was compressed, whereas when the oil pressure decreased, the gas expanded. The gas spring and damper formed a spring-damping assembly for the HPS strut. The HPS strut damper was located at the HPA inlet. The HPS damper with a central orifice provides damping for pressure fluctuations in the HPS strut with a two-way flow between the cylinder chamber and HPA. Gas springs and dampers provide a variety of options to change the characteristics of the HPS strut. The volume, pressure, and thermodynamic processes of gas are crucial for the properties of HPA. The damping efficiency of the HPS strut depends on the dimensions of the damper orifice and the working pressure in the hydraulic cylinder. The damping efficiency of the HPS strut could be improved by increasing the working pressure and reducing the dimensions of the damping elements [127].

In damping elements in the form of throttle bore, the small flow cross-section causes a high flow velocity of the hydraulic fluid, which generates high losses of pressure, which in laminar flow are proportional to the volumetric flow. Pressure losses are directly dependent on the viscosity of the hydraulic fluid, which is a significant characteristic of the throttle. This aspect is important because, in hydraulic fluids, viscosity is strongly dependent on temperature. Temperature has a significant impact on the damping effect of a throttle, which is unfavorable. At higher operating pressures, friction damping in the throttle may be beneficial due to increased fluid viscosity.

In damping elements in the form of the orifice bore, the cross-sectional fluid flow suddenly changes from wide to narrow areas or from narrow to wide areas. In the circular damping orifice, as opposed to the throttle, only a small amount of surface was in contact with turbulent fluid flow in regions with high flow velocities. Strong turbulence in the hydraulic fluid causes internal friction. The power loss caused by fluid flow is converted into heat, resulting in damping. This orifice type has a quadratic relationship between pressure loss and volume flow. This solution contributes to the design of new types of HPS systems with a better DPI for specific application areas.

The HPS system includes the HPS strut and other hydraulic components:

The hydraulic pump generates the fluid pressure required to charge the HPA and shift the cylinder piston.
The hydraulic fluid reservoir holds the volume of hydraulic fluid necessary for the HPS system to operate.
The hydraulic fluid transmits power within the system, functions as a lubricant to minimize wear and tear absorbs energy, and smooths out flow fluctuations.
The valves are designed to control the flow of fluid to the cylinders and can be adjusted to control the response of the suspension.

Figure 23 shows the hydraulic circuit diagram of the HPS system. The central valve allows two different operating modes: interconnected and closed. When the central valve is closed, the suspension units are separated from each other by the control valve and, therefore, act as individual springs. This causes additional roll stability compared to interconnected mode operation. If the level control valves are closed, greater ride stability can be achieved, especially during cornering and for 'sporty' driving, while for open level control valves, a soft suspension setup is obtained that provides a high level of ride comfort, which is typical for HPS.

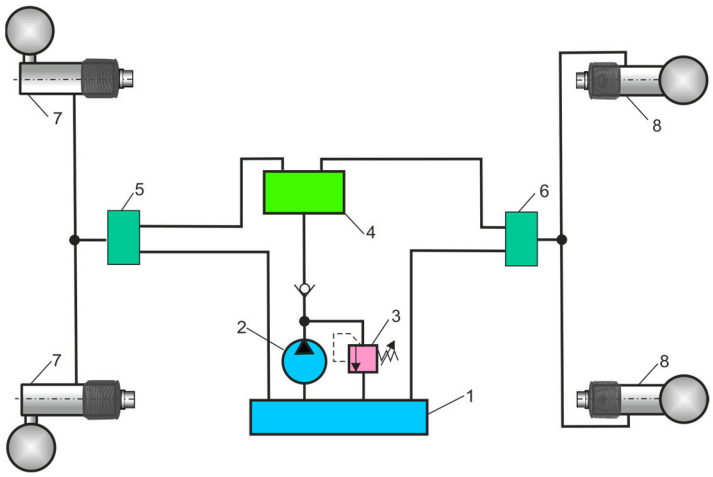

Figure 23. Diagram of the hydraulic circuit of the HPS system: 1—tank, 2—pump, 3—relief valve, 4—central control valve, 5—front level control valve, 6—rear level control valve, 7—front HPS struts, 8—rear HPS struts.

Advantages of the HPS system:

Comfort: HPS systems provide a smooth and comfortable ride with the help of shock absorbers caused by uneven terrain. Absorbs shock better than standard suspension. The car can be raised or lowered for better ground clearance.

Stability: HPS is able to maintain vehicle stability and height level even when performing hard braking, acceleration, and cornering. In addition, it offers compactness and high suspension efficiency. Keeps the vehicle stable on uneven roads, resulting in safer handling of the vehicle ride.

Durability: HPSs are highly durable and require minimal maintenance due to their simple design and construction.

Enhanced aerodynamics: These systems can also improve automobile aerodynamics by lowering the height at higher speeds.

Improved handling: They provide greater control over vehicle height and can be easily adjusted to improve handling and stability. However, they also include power, accuracy, efficiency, and ease of maintenance.

Disadvantages of the HPS system:

Cost: HPS can be expensive to install and maintain. High costs, particularly when high-efficiency units are used. Repairing is more costly due to specialized parts.

Weight: They can be heavier than other suspension systems, which can increase fuel consumption and degrade performance acceleration.

Complexity: The complexity of HPS systems can lead to significant repair costs and require specialized technicians.

Risk of failure: More points of potential failure in demanding riding conditions. Maintaining a hydraulic suspension requires a higher level of attention during service and maintenance.

Environmentally damaging: Toxic effects of hydraulic fluids caused by leaks and ruptured hoses of the hydraulic system.

4.2. Advances in HPS Systems Development

In [128], the performance of three types of heavy truck suspension systems, namely, HPS, leaf, and rubber springs, was investigated on the comfort of the cab ride. The results showed that the ride performance of the HPS system was much better than that of the rubber and leaf suspension systems. A review of publications on mathematical modeling and simulation of the HPS system was conducted. In [129], the study takes into account analytical modeling using nonlinear differential equations, simulation using Matlab/Simulink software, and experiments with an HPS system. In [130], a quarter model of a car suspension was presented to model mechanical systems and develop low-level suspension impedance control for high-speed multi-terrain vehicles. In [131], a mathematical model of a quarter-car HPS system was built and developed using the AMESim software, taking into account the random surface of the road. In [132], a simulation model was used to investigate how gas pressure and temperature affect the spring behavior of an HPS strut used in a wheeled armored personnel carrier. In [133], the aim of the study was to produce a simulation model in Adams/Car software for the eight-wheeled military vehicle Patria AMV and to investigate the influence of the settings of the HPS system on vehicle dynamics. The method of creating a numerical model that can simulate the safety of a wheeled armored combat vehicle with an HPS system was discussed in [134]. In [135], the objective of the project was to develop an HPS simulation model for the GINAF Dakar rally truck, which has the same HPS operation principles as the Citroen HydrActive system. In [136], the authors discuss the results of analyses of design and material solutions and

present the advantages of the commonly used HPS gas spring systems for passenger cars. In [137], the simulation and verification of the experimental suspension system of a self-propelled sprayer with high ground clearance were presented based on a fuzzy PID control strategy optimized by a genetic algorithm. In [138], a mathematical model was presented for a tracked chassis used in a road-rail vehicle with a multicylinder HPS system, which allows the vehicle to navigate uneven terrain and improve overall ride quality. In [139], a computational fluid dynamics (CFD) model was proposed to improve the damping and stiffness forces of HPS, considering the effect of different factors on the characteristics of HPS. In [140], a mathematical and simulation model was developed in the Simulink environment to describe the loading of the hydraulic suspension system. The dynamic properties of HPS were analyzed for step and sinusoidal signals of various frequencies. In [141], a model of the HPS system based on fractional order (HSM-FO) is proposed, which is advantageous in the modeling of viscoelastic materials considering the mechanical properties of the HPS multiphase medium. A detailed HSM-FO calculation method was developed using the Oustaloup filtering approximation algorithm, which is implemented in Matlab/Simulink. The study [142] introduced a new structure for HPS using high-speed in-off solenoid valves. This structure allows for the implementation of two spring force modes and four damping force modes. The fundamental principles of HPS functions with several force output modes were examined to create mathematical models that outline the properties of damping and stiffness. In [143], a semi-active HPS was investigated with four discrete spring characteristics and continuously variable damping controlled by two proportional solenoid valves capable of variable restricting flow to two accumulators. In [144], a study was carried out on the impedance of the active suspension with a transverse slope drive unit. The active HPS impedance model was created under slope conditions. The suspension system was tested using the first-order trajectory sensitivity method. In [145], a new suspension strut is designed to ensure a consistent bounce frequency regardless of the varying loads carried by the vehicle. To ensure a consistent resonance frequency, a non-linear spring stiffness was employed. The force-displacement relationships of this spring were determined using finite element analysis. In [146], an analytical model of the compact HPS strut is introduced, which includes the polytropic gas process, the nonlinear and hysteretic friction force, and turbulent flows through the damping orifices. In [147], the HPS wheel loader was developed using RecurDyn software in co-simulation with MATLAB/Simulink. RecurDyn is an interdisciplinary Computer-Aided Engineering (CAE) software package used to simulate the Multibody Dynamics (MBD) of suspension systems.

4.3. Models and Characteristics of HPA

When selecting an HPA in an HPS system, manufacturer catalogs and online tools such as Hydac ASPlight are useful, as they are used for optimal calculations of accumulators, such as usable volume, pressure ratio, maximum and minimum operating pressure, taking into account the behavior of real gases [148]. HPA calculation models must consider the following factors: type of construction gas, filling, installation, pressure gradient, volume and temperature changes, energy density, and heat exchange. The size of the HPA depends on many different parameters; therefore, computational methods based on thermodynamic principles should be used. According to the ideal gas law, pressure, volume, and temperature are important factors when selecting and sizing the HPA. HPA computational models found in the literature typically use isothermal or adiabatic gas compression and expansion processes [149]. The correct approach to calculating and selecting HPA should consider thermodynamic cycles that take into account the heat exchange of the gas with the ambient environment [150]. Various thermodynamic pressure-volume cycles (PV) based on the isothermal, adiabatic, isochoric, and isobaric processes

of an ideal gas can be considered during the determination and selection of HPA. In HPA, there is always some heat exchange with the ambient, which causes the thermodynamic compression and expansion of a diatomic gas (nitrogen) to proceed according to a polytropic process with exponent n, that is, between an isothermal process with exponent $n = 1$ and adiabatic processes with exponent $n = \kappa$, $1 \leq n \leq \kappa = 1.4$. The polytropic exponent is determined experimentally; therefore, in theoretical considerations, equations of adiabatic processes are generally used [151].

4.3.1. Thermodynamic Cycles of HPA

Thermodynamic PV cycles should be taken into account when selecting the HPA for the HPS system intended for a given vehicle. This is a task for vehicle designers, and auto repair shops should only list the original HPS struts. For the HPS system, a HPA thermodynamic PV cycle was considered, as shown in Figure 24.

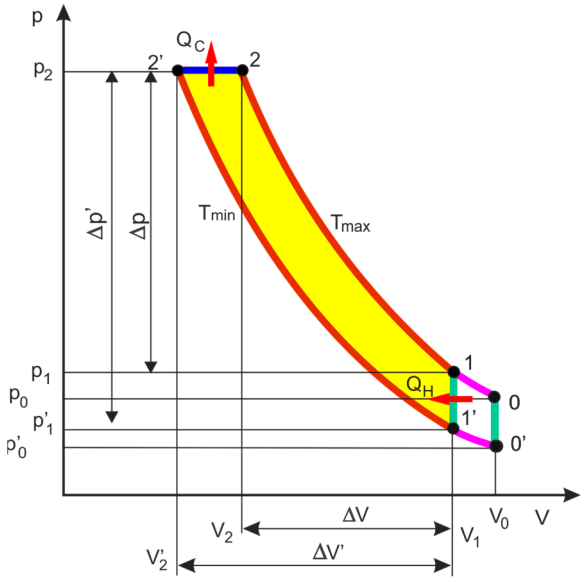

Figure 24. Thermodynamic PV cycle of HPA.

The thermodynamic processes of the ideal gas in the PV cycle of the HPA, shown in Figure 24, consist of isothermal compression under pre-charge $0 \rightarrow 1$, adiabatic compression $1 \rightarrow 2$, isobaric cooling $2 \rightarrow 2'$, adiabatic expansion $2' \rightarrow 1'$, isochoric heating $1' \rightarrow 1$, isothermal expansion to pre-charge state $1' \rightarrow 0'$, and isochoric heating under pre-charge state $0' \rightarrow 0$.

The thermodynamic processes that are highlighted in the PV cycle of HPA are determined by the equations below.

Isothermal compression under the pre-charge process $0 \rightarrow 1$, when the maximum ambient temperature $T_{a\max}$ is constant,

$$p_0 \, V_0 = p_1 \, V_1 \tag{46}$$

where V_0 and V_1 are the volumes of gas under pressures p_0 and p_1, respectively.

Isothermal expansion under the pre-charge process $1' \rightarrow 0'$, when the minimum ambient temperature $T_{a\min}$ is constant,

$$p'_1 \, V'_1 = p'_0 \, V'_0 \tag{47}$$

where V'_1 is the volume under pressure p'_1, V'_0 is the volume under pressure p'_0.

Adiabatic compression in process $1 \rightarrow 2$, with no heat exchange $Q = 0$,

$$p_1 \, V_1^{\kappa} = p_2 \, V_2^{\kappa} \tag{48}$$

where p_2 is the maximum operating pressure, V_2 is the gas volume under pressure p_2.

Adiabatic expansion in process $2' \rightarrow 1'$, with no heat exchange $Q = 0$,

$$p'_2 \, V'^{\kappa}_2 = p'_1 \, V'^{\kappa}_1 \tag{49}$$

where V'_1 is the volume of the gas under pressure p'_1, V'_2 is the volume of the gas under pressure p'_2.

Isochoric heating under the pre-charge process $0' \rightarrow 0$, when the volume V_1 is constant,

$$\frac{p'_0}{T'_0} = \frac{p_0}{T_0} \;\Rightarrow\; \frac{p'_0}{T_{a\min}} = \frac{p_0}{T_{a\max}} \tag{50}$$

where T_0 is the temperature under pressure p_0, equal to the temperature $T_{a\max}$, and T'_0 is the temperature under pressure p'_0, equal to the temperature $T_{a\min}$.

The heat of the isochoric heating process $0' \rightarrow 0$,

$$Q_H = \; c_{\mathrm{v}} \, m \, \left(T_0 - T'_0\right) = \frac{1}{\kappa - 1} V_1 \left(p_0 - p'_0\right) \tag{51}$$

Isochoric heating in process $1' \rightarrow 1$, when the volume V_1 is constant,

$$\frac{p'_1}{T'_1} = \frac{p_1}{T_1} \Rightarrow \; \frac{p'_1}{T_{a\min}} = \frac{p_1}{T_{a\max}} \tag{52}$$

where T_1 is the temperature under pressure p_1, equal to the temperature $T_{a\max}$, T'_1 is the temperature under pressure p'_1, equal to the temperature $T_{a\min}$.

The heat of the isochoric heating process $1' \rightarrow 1$,

$$Q_H = \; c_{\mathrm{v}} \, m \, \left(T_1 - T'_1\right) = \frac{1}{\kappa - 1} V_1 \left(p_1 - p'_1\right) \tag{53}$$

where c_{v} is the specific heat at constant volume, and m is the mass of the gas.

Isobaric cooling in process $2 \rightarrow 2'$, when the pressure p_2 is constant,

$$\frac{V'_2}{T'_2} = \frac{V_2}{T_2} \tag{54}$$

where V_2, V'_2 are the volumes of gas under pressure p_2 and at temperatures T_2, T'_2.

The heat of the isobaric cooling process $2 \rightarrow 2'$,

$$Q_C = m \, c_p \, \left(T_2 - T'_2\right) = \frac{\kappa}{\kappa - 1} p_2 \, \left(V_2 - V'_2\right) \tag{55}$$

where c_p is the specific heat at constant pressure.

4.3.2. HPA Selection Criteria

The HPA selection criteria for an HPS system based on the thermodynamic PC cycle should consider the fulfillment of the required useful volume ΔV_r, the required pressure drops Δp_r, and the required work W_r.

Determination of required useful volume ΔV_r.

The required useful volume ΔV_r in the HPS should be less than or equal to the useful volume ΔV in the HPA,

$$\Delta V_r \leq \Delta V = V_1 - V_2 \tag{56}$$

The useful volume of HPA is due to the adiabatic compression of the gas after taking into account the isothermal compression under pre-charge,

$$\Delta V_r \leq \Delta V = V_0 \frac{p_0}{p_1}\left[1 - \left(\frac{p_1}{p_2}\right)^{1/\kappa}\right] \Rightarrow \frac{\Delta V_r}{V_0} \leq \frac{p_0}{p_1}\left[1 - \left(\frac{p_1}{p_2}\right)^{1/\kappa}\right] \tag{57}$$

When selecting diaphragm accumulators, it is important to introduce the pressure ratios recommended by the manufacturers. Generally, the pressure ratios for diaphragm accumulators are within the following limits [45,152]:

$$\frac{p_0}{p_1} \leq 0.9 \text{ and } \frac{p_0}{p_2} \geq 0.1 \text{ company} \tag{58}$$

By introducing in (57) the pressure ratios p_0/p_1 and p_0/p_2 and the isochoric heating equation, the condition of the required usable volume is as follows:

$$\frac{\Delta V_r}{V_0} \leq \frac{p_0}{p_1}\left[1 - \left(\frac{\frac{p_0}{p_2}}{\frac{p_0}{p_1}}\right)^{1/\kappa}\right] = \frac{p'_0}{p_1}\frac{T_{a\max}}{T_{a\min}}\left[1 - \left(\frac{\frac{p_0}{p_2}}{\frac{p_0}{p_1}}\right)^{1/\kappa}\right] \tag{59}$$

Determination of required pressure drop Δp_r.

The required pressure drop Δp_r in the HPS should be greater than or equal to the useful pressure drop Δp in the HPA,

$$\Delta p_r \geq \Delta p = p_2 - p'_1 \tag{60}$$

Introducing in (60) the pressure p'_1 of the isochoric heating process and the pressure p_0 results in the following relation

$$\Delta p_r \geq \Delta p = p_2 - \frac{p_1 T_{a\min}}{T_{a\max}} \Rightarrow \frac{\Delta p_r}{p_2} \geq 1 - \frac{\frac{T_{a\max}}{T_{a\min}}}{\frac{p_0}{p_1}}\frac{p_0}{p_2} \tag{61}$$

This condition will be satisfied for a given pressure drop Δp_r when the pressure ratio p_0/p_2 is greater than or equal to

$$\frac{p_0}{p_2} \geq \frac{\frac{p_0}{p_1}}{\frac{T_{a\max}}{T_{a\min}}}\left(1 - \frac{\Delta p_r}{p_2}\right) \tag{62}$$

Determination of the required work W_r.

The required work W_r in the HPS should be less than or equal to the useful compression work W_{12} specified for the HPA thermodynamic cycle,

$$W_r \leq W_{12} = \frac{p_1 V_1}{\kappa - 1}\left[1 - \left(\frac{p_1}{p_2}\right)^{\frac{1-\kappa}{\kappa}}\right] \tag{63}$$

Introducing in (63) the equations of the isothermal process and the isochoric heating, as well as the pressure p_2, results in the following relation.

$$\frac{W_r}{V_0\, p_2} \leq \frac{1}{\kappa - 1}\frac{p_0}{p_2}\left[1 - \left(\frac{\frac{p_0}{p_2}}{\frac{p_0}{p_1}}\right)^{\frac{1-\kappa}{\kappa}}\right] = \frac{1}{\kappa - 1}\frac{p'_0}{p_2}\frac{T_{a\max}}{T_{a\min}}\left[1 - \left(\frac{\frac{p_0}{p_2}}{\frac{p_0}{p_1}}\right)^{\frac{1-\kappa}{\kappa}}\right] \tag{64}$$

According to the ideal gas law, a change in gas temperature will result in a corresponding change in pressure and volume in the HPA. Temperature is an important consideration when sizing the HPA. When HPA is selected on the basis of catalogs, engineering calculations, and computer simulations, the thermodynamic processes of the ideal gas are assumed. For real gases, appropriate correction factors are introduced with respect to volume change [153].

4.3.3. Times Characteristics of HPA Thermodynamic Processes

When considering isochoric heating, the change in gas temperature is as follows [154],

$$\frac{T - T'_1}{T_1 - T'_1} = 1 - e^{-t/\tau} \tag{65}$$

where τ is the thermal time constant of HPA.

For an ideal gas process, T/p = constant, the pressure changes with time during the heating process $1' \rightarrow 1$ is defined as follows:

$$\frac{p_H - p'_1}{p_1 - p'_1} = 1 - e^{-t/\tau} \Rightarrow \; p_H(t) = p'_1 + \left(p_1 - p'_1\right)\left(1 - e^{-t/\tau}\right) \tag{66}$$

When considering isobaric cooling, the gas temperature change is as follows:

$$\frac{T - T'_2}{T_2 - T'_2} = e^{-t/\tau} \tag{67}$$

For an ideal gas process V/T = constant, the volume changes with time during the cooling process $2 \rightarrow 2'$ is defined as follows:

$$\frac{V_C - V_{2'}}{V_2 - V_{2'}} = e^{-t/\tau} \Rightarrow \; V_C(t) = V'_2 + \left(V_2 - V'_2\right) e^{-t/\tau} \tag{68}$$

Based on the type of membrane HPA tests performed in [155] and the computing parameters, the thermal time constant τ = 6 s at the initial volume of V_0 = 0.001 m^3 and the initial pressure of p_0 = 5 MPa was selected. In the calculation example, the following pressure was adopted: p_1 = 5 MPa, p_1'= 0.9 p_1, V_2 = 10 MPa, V_2' = 0.8 p_2. According to the membrane deformation criteria in HPA with a pre-charge pressure p_0 and volume V_0, the volume change range is 0.1 $V_0 \leq V_2 \leq$ 0.9 V_0. The diaphragm should be in the middle position of the HPS so that the hydraulic cylinder piston is also in the center position. This ensures the maximum possible margins for membrane deformation on both sides. The middle position of the diaphragm means V_2 = 0.5 V_0. Figure 25 shows the HPA time characteristics.

4.4. HPA Simulation Modeling

Various HPA model blocks are used in hydraulic system simulations. Hydraulic libraries with HPA blocks are available in fluid simulation software, such as Matlab/Simulink and Simscape Toolbox. HPA simulation blocks include ideal or real gas, constant and variable oil compressibility, isothermal, and adiabatic processes. The HPA dynamic models are not well defined in most of the literature. Figure 26 shows the graphics of the HPA simulation blocks.

When in the HPA, there is compression and expansion of gas, the flow rate balance for the HPA joint is considered,

$$q_a = \sum_{i=1}^{n} q_{\mathrm{v}i} \tag{69}$$

where q_a is the flow rate of the fluid in the HPA, and $q_{\mathrm{v}i}$ is the flow rate of the fluid in the HPA joint.

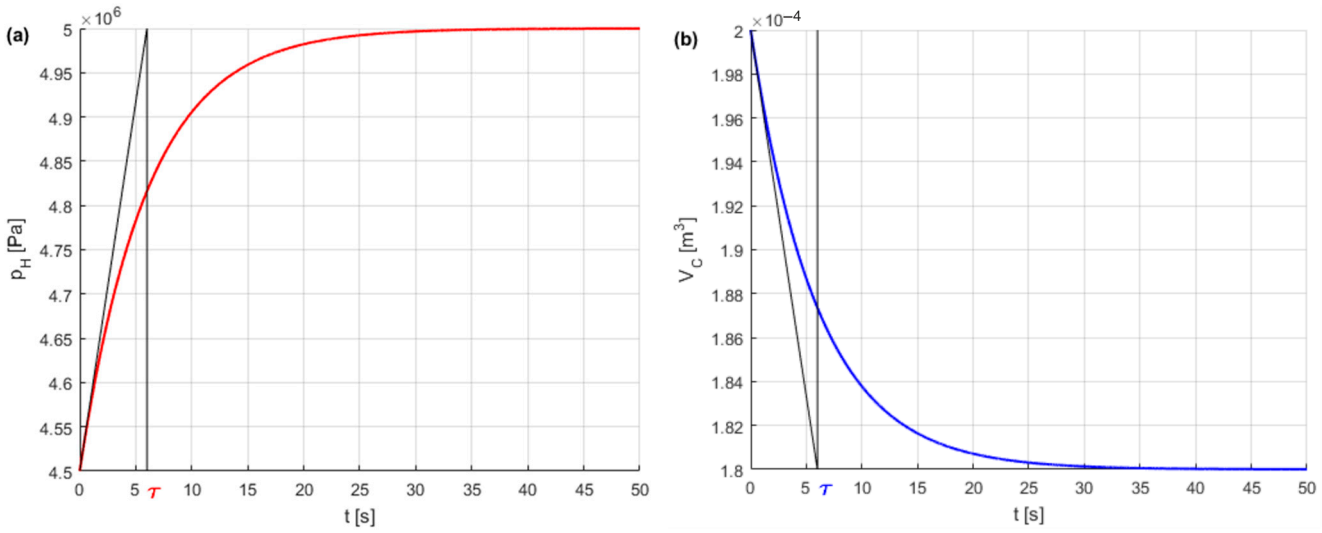

Figure 25. HPA time characteristics: (**a**) pressure time curve during isochoric heating; (**b**) volume time curve during isobaric cooling.

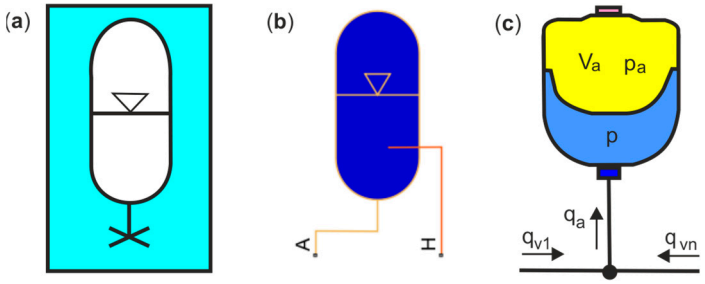

Figure 26. HPA simulation block model: (**a**) general simulation block, (**b**) Simscape simulation block, (**c**) calculation block.

In the HPA simulation block, the compression pressure and volume are calculated on the basis of the adiabatic process of the ideal gas,

$$p_a\, V_a^{\kappa} = p_0\, V_0^{\kappa} \Rightarrow\ p_a = \left(\frac{V_0}{V_a}\right)^{\kappa} p_0 \tag{70}$$

where p_a and V_a are the instantaneous pressure and volume, p_0 is the gas pressure, V_0 is the volume of the gas chamber in the pre-charge state, and κ is the adiabatic exponent of nitrogen.

After differentiation, the dp_a/dV_a of (70) is obtained,

$$\frac{dp_a}{dV_a} = -\kappa\, \frac{p_0\, V_0^{\kappa}}{V_a^{\kappa+1}} = -\,\kappa\, \frac{p_a\, V_a^{\kappa}}{V_a^{\kappa+1}} = -\frac{\kappa\, p_a}{V_a} \tag{71}$$

After differentiation (71) in time, the pressure impulse in HPA is as follows:

$$\frac{p_a}{dt} = -\frac{\kappa\, p_a}{V_a}\, \frac{dV_a}{dt} = -\frac{\kappa\, p_a}{V_a}\, q_a \Rightarrow\ q_a = -\frac{V_a}{\kappa\, p_a}\, \frac{p_g}{dt} = -\,C\, \frac{p_a}{dt} \tag{72}$$

where C is the HPA capacitance, which is defined as the change in volume with pressure under constant entropy

$$C = -\frac{dV_a}{dp_a} = -\frac{V_a}{\kappa\, p_a} \tag{73}$$

C is simplified for the pre-charging state in the adiabatic process of an ideal gas

$$C \approx \frac{V_0}{\kappa\, p_0} \tag{74}$$

4.4.1. HPA–DT Dynamic Model

Figure 27 shows a functional diagram of an HPS strut in which the HPA–DT serial connection is distinguished.

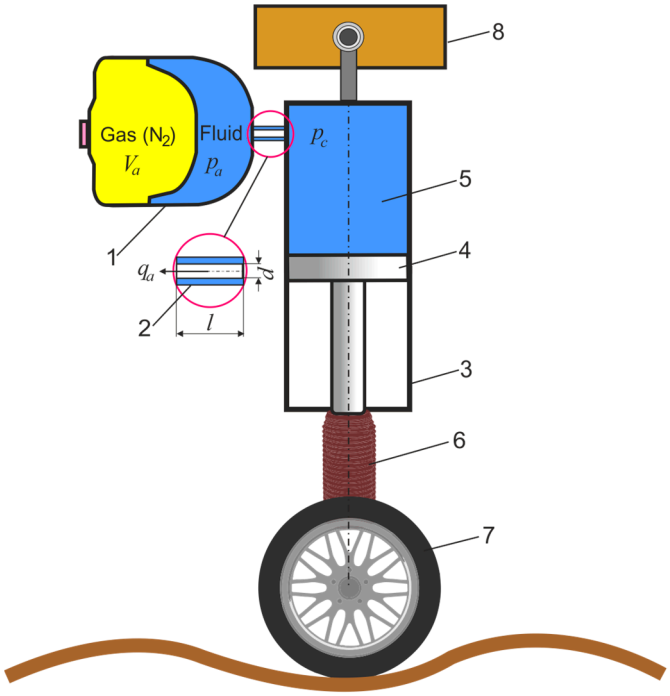

Figure 27. Functional diagram of the HPS strut with HPA–DT connection: 1—HPA, 2—DT, 3—hydraulic cylinder, 4—piston of cylinder, 5—chamber of cylinder, 6—dust protector, 7—wheel, 8—vehicle body.

The DT is connected to a chamber of the hydraulic cylinder. The piston rod of the cylinder is connected to the suspension arm of the wheel, and the barrel of the cylinder is connected to the body of the vehicle.

The dynamic modeling of HPA–DT is critical to the simulation and control of the HPS strut and must also meet key performance indicators (KPIs) of the suspension systems. KPIs are used to gain an understanding of how an HPS system will perform under various driving conditions, including cornering, braking, and steering.

HPA–DT can be modeled by RLC lumped elements based on the analogy between hydraulic and electrical circuits [156], where R is the hydraulic resistance, L is the hydraulic inductance, C is the hydraulic conductance,

$$L\,\frac{dq_a}{dt} + R\,q_a = p_c - p_a \tag{75}$$

$$q_a = C\,\frac{dp_a}{dt} \Rightarrow \quad \frac{dp_a}{dt} = \frac{1}{C} q_a \tag{76}$$

where p_c is the pressure in the hydraulic cylinder chamber.

In the case of a DT in the form of a resistor throttle with laminar flow, the pressure drop is proportional to the volumetric flow rate, depending on the density and viscosity of the hydraulic fluid, as well as the Reynolds number and dimensions. In hydraulic

fluids, the viscosity strongly depends on the temperature, which has a significant impact on the damping effect of a throttle. At higher temperatures, the viscosity is lower, which unfavorably affects the damping of the resistor throttle. The viscosity of the fluid increases as the pressure increases, which is favorable for viscous damping. This characteristic must be taken into account when pressures exceed 200 bar.

The resistance R of the DT for laminar flow is determined from the Hagen–Poiseuille equation,

$$R = \frac{128\ l\ \nu\ \rho}{\pi\ d^4} \tag{77}$$

where d, l are the diameter and length of the DT, ρ is the oil density, and ν is the kinematic viscosity of the hydraulic oil.

Specification of the RAVENOL E- PSF fluid, which is specially developed for use in the hydropneumatic Hydractive III and Hydractive III+ suspension of Citroën, density 821 kg/m^3 at 20 °C according to EN ISO 12185 [157], and kinematic viscosity 19 mm^2/s (19 10^{-6} m^2/s) at 40 °C according to DIN 53000-1 [158].

The hydraulic inductance of DT is as follows.

$$L = \frac{\rho\ l}{A} = \frac{4\ \rho\ l}{\pi\ d^2} \tag{78}$$

where A is the cross-section area of the DT, $A = \pi\ d^2/4$.

The HPA–DT simulation model with a hydraulic cylinder as a pressure source p_c,

$$\begin{cases} \dot{V}_a = q_a \\ \dot{q}_a = \frac{1}{L}(-\ R\ \ q_a - p_a + p_c) \\ \dot{p}_a = \frac{1}{C}\ \ q_a \end{cases} \tag{79}$$

Based on the dynamic HPA–DT model of the HPS strut, the responses of the dynamic parameters of the HPA to the input pressure signal generated by the displacement of the cylinder piston and the vehicle wheel were simulated.

Figure 28 shows the input pressure signal and the dynamic response of the HPA pressure. Figure 29 shows the dynamic response of the HPA volume and the flow rate.

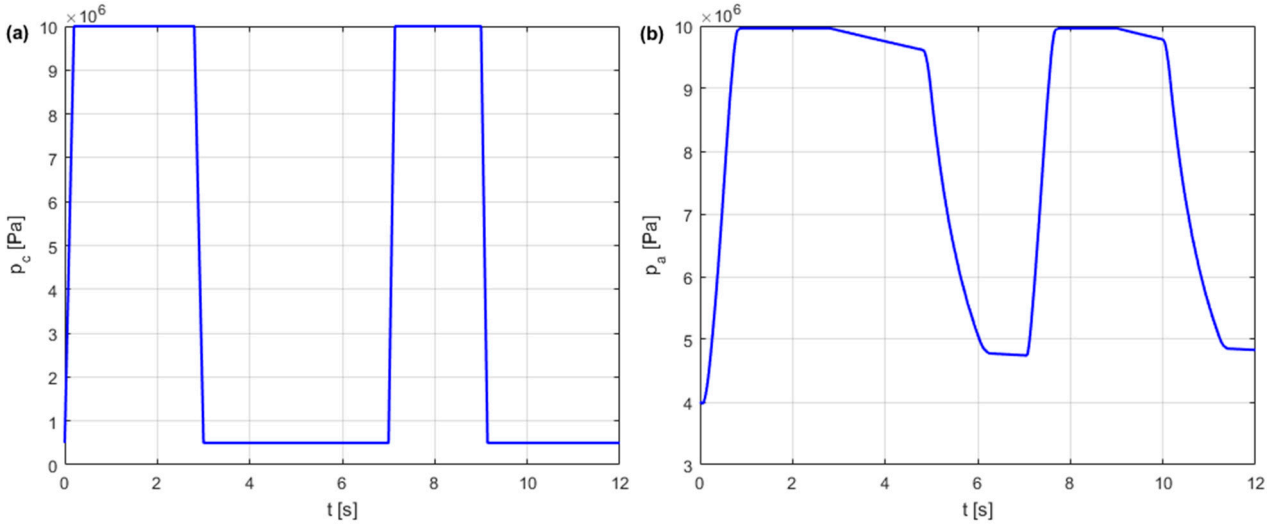

Figure 28. Simulation input pressure signal (**a**) and dynamic response of the HPA pressure (**b**).

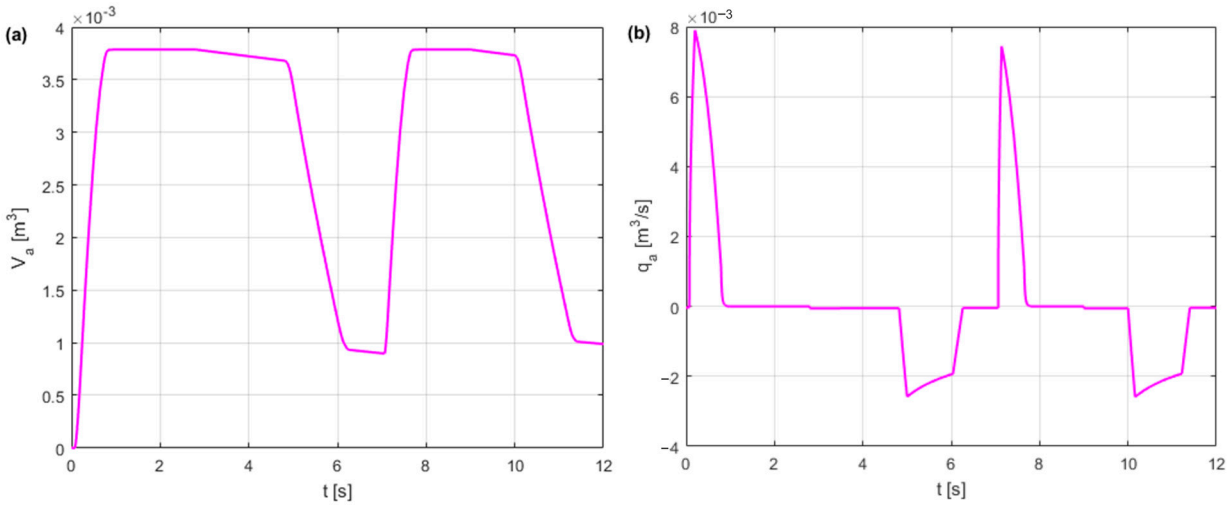

Figure 29. Simulated dynamic responses of HPA parameters: volume (**a**) and flow rate (**b**).

4.4.2. HPA–DT Impedance Modeling

To determine the dimensionless frequency characteristics of HPA-DT, such as amplitude and phase curves, as well as damping efficiency index curves, impedance modeling was used.

HPA–DT frequency analysis was performed using hydraulic impedance modeling, which is analogous to electrical impedance modeling. For this purpose, a dynamic RLC model was used, from which, after differentiation (75) and insertion (76), a second-order differential equation was obtained in the following form,

$$C\,L\,\frac{d^2q_a}{dt^2} + C\,R\,\frac{dq_a}{dt} + q_a = C\,\frac{dp_c}{dt} \tag{80}$$

From (80), the transfer function $G(s)$ of HPA–DT is obtained in the domain of the Laplace operator s,

$$G(s) = \frac{q_a(s)}{p_c(s)} = \frac{C\,s}{C\,L\,s^2 + C\,R\,s + 1} = \frac{C\,s}{\frac{1}{\omega_n^2}\,s^2 + \frac{2\,\zeta}{\omega_n}\,s + 1} \tag{81}$$

where ω_n is the natural frequency,

$$\omega_n = \frac{1}{\sqrt{C\,L}}, \tag{82}$$

where ζ is the damping ratio,

$$\zeta = \frac{1}{2}\,C\,R\,\omega_n. \tag{83}$$

The transfer function $G(s)$ of HPA–DT is transformed into the frequency domain by replacing the operator $s = j\omega$; therefore, the Laplace transform is replaced by the Fourier transform as follows:

$$G(j\omega) = \frac{q_a(j\omega)}{p_c(j\omega)} = \frac{j\,C\,\omega}{1 - \frac{\omega^2}{{\omega_n}^2} + j2\,\zeta\frac{\omega}{\omega_n}} \tag{84}$$

By substituting $s = j\omega$, the analysis of the steady-state system focuses on the frequency response, which simplifies the mathematical operations involved in the frequency response analysis, such as the calculation of transfer functions, frequency response functions, and

their graphical representations. This reduces computational complexity and makes analysis more straightforward, particularly for vibration systems.

Equation (83) is transformed into the following form,

$$G(j\omega) = \frac{q_a(j\omega)}{p_c(j\omega)} = \frac{1}{\alpha\left[\beta + j\left(\frac{\omega}{\omega_n} - \frac{\omega_n}{\omega}\right)\right]} \tag{85}$$

where α and β are the constant coefficients,

$$\alpha = \frac{1}{C\,\omega_n}, \tag{86}$$

$$\beta = 2\,\zeta. \tag{87}$$

Fluid flow in the HPA–DT can be modeled in the frequency domain using the impedance $Z(j\omega)$, which is determined by the ratio of pressure $p_c(j\omega)$ to flow rate $q_a(j\omega)$, j similar to the electrical impedance in an AC circuit,

$$Z(j\omega) = \frac{1}{G(j\omega)} = \frac{p_c(j\omega)}{q_a(j\omega)} = \alpha\,\beta + \alpha\,j\left(\frac{\omega}{\omega_n} - \frac{\omega_n}{\omega}\right) \tag{88}$$

The impedance $Z(j\omega)$ takes into account the hydraulic resistance R and the hydraulic reactance X, added in the complex,

$$Z(j\omega) = \alpha\,\beta + j\left(\alpha\frac{\omega}{\omega_n} - \alpha\frac{\omega_n}{\omega}\right) = R + jX = R + j(X_L - X_C) \tag{89}$$

where R is the resistance,

$$R = \alpha\,\beta \tag{90}$$

X_L is the inductive reactance, after considering (86) and (87) is as follows:

$$X_L = \alpha\frac{\omega}{\omega_n} = L\,\omega \tag{91}$$

X_C is the capacitive reactance after considering (86) is as follows:

$$X_C = \alpha\frac{\omega_n}{\omega} = \frac{1}{C\,\omega} \tag{92}$$

From (88), the modulus (amplitude) and argument (phase) of the impedance of $Z(j\omega)$ of the HPA–DT were determined

$$|Z(j\omega)| = \alpha\sqrt{\beta^2 + \left(\frac{\omega_n}{\omega} - \frac{\omega}{\omega_n}\right)^2}; \tag{93}$$

$$\arg[Z(j\omega)] = \arctan\frac{\left(\frac{\omega_n}{\omega} - \frac{\omega}{\omega_n}\right)}{\beta}. \tag{94}$$

The impedance modulus curves are presented in dimensionless form

$$|Z_d(j\omega)| = \frac{|Z(j\omega)|}{\alpha} = \sqrt{\beta^2 + \left(\frac{\omega_n}{\omega} - \frac{\omega}{\omega_n}\right)^2}. \tag{95}$$

Based on (93) and (94), the impedance curves versus the frequency of the HPA–DT system are determined, the dimensionless amplitude curve and a phase curve for the HPA param-

eters p_1 = 7 MPa and V_1 = 0.001 m^3 (1 L), and the DT parameters l = 0.05 m and d = 0.008 m, shown in Figure 30.

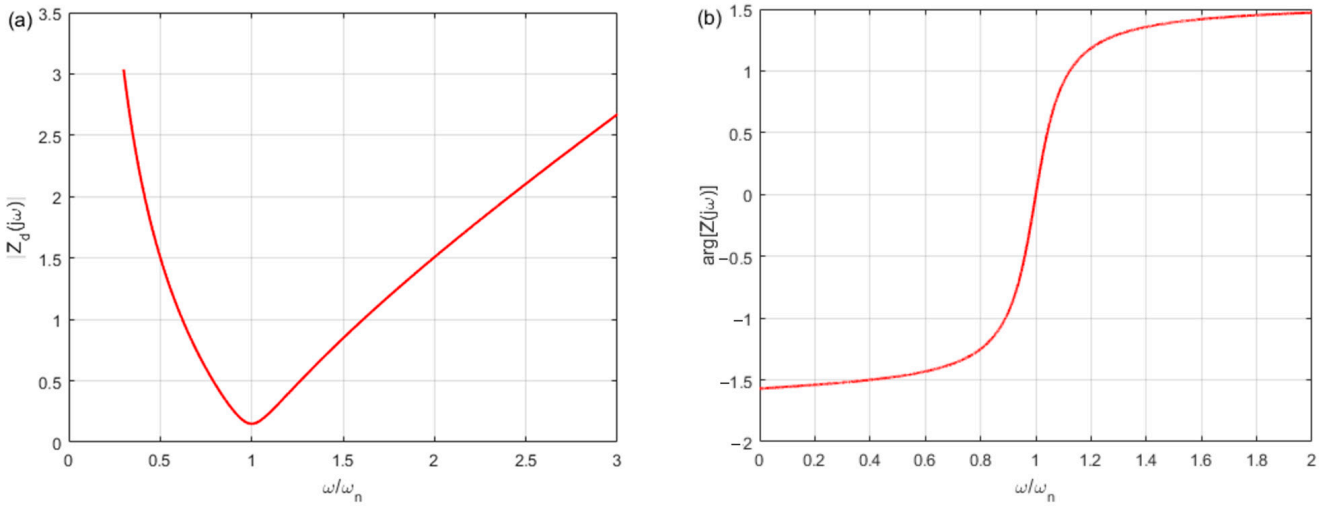

Figure 30. Impedance resonance versus frequency curves of the HPA–DT system: (**a**) dimensionless impedance amplitude curve; (**b**) impedance phase curve.

The curve of impedance versus frequency shows that the value of the impedance amplitude is the lowest at the impedance resonance. In resonance, when $\omega = \omega_n$, the impedance $Z(j\omega)$ is equal to the resistance R, the reactance $X = 0$, and then the phase angle φ is equal to zero. The capacitive reactance of X_C is dominant at low frequencies ($X_C > X_L$), whereas the inductive reactance of X_L is dominant at high frequencies ($X_L > X_C$). The HPA–DT system is recommended for use in the dominant capacitive reactance range. Resonance impedance must be avoided, during which an uncontrolled increase in pressure may occur in the upper chamber of the hydraulic cylinder.

When HPA and DT are selected, the influence of their parameters on the impedance curves of the HPA–DT system is important. Figure 31 shows the influence of HPA parameters, volume V_{a0} and pressure p_{a0}, on the impedance curves of the HPA–DT system. Figure 32 shows the influence of the DT parameters, diameter d and length l, on the impedance curves of the HPA–DT system.

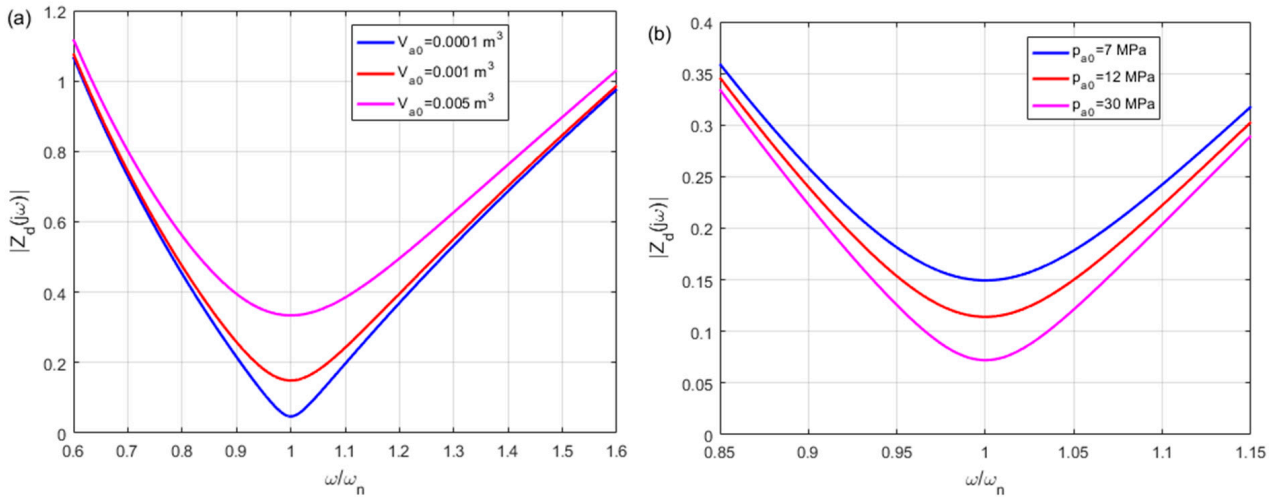

Figure 31. HPA–DT impedance curves for various dimensions of the HPA: (**a**) various initial volumes V_{a0} at pressure p_{a0} = 7 MPa, (**b**) various initial pressures p_{a0} at volume V_{a0} = 0.001 m.

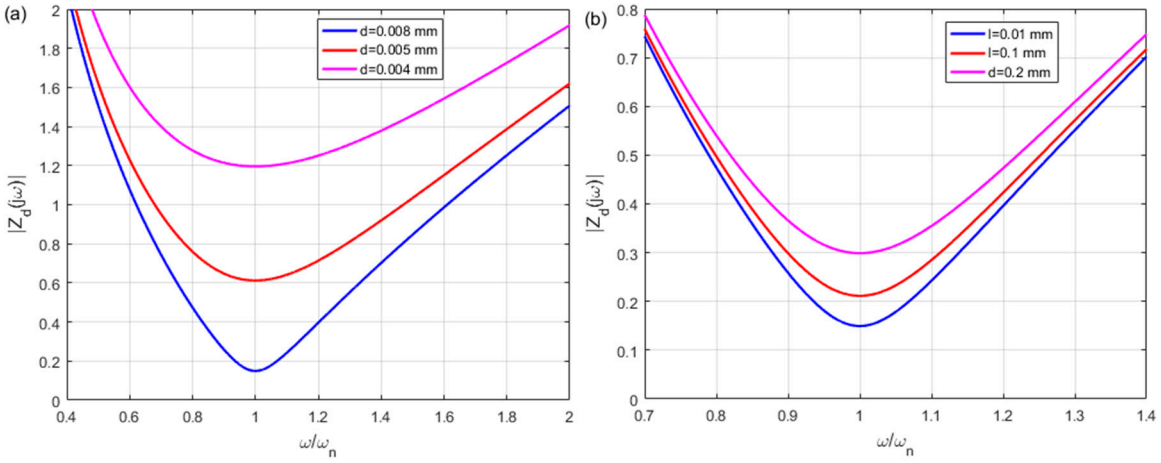

Figure 32. HPA–DT impedance curves for various dimensions of the DT: (**a**) various diameters d at length l = 0.05 m, (**b**) various lengths l at diameter d = 0.005 m.

4.4.3. DPI of the HPA–DT

Wheel vibrations are unavoidable and come from different sources, such as tire-road interaction, engine, wind, or potholes. Vibration can cause minor inconveniences, but it can also cause serious problems, such as unsafe driving conditions. Vibrations can cause premature damage to parts of the vehicle due to fatigue and abrasion, contribute to excessive noise, and adversely affect people and sensitive devices. To assess the effectiveness of pressure shock suppression in the HPS, a DPI in the form $D(j\omega)$ was used, which considers the relationship between the downstream pressure p_a and the upstream pressure p_c of the DT. When considering the flow resistance R of the DT and the impedance $Z(j\omega)$ of the HPA–DT, the following relationship is used,

$$q_a(j\omega) = \frac{p_c(j\omega)}{Z(j\omega)} = \frac{\Delta p(j\omega)}{R(j\omega)} = \frac{p_a(j\omega) - p_c(j\omega)}{R(j\omega)} \tag{96}$$

The pressure transfer function $H_a(j\omega)$ of the HPA–DT model result from (96) is as follows:

$$H(j\omega) = \frac{p_a(j\omega)}{p_c(j\omega)} = 1 + \frac{R(j\omega)}{Z(j\omega)} = 1 + \frac{R(j\omega)}{\alpha\ \beta + \alpha j\left(\frac{\omega_n}{\omega} - \frac{\omega}{\omega_n}\right)} \tag{97}$$

From (97), the module of the transfer function $H(j\omega)$ is determined,

$$|H(j\omega)| = \sqrt{1 + \frac{R^2 + 2\ R\ \alpha\ \beta}{(\alpha\ \beta)^2 + \alpha^2\left(\frac{\omega_n}{\omega} - \frac{\omega}{\omega_n}\right)^2}} \tag{98}$$

HPS–DT was evaluated using the following $D(j\omega)$ [159],

$$D(j\omega) = 20\ \log|H(j\omega)|\quad dB \tag{99}$$

Figure 33 shows the curves of the $D(j\omega)$ of the HPA–DT for various diameters d and the length l of the DT.

The curves show that the $D(j\omega)$ is highest when the natural frequency HPA–DT coincides with the excitation frequency, which is reduced. As expected, the index D increases with a decrease in diameter d and an increase in length l of the DT. The results of the $D(j\omega)$ may constitute the basis for a selection of HPS systems for driving conditions.

Hydraulic systems are widely discussed as sources and receivers of vibrations with a wide frequency spectrum in the book [160]. The influence of mechanical vibrations on the pressure pulsation range in hydraulic systems was studied.

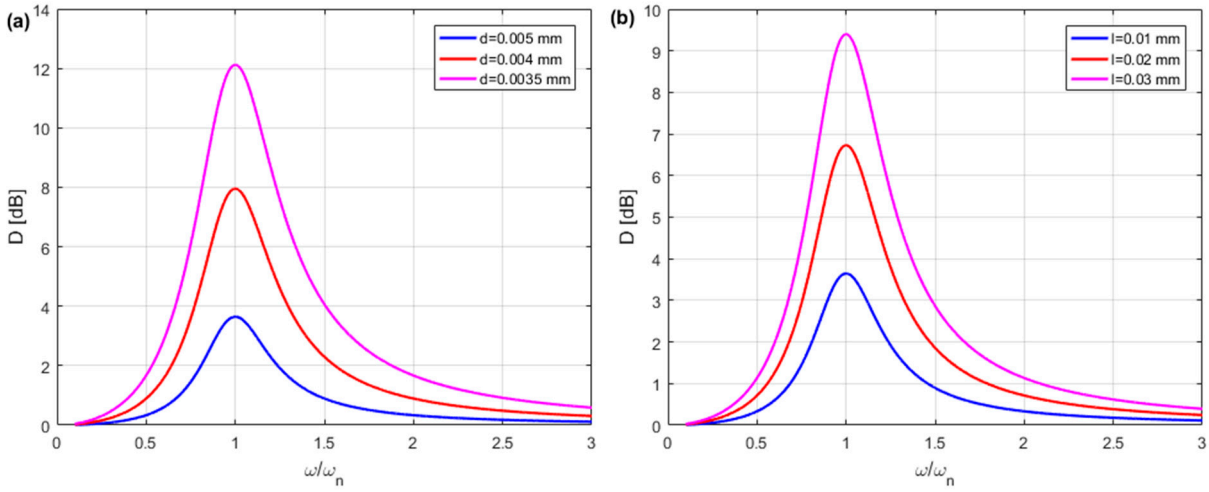

Figure 33. Curves of the $D(j\omega)$ of HPA–DT: (**a**) various diameters d at length l = 0.01 m; (**b**) various lengths l at diameter d = 0.005 m.

4.5. Trends and Challenges in HPS Systems

The main trends and challenges in the development of HPS systems are the following.

HPS systems increase and improve the efficiency of energy recovery and harvesting. In [161], a new hydropneumatic suspension system with an embedded piezoelectric power harvester was proposed, which allows self-powered monitoring and diagnosis of a vehicle or its subsystems. In [162], the simulation of a hydropneumatic regenerative suspension system (HPRSS) using AMEsim software was discussed. The results show that HPRSS performs better than conventional HPS in reducing vibration and increasing the energy harvested. Additionally, the impact of utilizing various standard HPA sizes, road profiles, and external load resistances was examined. It was emphasized that the size of the HPA had a significant effect on the damping force of the energy suspension system and the energy harvesting from road vibrations. In [163], the review discussed HPS systems of vehicles with energy recovery. The energy recovery system converts vibrational energy into electrical energy to supply energy to vehicle equipment. In [164], a force generator was added to form an active regenerative suspension system of HPS, which improved its vibration-causing characteristics. Regenerative HPS can only be effective when vibration reduction performance and energy harvesting efficiency are combined.

Implementation of smart HPS systems that utilize sensors, connectivity, and advanced control algorithms to improve their accuracy, efficiency, and energy performance. Smart HPS systems are monitored in real-time, and suspension data analysis allows energy optimization, contributing to a more sustainable and cost-effective operation, which reduces maintenance costs and downtime.

Integrating the HPS system with electrohydraulic control using servo valves and proportional valves combines the advantages of hydraulic power with the accuracy and control provided by electronic systems.

The growing adoption of lightweight materials, such as high-strength alloys and composites, supports conventional materials in the production of hydraulic components used in HPS systems. This trend not only aids in reducing weight but also improves the overall performance of the HPS system, making it better suited to contemporary engineering design challenges.

The emphasis on compliance of HPS systems with environmental regulations results in the use of biodegradable hydraulic fluids and the design of hydraulic components with low environmental impact and low ecological footprint.

Customized HPS solutions enhance vehicle efficiency, reliability, and safety and are tailored to meet the specific requirements of various vehicles.

5. Discussion of Impedance Modeling of HPS Strut with a PFD

Vehicles traveling on uneven roads with unpaved surfaces experience strong vibrations and poor stability. In such cases, the aim is to improve the functional properties of the HPS strut at the component level, which also brings economic benefits. New innovative solutions for the HPS system with a PFD were proposed to improve its damping performance in different road conditions, especially on terrain or off-road. The PFD is placed between the piston and the HPA in the hydraulic cylinder. Therefore, the PFD separates the cylinder chamber into two parts: the upper and lower parts. There is a flow resistor in the center of the PFD, which can be in the form of an orifice with turbulent flow or a throttle with laminar flow.

For the purposes of impedance modeling of the HPS strut, the functional diagram with PFD was adopted, in which a fixed-shaped resistor orifice is placed. Figure 34 shows the functional diagram of the HPS strut with PFD.

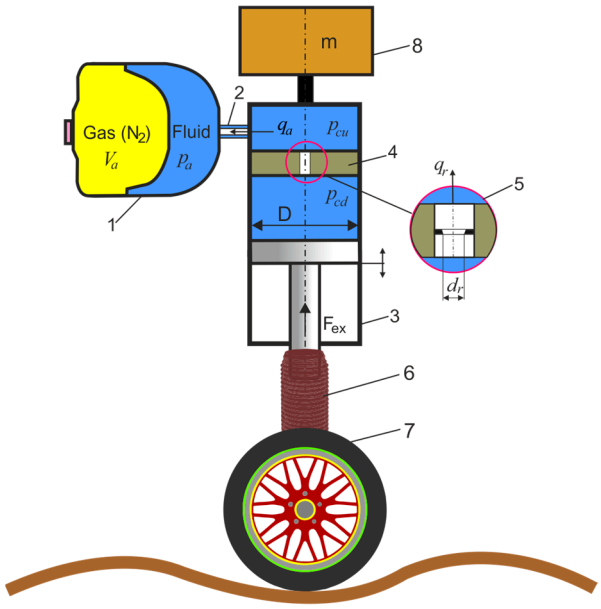

Figure 34. Functional model diagram of HPS strut with PFD: 1—HPA, 2—DT, 3—hydraulic cylinder, 4—PFD, 5—fixed shape of resistor orifice, 6—dust protector, 7—wheel, 8—vehicle body.

For an HPS system with HFD, the flow continuity equation and flow rate through the resistor orifice were formulated,

$$\begin{cases} q_a = q_r \\ q_r = \frac{1}{Z_r}\,\Delta p = \frac{1}{Z_r}\,(p_{cd} - p_{cu}) \end{cases} \tag{100}$$

where q_r is the flow rate through the flow resistor, Δp is the pressure drop in the flow resistor, p_{cd} is the pressure in the upper chamber of the cylinder, p_{cu} is the pressure in the lower chamber of the cylinder, Z_r is the hydraulic impedance of the flow resistor.

The pressure p_{cd} in the down chamber of the cylinder is the result of the sprung mass, the excitation force and the friction force,

$$p_{cd} = \frac{4\,(F_{ex} + F_t + m\,g)}{\pi\,D_c^2} \tag{101}$$

where m is the sprung mass of the vehicle body, g is the acceleration of gravity, F_t is the friction force, D_c is the diameter of the cylinder bore (piston diameter, inside barrel diameter), and F_{ex} is the force exerted by the wheel. Refs. [165,166],

$$F_{ex} = m_u\,r_w\,\omega^2\,\sin(\theta + \varphi) \tag{102}$$

where m_u is the unbalanced mass, r_w is the radius of the wheel, ω is the angular speed of the wheel, θ is the position of the mass, and is the phase shift.

The flow resistors can be in the form of a resistor throttle or an orifice resistor. Flow resistors in a hydraulic circuit are elements analogous to electrical resistors in an electrical circuit. The flow resistor, as a result of the resistance of the fluid flow through the orifice or throttle located in the PFD, dampens pressure fluctuations during HPS operation. The turbulent fluid flow in the resistor orifice suddenly changes from a wide to a narrow area and from a narrow to a wide area. In the orifice, only a small area of the surface coincided with turbulent fluid flow in regions with high flow velocities. Strong flow turbulence in the orifice causes internal friction and loss of hydraulic power, resulting in energy dissipation and a damping effect. The orifice exhibits a quadratic relationship between pressure drop and flow rate. The flow rate through the resistor orifice is determined by the Bernoulli equation, which determines the relationship between the pressure drop and the flow rate of an incompressible fluid through an orifice,

$$q_r = C_d\,A_r\,\sqrt{\frac{2}{\rho}}\,\sqrt{\Delta p} \tag{103}$$

where C_d is the flow discharge coefficient determined by the geometry of the resistor orifice and the Reynolds number, A_r is the cross-sectional area of the resistor orifice,

$$A_r = \frac{\pi\,d_r^2}{4} \tag{104}$$

where d_r is the diameter of the resistor orifice.

The square root of the pressure drop used to model the flow rate through the resistor orifices causes computational problems in the frequency domain. For small values of the pressure drop, it is more appropriate to assume that the flow rate depends linearly on the pressure drop. The orifice model for the laminar condition has been used in the Simscape library of Simulink R2020 software by Mathworks. In [167], an empirical formula for C_d was proposed that provides a linear relation of the flow rate for small pressure differences in the orifice,

$$C_d = \frac{C_{dt}}{\sqrt{\mathrm{Re}_{cr}}}\,\sqrt{\mathrm{Re}} \tag{105}$$

where C_{dt} is the turbulent flow discharge coefficient of the orifice, C_{dt} = 0.61 [168]; Re_{cr} is the critical Reynolds number for laminar flow, the default value of 12, corresponds to a round orifice made of thin material with sharp edges; Re is the Reynolds number,

$$\mathrm{Re} = \frac{d_r\,v_r}{\nu} = \frac{d_r\,q_r}{A_r\,\nu} \tag{106}$$

where ν is the kinematic viscosity of the hydraulic fluid, v_r is the velocity in the resistor orifice.

Substituting (106) into (105) and then into (103) and squaring them, the linear flow rate versus pressure drop is determined as follows:

$$q_r = \frac{\pi\, d_r^3}{2\,\rho\,\nu}\,\frac{C_{dt}^2}{\mathrm{Re}_{cr}}\,\Delta p \;\Rightarrow\; \Delta p = \frac{2\,\rho\,\nu\,\mathrm{Re}_{cr}}{\pi\, d_r^3\, C_{dt}^2} = R_r\, q_r \tag{107}$$

where R_r is the resistance of the resistor orifice,

$$R_r = \frac{2\,\rho\,\nu\,\mathrm{Re}_{cr}}{\pi\, C_{dt}^2\, d_r^3} \tag{108}$$

The flow through the resistor orifice is observed to be characterized by the resistance R_r and the inductive reactance L_r, which result from the high flow speed. The impedance of the flow resistor has the following form,

$$Z_r(j\omega) = \frac{\Delta p(j\omega)}{q_r(j\omega)} = R_r + j\omega\, L_r \tag{109}$$

where ω is the angular frequency of the pulsatile flow.

The impedance of the flow resistor orifice (109) is closer to a simple resistance model in the following form,

$$Z_r(j\omega) \approx R_r \tag{110}$$

From the continuity of flow in the analyzed HPS system, and after taking into account (85) and (110) is obtained,

$$q_a = q_r \;\Rightarrow\; \frac{1}{Z(j\omega)}p_{cu} = \frac{1}{Z_r(j\omega)}\,(p_{cd} - p_{cu}) \tag{111}$$

The pressure transfer function $H(j\omega)$ of the HPS strut with PFD resulting from (111) is as follows:

$$H(j\omega) = \frac{p_{cd}}{p_{cu}} = 1 + \frac{Z_r(j\omega)}{Z(j\omega)} \tag{112}$$

Taking into account the impedances Z and $Z_{r,}$ the transfer function $H(j\omega)$ is as follows:

$$H(j\omega) = 1 + \frac{Z_r(j\omega)}{Z(j\omega)} = 1 + \frac{R_r}{\alpha\,\beta + \alpha j\left(\frac{\omega_n}{\omega} - \frac{\omega}{\omega_n}\right)} \tag{113}$$

Based on (112), the module of the $H(j\omega)$ transfer function was determined as follows:

$$|H(j\omega)| = \sqrt{1 + \frac{R_r^2 + 2\,R_r\,\alpha\,\beta}{(\alpha\,\beta)^2 + \alpha^2\left(\frac{\omega_n}{\omega} - \frac{\omega}{\omega_n}\right)^2}} \tag{114}$$

HPS strut with PFD was evaluated using the following $D(j\omega)$,

$$D(j\omega) = 20\,\log|H(j\omega)|\;dB \tag{115}$$

Figure 35 shows the curves of the $D(j\omega)$ of the HPS strut with PFD for various diameters d_r for the fixed resistor orifice.

The curves of the $D(j\omega)$ show the expected results that index D increases with a decrease in the diameter d_r of the fixed resistor orifice of the PFD. The results of the model tests of the $D(j\omega)$ of the HPS strut with PFD may constitute the basis for the possibility of using a semi-active HPS system by applying a resistor orifice of the PFD with variable cross-sectional area $A_r(d_r)$.

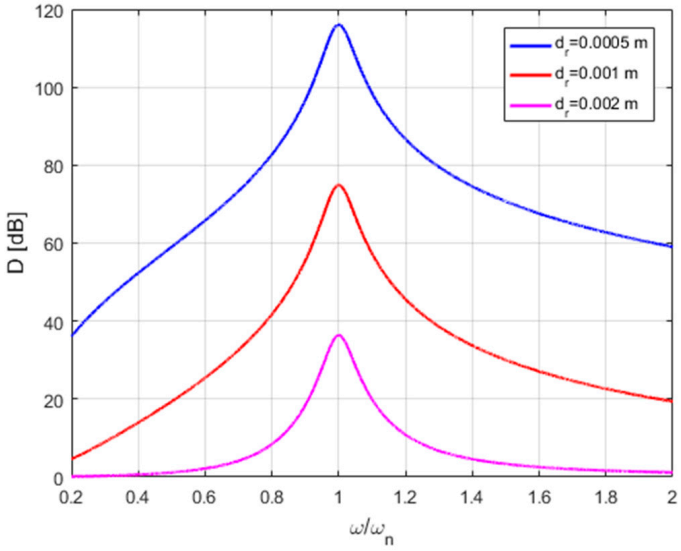

Figure 35. Curves of the $D(j\omega)$ of the HPS strut with PFD for various diameters d_r of the fixed resistor orifice.

Figure 36 shows a comparison of the curves of the $D(j\omega)$ of the HPS with and without the PFD. Impedance modeling confirmed that the use of PFD in the HPS strut with damping elements (resistor orifice) significantly improved the $D(j\omega)$ of the HPS strut. The results of the model tests can be the basis for the design of new HPS struts with better performance parameters for specific application areas, especially off-road vehicles.

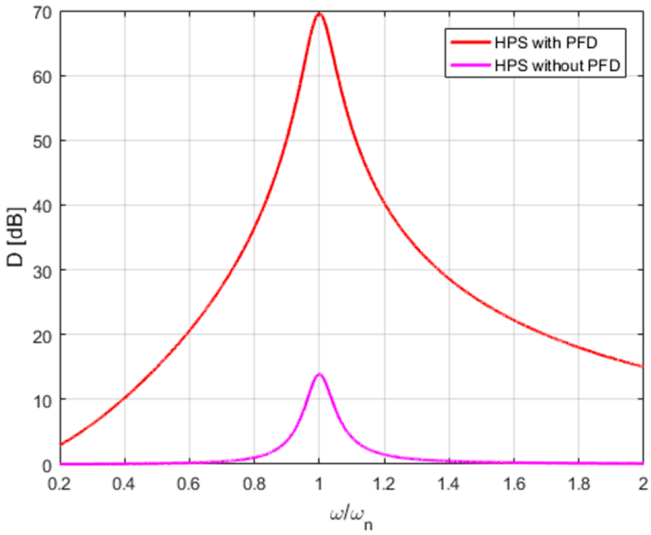

Figure 36. Comparison of the curves of the $D(j\omega)$ of HPS with and without PFD.

From the results of the impedance modeling, it was found that the PFD was most effective when its natural frequency coincided with the reduced excitation frequency. This indicates the possibility of adjusting the PFD to the conditions of the road, which are the sources of excitation vibrations. Therefore, an adjustable resistor should be used in the PFD, and the design of HPS struts with the PFD is the starting point for creating a new type of adaptive suspension. The adaptive HPS system has been successfully designed for high-performance cars, which are becoming more common. The next step in the development of the HPS strut is to create an HPS capable of storing unwanted energy from the relative movements of the body and reusing it. Energy regenerative and energy-harvesting systems may pose another challenge in improving the energy performance of HPS systems.

6. Conclusions

The primary contribution of this review is a comprehensive comparison of advances in and effectiveness in the operation, control, and application of PS and HPS systems. The PS system was compared with the HPS system, and these two systems were compared with the classical passive, semi-active and active vehicle suspension systems. This review contributes to the development of vehicle nonconventional PS and HPS systems by providing a detailed and up-to-date assessment of their advantages, disadvantages, and potential future developments. This review is a valuable resource for researchers, engineers and industry professionals in the fields of vehicle suspension and vibration isolation.

The greatest contribution of this review is to guide future studies in the field of PS and HPS systems. The importance and purpose of this review are as follows.

1. This review presents unique solutions for the calculation, modeling, and simulation of air springs in PS systems, as well as the interconnections of HPA with DT and PFD in HPS systems, which are not commonly discussed in the literature.
2. A review of PS systems includes the principles of operation and progress in development. It also covers the specific principles of air spring operation, including characteristics, simulation models, and vibration isolation.
3. The useful solutions for the design of PS systems were presented: the model solutions for air springs, which included an effective area depending on pressure and volume, the volume increment and the volume gradient dependent on stroke and the pressure, and stiffness dependent on pressure, volume and effective area. These relationships were used to present the 2D and 3D curves.
4. The air spring as a vibroisolator was analyzed using models of the mass air spring stiffness system and the mass air spring-damping system. The vibration transmissibility T and the isolation rate IR were used to evaluate the air spring as a vibroisolator.
5. The dynamic response of the spring obtained using the dynamic model using the Simscape block is applied in modeling PS systems.
6. The HPA practical selection criteria for an HPS system based on the thermodynamic PC cycle are presented, which consider the fulfillment of the required useful volume ΔV_r, required pressure drop Δp_r, and required work W_r.
7. This review includes the time characteristics of HPA thermodynamic processes that are useful for the design of HPS systems.
8. Dynamic modeling of HPA–DT with RLC lumped parameters is critical to simulate and control the HPS strut and must meet KPIs depending on the requirements of the HPS system.
9. The impedance modeling of HPA–DT allowed the determination of its dimensionless resonance impedance curves and $D(j\omega)$ curves. Impedance modeling is a significant contribution to this review because frequency characteristics are neglected in the analysis of suspension systems, although they are vibration systems.
10. In this review, new trends in HPS development are discussed, including the effect of an additional pressure fluctuation damper (PFD) placed in a hydraulic cylinder on the DPI of the HPS in off-road driving conditions.

A comprehensive comparative review of the advances in the effectiveness of PS and HPS systems led to the following conclusions.

1. Increasing vehicle safety by equipping vehicles with advanced PS and HPS systems can lead to a better vehicle response to sudden maneuvers and emergency situations, which in turn improves vehicle traction and stability.

2. A more stable and pleasant ride for both the driver and passengers can be achieved by appropriately tuning the PS and HPS systems according to the driving characteristics of the vehicle.
3. The better performance of the PS and HPS systems increases the wheel grip, reduces body roll, provides a more precise steering response, and improves acceleration, braking, and cornering performance.
4. Customization of the PS and HPS systems through simple adjustments or fine-tuning based on the individual preferences of drivers and passengers allows vehicle handling characteristics to adapt to specific driving styles or road conditions.

Future-proof innovation of solutions in such a dynamic field as automotive technology requires a balanced approach that considers both technical progress in suspension system solutions that consider the response of the steering and braking systems, as well as the expectations of drivers and passengers, and economic and ecological issues. Among the new challenges of car suspension, user feedback, testing before mass production, and affordability are the most important. Innovations in suspension solutions bring tangible benefits to consumers, such as reduced fuel consumption, lower vehicle maintenance costs, higher value of used cars, and higher resale value.

The concept of innovative development of PS and HPS systems should be considered.

1. Real-time data analysis, in which modern suspension systems can collect data from roads in real time.
2. Predictive control, in which advanced suspension systems predict future road conditions based on current data.
3. Advanced suspension systems are integrated with other vehicle systems and operate as part of a cohesive system that includes steering, braking, and driving systems.
4. The use of IoT in information technology (IT) and AI systems related to suspension systems consists of transmitting data about road conditions and traffic (road damage) and enabling communication with road officials and drivers about road conditions (adapting the suspension to expected disruptions).
5. The use of PS systems in EVs and AVs is a desirable solution due to its ability to provide better ride quality and stability, which is desirable given the heavy weight of EV batteries.
6. Sensor technology has become increasingly important and popular in vehicle suspension systems for its control and monitoring.
7. The development of hybrid suspension systems as a combination of hydraulic, pneumatic, electric and electromagnet elements.

Risks associated with innovative advanced PS and HPS solutions

1. Active suspension systems have become increasingly connected to information networks, rendering them vulnerable to cyberattacks.
2. The high cost of integrating advanced technologies into suspension systems is expensive and may drive-priced vehicles.
3. Maintenance of advanced suspensions requires advanced mechanical training and incurs increased costs.
4. Sensor faults endanger the reliability and safety of suspension systems and have raised broad concerns.

Funding: This research received no external funding.

Data Availability Statement: Data are contained within the article.

Conflicts of Interest: The author declares no conflicts of interest.

Abbreviations

AS	air suspension
AV	autonomous vehicle
DT	damping tube
EV	electric vehicle
HPA	hydro-pneumatic accumulator
HPS	hydro-pneumatic suspension
IR	isolation rate
KPI	key performance indicator
PFD	pressure fluctuation damper
PS	pneumatic suspension

References

1. Tata, R.P. *Automotive Suspension Systems*; Course No: M02-038; Continuing Education and Development, Inc.: Stony Point, NY, USA, 2012.
2. Goodarzi, A.; Khajepour, A. *Vehicle Suspension System Technology and Design*; Synthesis lectures on advances in automotive technology; Springer: Cham, Switzerland, 2017.
3. Sezgin, A.; Yagiz, N. Analysis of passenger ride comfort. In Proceedings of the International Conference on Structural Nonlinear Dynamics and Diagnosis (CSNDD 2012), Marrakech, Morocco, 30 April–2 May 2012; MATEC Web of Conferences; Volume 1, p. 03003.
4. *ISO 2631-1:1997/Amd 1:2010*; Mechanical Vibration and Shock—Evaluation of Human Exposure to Whole-Body Vibration. Part 1: General Requirements. ISO: Geneva, Switzerland, 2010. Available online: https://www.iso.org/standard/45604.html (accessed on 10 July 2010).
5. Reimpell, J.; Stoll, H. *Fahrwerktechnik: Stoβ- und Schwingungsdämpfer*; Vogel- Fachbuch Technik Kraftfahrzeugwesen; Vogel-Buchverlag: Würzburg, Germany, 1989.
6. Heissing, B.; Ersoy, M. *Fahrwerkhandbuch, Grundlagen, Fahrdynamik, Komponenten, Systeme, Mechatronik, Perspektiven*; Vieweg+Teubner Verlag: Wiesbaden, Germany, 2008.
7. Jain, S.C.; Sharma, P.K.; Vadodaria, D. McPherson suspension system—A review. *Int. J. Technol. Res. Eng.* **2014**, *1*, 1496–1498.
8. Lopes, R.; Farahani, B.V.; Queirós de Melo, F.; Moreira, P.M.G.P. A dynamic response analysis of vehicle suspension system. *Appl. Sci.* **2023**, *13*, 2127. [CrossRef]
9. Seelam, A.B.; Kumaran, M.S.; Sachidananda, K.H. Design and analysis of suspension strut in automobile vehicles. *Mat. Mod. Eng. Prob.* **2020**, *7*, 587–596. [CrossRef]
10. Dixon, J.C. The shock absorber. In *Handbook*, 2nd ed.; John Wiley and Sons, Ltd.: West Sussex, UK, 2007.
11. Gong, M.; Chen, H. Variable damping control strategy of a semi-active suspension based on the actuator motion state. *J. Low Freq. Noise Vib. Act. Control* **2020**, *39*, 787–802. [CrossRef]
12. Wang, X.; Liu, X.; Shan, Y.; Shen, Y.; He, T. Analysis and optimization of the novel inerter-based dynamic vibration absorbers. *IEEE Access* **2018**, *6*, 33169–33182. [CrossRef]
13. Smith, M.C. Synthesis of mechanical networks: The inerter. *IEEE Trans. Autom. Control* **2002**, *47*, 1648–1662. [CrossRef]
14. Gholkar, M.D.; Salokhe, V.S. Methods for attenuating mechanical vibrations: A review with agricultural tractor perspective. In Proceedings of the 9th International Agricultural Engineering Conference (IAEC), Bangkok, Thailand, 3–6 December 2007.
15. Guglielmino, E.; Sireteanu, T.; Stammers, C.W.; Ghita, G.; Giuclea, M.; Casey, T. Semi-active suspension control: Improved vehicle ride and road friendliness. *Noise Control. Eng. J.* **2009**, *57*, 155. [CrossRef]
16. Poussot, V.C.; Spelta, C.; Sename, O.; Savaresi, S.; Dugard, L. Survey and performance evaluation on some automotive semi-active suspension control methods: A comparative study on a single-corner model. *Annu. Rev. Control* **2012**, *36*, 148–160. [CrossRef]
17. Fujita, T.; Fukao, T.; Kinoshita, T.; Itagaki, N. Semi-active suspension improving both ride comfort and handling feel. *IFAC Proc.* **2013**, *46*, 225–230. [CrossRef]
18. Hamersma, H.; Schalk, P. Improving the braking performance of a vehicle with ABS and a semi-active suspension system on a rough road. *J. Terramech.* **2014**, *56*, 91–101. [CrossRef]
19. Chen, M.Z.Q.; Hu, Y.; Li, C.; Chen, G. Application of semi-active inerter in semi-active suspensions via force tracking. *J. Vib. Acoust.* **2016**, *138*, 041014. [CrossRef]
20. Liu, C.; Chen, L.; Yang, X.; Zhang, X.; Yang, Y. General Theory of Skyhook Control and its Application to Semi-Active Suspension Control Strategy Design. *IEEE Access* **2019**, *7*, 101552–101560. [CrossRef]
21. Jayabalan, A.; Kumar, N.K.S. Vibration suppression of quarter car using sliding-mode and internal model-based skyhook controller. *J. Vib. Eng. Technol.* **2018**, *6*, 117–126. [CrossRef]

22. Mardani, A. Energy harvesting, handling and ride comfort trade-off between passive and active suspension systems of half vehicle model using PID controller for off-road vehicles. *J. Adv. Veh. Eng.* **2017**, *3*, 150–160.
23. Yao, J.; Li, Z.; Wang, M.; Yao, F.; Tang, Z. Automobile active tilt control based on active suspension. *Adv. Mech. Eng.* **2018**, *10*, 1687814018801456. [CrossRef]
24. Yim, S.J.; Park, Y.J.; Yi, K. Design of active suspension and electronic stability program for rollover prevention. *Int. J. Automot. Technol.* **2010**, *11*, 147–153. [CrossRef]
25. Nguyen, D.N.; Nguyen, T.A.; Shao, X. The dynamic model and control algorithm for the active suspension system. *Math. Prob. Eng.* **2023**, *9*, 2889435. [CrossRef]
26. Riduan, A.F.M.R.; Tamaldin, N.; Sudrajat, A.; Ahmad, F. Review on active suspension system. *SHS Web Conf.* **2018**, *49*, 02008. [CrossRef]
27. Jiregna, I.; Sirata, G. Review of the vehicle suspension system. *J. Mech. Ener. Eng.* **2020**, *4*, 109–114. [CrossRef]
28. Sanchez, E.J.A. A quarter-car suspension system: Car body mass estimator and sliding mode control. *Procd. Technol.* **2013**, *7*, 208–214. [CrossRef]
29. Siswoyo, H.; Mir-Nasiri, N.; Ali, M.H. Design and development of a semi-active suspension system for a quarter car model using PI controller. *J. Autom. Mob. Robot. Intell. Syst.* **2017**, *11*, 26–33. [CrossRef]
30. Al-Mutar, W.; Abdalla, T. Quarter car active suspension system control using fuzzy controller tuned by PSO. *Int. J. Comput. Appl.* **2015**, *127*, 38–43.
31. Shahid, Y.; Wei, M. Comparative analysis of different model-based controllers using active vehicle suspension system. *Algorithms* **2020**, *13*, 10. [CrossRef]
32. Kawamoto, Y.; Suda, T.; Inoue, H.; Kondo, T. Electro-mechanical suspension system considering energy consumption and vehicle manoeuvre. *Veh. Syst. Dyn.* **2008**, *46*, 1053–1063. [CrossRef]
33. Amati, N.; Tonoli, A.; Castellazzi, L.; Ruzimov, S. Design of electromechanical height adjustable suspension. *Proc. Inst. Mech. Eng. Part D J. Auto. Eng.* **2018**, *232*, 1253–1269. [CrossRef]
34. Wilfride, M. Strut for a Wheel Suspension of Motor Vehicles. US Patent 8,573,604 B2, 20 July 2011.
35. Hakui, T.; Hirata, H.; Kajiwara, H.; Nakajima, K.; Akuta, Y.; Hatano, K. Vehicle Height Adjusting System. US Patent 7,922,181, 12 April 2011.
36. Kim, J.M.; Jang, S.B.; Kim, B.M.; Ko, D.S. Electronic Control Suspension System for Vehicles. US Patent 8,833,775, 15 September 2014.
37. Suda, Y.; Shiba, T.; Hio, K.; Kawamoto, Y.; Kondo, T.; Yamagata, H. Study on electromagnetic damper for automobiles with nonlinear damping force characteristics. *Veh. Syst. Dyn.* **2004**, *41*, 637–646.
38. Gysen, B.L.J.; Paulides, J.J.H.; Janssen, J.L.G.; Lomonova, E.A. Active electromagnetic suspension system for improved vehicle dynamics. *IEEE Trans. Veh. Technol.* **2010**, *59*, 1156–1163. [CrossRef]
39. Tu, F.; Yang, Q.; He, C.; Wang, L. Experimental study and design on automobile suspension made of magneto-rheological damper. *Ener. Proc.* **2012**, *16*, 417–442. [CrossRef]
40. Zhang, H.; Liu, J.; Wang, E.; Rakheja, S.; Su, C.Y. Nonlinear dynamic analysis of a skyhook-based semi-active suspension system with magneto-rheological damper. *IEEE Trans. Veh. Technol.* **2018**, *67*, 10446–10456. [CrossRef]
41. Turnip, A.; Panggabean, J.H. Hybrid controller design-based magneto-rheological damper lookup table for quarter car suspension. *Int. J. Artif. Intell.* **2020**, *18*, 193–206.
42. Shojaei, A.; Metered, H.; Shojaei, S.; Olutunde Oyadiji, S. Theoretical and experimental investigation of magneto-rheological damper based semi-active suspension systems. *Int. J. Veh. Struct. Syst.* **2013**, *5*, 109. [CrossRef]
43. Jeyasenthil, R.; Choi, S.B. A novel semi-active control strategy based on the quantitative feedback theory for a vehicle suspension system with magneto-rheological damper saturation. *Mechatronics* **2018**, *54*, 36–51. [CrossRef]
44. Edgar, J. *Custom Air Suspension*; Veloce Publishing: Poundbury, UK, 2017.
45. Bauer, W. *Hydropneumatic Suspension Systems*; Springer: Berlin/Heidelberg, Germany, 2011.
46. *ISO 2631-1:1997*; Mechanical Vibration and Shock—Evaluation of Human Exposure to Whole-Body Vibration. Part 1: General Requirements. ISO: Geneva, Switzerland, 1997. Available online: https://www.iso.org/standard/7612.html (accessed on 2 February 1997).
47. Buhari, R.; Rohani, M.M.; Abdullah, M.E. Dynamic load coefficient of tyre forces from truck axles. *App. Mech. Mat.* **2013**, *405–408*, 1900–1911. [CrossRef]
48. Long, L.X.; Quynh, L.V.; Liem, N.V.; Cuong, B.V.; Hien, V.T.; Tan, H.A. Ride performance evaluation of air and hydro-pneumatic springs of suspension system. *Int. J. Adv. Res. Eng. Technol.* **2021**, *12*, 439–447.
49. Goodarzi, A.; Lu, Y.; Khajepour, A. Adaptive Suspension Systems Design. In *Vehicle Suspension System Technology and Design*; Synthesis Lectures on Advances in Automotive Technology; Springer: Cham, Switzerland, 2023.
50. Slaski, G. Simulation and experimental testing of adaptive suspension damping control depending on the frequency of a sinusoidal kinematic input. *Arch. Auto. Eng. Arch. Moto.* **2014**, *64*, 65–78.

51. Wu, X.; Shi, W.; Zhang, H.; Chen, Z. Adaptive suspension state estimation based on IMMAKF on variable vehicle speed, road roughness grade and sprung mass condition. *Sci. Rep.* **2014**, *14*, 1740. [CrossRef] [PubMed]
52. Dwivedi, R.; Kandpal, N.; Shukla, A. Adaptive suspension system. In Proceedings of the 2nd IEEE International Conference on Information and Financial Engineering, Chongqing, China, 17–19 September 2010; pp. 694–697.
53. Mihaly, A.; Kisari, A.; Gaspar, P.; Nemeth, B. Adaptive semi-active suspension design considering cloud-based road Information. *IFAC-Pap. OnLine* **2019**, *52*, 249–254. [CrossRef]
54. Bououden, S.; Chadli, M.; Karimi, H.R. A robust predictive control design for nonlinear active suspension systems. *Asian J. Control* **2016**, *18*, 122–132. [CrossRef]
55. Malekshahi, A.; Mirzaei, M.; Aghasizade, S. Non-linear predictive control of multi-input multi-output vehicle suspension system. *J. Low Freq. Noise, Vib. Act. Control.* **2015**, *34*, 87–105. [CrossRef]
56. Li, Q.; Chen, Z.; Song, H.; Dong, Y. Model predictive control for speed-dependent active suspension system with road preview information. *Sensors* **2024**, *24*, 2255. [CrossRef] [PubMed]
57. Theunissen, J.; Sorniotti, A.; Gruber, P.; Fallah, S.; Ricco, M.; Kvasnica, M.; Dhaens, M. Regionless explicit model predictive control of active suspension systems with preview. *IEEE Trans. Ind. Electron.* **2019**, *67*, 4877–4888. [CrossRef]
58. Pedro, J.O.; Nhlapo, S.M.; Mpanza, L.J. Model predictive control of half-car active suspension systems using particle swarm optimization. *IFAC-Pap. OnLine* **2020**, *53*, 14438–14443. [CrossRef]
59. Continuous Damping Control (CDC). Available online: https://www.zf.com/products/en/cars/products_64273.html (accessed on 15 July 2024).
60. Vehicle Suspension Control. Available online: https://www.bilstein-shocks.co.uk/pages/vehicle-suspension-control (accessed on 15 May 2024).
61. Monroe Intelligent Suspension. Available online: https://www.monroe.com/products/restore-your-ride/intelligent-suspension-ridesense.html (accessed on 15 July 2024).
62. Kayaba's DRC Suspension Systems. Available online: https://www.vwvortex.com/threads/kayabas-drc-suspension-system-has-been-selected-for-audis-new-rs6-quattro.1660144 (accessed on 30 October 2004).
63. General Motors Magnetic Ride Control Technology. Available online: https://gmauthority.com/blog/gm/general-motors-technology/gm-chassis-suspension-technology/gm-magnetic-ride-control-technology/ (accessed on 15 July 2024).
64. Computer Active Technology Suspension (CATS) Tech Guide. Available online: https://prestigeandperformancecar.com/jaguar/computer-active-technology-suspension-cats-tech-guide (accessed on 15 July 2024).
65. Pneumatic Damping Control Shock Absorbers. Available online: https://www.dynarev.com/Audi_fuel_exhaust.html (accessed on 15 July 2024).
66. Hydractive 3rd Generation Suspension. Available online: https://www.citroenet.org.uk/miscellaneous/hydraulics/hydraulics-13.html (accessed on 15 May 2024).
67. Electronically Controlled Air Suspension (ECAS). Available online: https://www.wabco-customercentre.com/catalog/en/2003001020 (accessed on 15 June 2024).
68. HÜBNER Presents Innovations for e-Buses. Available online: https://www.hubner-group.com/en/press/press-release/huebner-presents-innovations-for-e-buses-at-mobility-move-24-hydraulic-chassis-for-increased-energy-efficiency (accessed on 1 March 2024).
69. Atindana, V.A.; Xu, X.; Nyedeb, A.N.; Quaisie, J.K.; Nkrumah, J.K.; Assam, S.P. The evolution of vehicle pneumatic vibration isolation: A systematic review. *Shock. Vib.* **2023**, *2023*, 1716615. [CrossRef]
70. Andrea, F. *Air Springs for Air Suspension Vehicle: Fundamental Characteristics, Design in First Approximation, Fatigue Testing and Failure Modes*; Smashwords: Broken Arrow, OK, USA, 2019.
71. Faussone, A. *Air Springs for Air Suspension Vehicle*; Smashwords Inc.: Los Gatos, CA, USA, 2019.
72. Fish, M. *Air Suspension Design*; Pedantic Publishing: Pittsburgh, PA, USA, 2016.
73. Kevin Whipps, K. *How to Install Air Ride Suspension Systems*; CarTech: Ypsilanti, MI, USA, 2020.
74. Edgar, J. *Custom Air Suspension: How to Install Air Suspension in Your Road Car*; Veloce Publishing Ltd.: Dorchester, UK, 2017.
75. Wanen, M. *Workshop Manual Air Suspensions*; BPW: Wiehl, Germany, 2021.
76. Spender, J. *Car Suspension: Repair, Maintenance and Modification*; Crowood Press: Marlborough, UK, 2020.
77. WABCO. *Luftfedern für Nutzfahrzeuge*; WABCO: Brussels, Belgium, 2010.
78. TIMMER. *Bagzylinder*; Timmer-Pneumatik GmbH: Neuenkirchen, Germany, 2010.
79. SCHILTZ Norm. *Hefkussen*; Schlitz Norm: Brussels, Belgium, 2020.
80. PARKER Pneumatic. *Balgzylinder Pneuride*; Parker Pneumatic: Richland, MI, USA, 2020.
81. FIRESTONE. *Airstroke, Airmount*; Firestone: Hamilton, IN, USA, 2021.
82. FESTO. *Bellows Cylinders*; Festo GmbH: Esslingen, Germany, 2024.
83. GRANNING. *Air Springs*; Granning UK Ltd.: Cheshire, UK, 2024.
84. WEFORMA. *Air Springs*; Weforma Dämpfungstechnik GmbH: Stolberg, Germany, 2024.

85. CONITECH. *Luftfedersysteme*; ContiTech Luftfedersysteme GmbH: Hanower, Germany, 2024.
86. Li, C.; Jing, Y.; Ni, J. Uncertainty analysis and design of air suspension systems for city buses based on neural network model and true probability density. *Machines* **2023**, *11*, 791. [CrossRef]
87. Lee, S.J. Development and analysis of an air spring model. *Int. J. Automot. Technol.* **2010**, *11*, 471–479. [CrossRef]
88. Spiroiu, M.A. Railway vehicle pneumatic rubber suspension modelling and analysis. *Mater. Plast.* **2018**, *55*, 24–27. [CrossRef]
89. Armansyah, A.; Ahmad, K.; Amin, K.; Ferdyanto, F.; Muhammad, M. Optimization of air suspension system for improved ride and handling performance in road vehicles dynamic. *Mech. Eng. Soc. Indu.* **2024**, *4*, 277–293. [CrossRef]
90. Hirose, M.; Matsushige, S.; Buma, S.; Kamiya, K. Toyota electronic modulated air suspension system for the 1986 Soarer. *IEEE Trans. Ind. Electron.* **1988**, *35*, 193–200. [CrossRef]
91. Tener, D.R. *Overcoming the Ride/Handling Compromise—A Cockpit Adjustable Suspension System*; SAE Technical Paper; SAE International: Warrendale, PA, USA, 2004; pp. 1–6.
92. Zhou, R.; Zhang, B.; Li, Z. Dynamic modeling and computer simulation analysis of the air spring suspension. *J. Mech. Sci. Technol.* **2022**, *36*, 1719–1727. [CrossRef]
93. Nazemian, H.; Masih-Tehrani, M. Development of an optimized game controller for energy saving in a novel interconnected air suspension system. *Proc. Inst. Mech. Eng. Part D J. Automob. Eng.* **2020**, *234*, 3068–3080. [CrossRef]
94. Jiang, X.; Xu, X.; Shi, T.; Atindana, V.A. Nonlinear characteristic analysis of gas-interconnected quasi-zero stiffness pneumatic suspension system: A Theoretical and Experimental Study. *Chin. J. Mech. Eng.* **2024**, *37*, 58. [CrossRef]
95. Kim, J.; Lee, T.; Cheol-Joong Kim, C.-J.; Yi, K. Development of data-based model predictive control for continuous damping and air spring suspension system. *Control Eng. Pract.* **2024**, *142*, 105777. [CrossRef]
96. Jiang, X.; Cheng, T. Design of a BP neural network PID controller for an air suspension system by considering the stiffness of rubber bellows. *Alex. Eng. J.* **2023**, *74*, 65–78. [CrossRef]
97. Kuzyshyn, A.Y.; Sobolevska, Y.H.; Kostritsa, S.A.; Voznyak, O.M. Research of the characteristics of an air spring under cyclic load. *IOP Conf. Ser. Mater. Sci. Eng.* **2023**, *1277*, 012010. [CrossRef]
98. Urbansky, M.; Homisin, J.; Kassay, P.; Krajnak, J. Measurement of air springs volume using indirect method in the design of selected pneumatic devices. *Acta Mech. Autom.* **2018**, *12*, 19–22. [CrossRef]
99. Larten, C.-P. Modeling and Identification of Air Suspension in Heavy-Duty Vehicles. Master's Thesis, Division of Automatic Control, Department of Electrical Engineering, Linköping University, Linköping, Sweden, 2016.
100. Sreenivasan, G.P.; Keppanan, M.K. Analytical approach for the design of convoluted air suspension and experimental validation. *Acta Mech. Sin.* **2019**, *35*, 1093–1103. [CrossRef]
101. De Melo, F.J.M.Q.; Pereira, A.B.; Morais, A.B. The Simulation of an automotive air spring suspension using a pseudo-dynamic procedure. *Appl. Sci.* **2018**, *8*, 1049. [CrossRef]
102. Locken, F.; Welsch, M. The dynamic characteristic and hysteresis effect of an air spring. *Int. J. Appl. Mech. Eng.* **2015**, *20*, 127–145. [CrossRef]
103. Vo, N.Y.P.; Le, T.D. Analysis model of restoring force of a rubber air spring. *J. Vibr.* **2021**, *23*, 1138–1147. [CrossRef]
104. Breitenbach, S.; Skoglund, M.; Lillepärg, J.; Emmler, T.; Frank Mantwill, F. On the influence of sorbents on the static stiffness of Air Springs. *Forsch Ingenieurwes* **2024**, *88*, 32. [CrossRef]
105. Pahl, H.J. *Luftfedern in Nutzfahrzeuge, Auslegung, Berechnung, Praxis*; LFT Luftfedertechnik GmbH: Neuss, Germany, 2002.
106. Takosoglu, J.; Ziejewski, K.; Dindorf, R.; Wos, P.; Chlopek, L. Design of the stand for experimental tests of pneumatic bellows actuators. In Proceedings of the International Scientific-Technical Conference on Hydraulic and Pneumatic Drives and Control NSHP 2023: Advances in Hydraulic and Pneumatic Drives and Control 2023, Piechowice, Poland, 11–13 October 2023; Stryczek, J., Warzynska, U., Eds.; Lecture Notes in Mechanical Engineering. Springer: Cham, Switzerland, 2024; pp. 152–161.
107. Continental. *ContiTech Luftfedersysteme Catalog*; Continental GmbH: Hanower, Germany, 2012.
108. FABREEKA. *Vibration Damping with Low-Frequency Air Springs*; Technical Specifications; Fabreeka International, Inc.: Boston, MA, USA, 2020.
109. Hu, Y.; Zhang, J.; Long, J. Influence of rubber's viscoelasticity and damping on vertical dynamic stiffness of air spring. *Sci. Rep.* **2023**, *13*, 9886. [CrossRef] [PubMed]
110. Gavriloski, V.; Jovanova, J. Dynamic behaviour of an air spring element. *J. Mach. Technol. Mat.* **2010**, *4–5*, 24–27.
111. Zhu, H.; Yang, J.; Zhang, Y.; Feng, X. A novel air spring dynamic model with pneumatic thermodynamics, effective friction and viscoelastic damping. *J. Sound Vib.* **2017**, *408*, 87–104. [CrossRef]
112. Berg, M. A non-linear rubber spring model for rail vehicle dynamics analysis. *Veh. Syst. Dyn.* **1998**, *30*, 197–212. [CrossRef]
113. Na, S.-D.; Yoo, W.-S. Improvement in the dynamic responses of the semiempirical vehicle model using the Maxwell force model for the suspension forces. *Proc. Inst. Mech. Eng. Part D J. Automob. Eng.* **2015**, *229*, 1996–2006. [CrossRef]
114. Huang, C.; Zeng, J. Comparison of the Maxwell model and a simplified physical model for a railway yaw damper in damping characteristics and vehicle stability assessment. *Proc. Inst. Mech. Eng. Part F J. Rail Rapid Transit* **2022**, *236*, 275–287. [CrossRef]

115. Fongue, W.A.; Pelz, P.F.; Kieserling, J. The dynamic performance of air spring air damping systems by means of small excitations. In Proceedings of the 25th International Conference on Noise and Vibration Engineering (ISMA2012), Leuven, Belgium, 17–19 September 2012.
116. Presthus, M. Derivation of Air Spring Model Parameters for Train Simulation. Master's Thesis, Department Applied Physic and mechanical Engineering, Lulea University of Technology, Lulea, Sweden, 2002.
117. Franz, D. Simulink Control Model of an Active Pneumatic Suspension System in Passenger Cars. Master's Thesis, Department of Control and Computer Engineering, Politecnico di Torino, Turin, Italy, 2019.
118. Zhou, Q.; Yuan, P.; Tudor, T.; Wang, X.; Guo, Z.; Huang, Y.; Sun, J.; Wang, B. Method for determining accurate initial air pressure range of air suspension airbag based on vehicle ride comfort simulation analysis. *IOP Conf. Ser. Mat. Sci. Eng.* **2019**, *538*, 012068. [CrossRef]
119. Ingale, A.; Daga, A.; Naik, R. Modeling Mass-Spring-Damper System using Simscape. *J. Eng. Res. App.* **2018**, *8*, 30–33.
120. Abid, H.J.; Chen, J.; Nassar, A.A. Equivalent air spring suspension model for quarter-passive model of passenger vehicles. *Int. Sch. Res. Not.* **2015**, *2015*, 974020.
121. Zhang, H.; Zhang, H.; Zhao, L.; Ou, C.; Liu, Y.; Shan, X. Height Control Strategy Design and Simulation of Electronic Control Air Suspension for Trucks. *World Electr. Veh. J.* **2024**, *15*, 273. [CrossRef]
122. Nieto, A.J.; Morales, A.L.; González, A.; Chicharro, J.M.; Pintado, P. An analytical model of pneumatic suspensions based on an experimental characterization. *J. Sound. Vib.* **2008**, *313*, 290–307. [CrossRef]
123. Eskandary, P.K.; Khajepour, A.; Wong, A.; Ansari, M. Analysis and optimization of air suspension system with independent height and stiffness tuning. *Int. J. Automot. Technol.* **2016**, *17*, 807–816. [CrossRef]
124. Yin, Z.; Jiang, J.; Shangguan, W.-B. Complex stiffness model of an air spring with auxiliary chamber considering inertial effects of gas in connecting pipeline. *Proc. Inst. Mech. Eng. Part D J. Automob. Eng.* **2023**, *237*, 145–158. [CrossRef]
125. Murrenhoff, H.; Wallentowitz, H. *Fluidtechnik für Mobile Anwendungen, Reihe Fluidtechnik*; Verlag Mainz: Aachen, Germany, 1998.
126. Citroën Hydraulics System. Available online: https://www.citroenet.org.uk/miscellaneous/hydraulics/hydraulics-1.html (accessed on 12 April 2024).
127. Zhu, W.; Zhao, Z.; Zhou, X.; Cao, X.; Ye, M.; Cao, C.; Alam, M.M. Research on damping hole optimization of hydro-pneumatic suspension for mining trucks under variable load conditions. *Actuators* **2024**, *13*, 163. [CrossRef]
128. Longa, L.X.; Quynh, L.V.; Liemb, N.V.; Cuongc, B.V.; Tand, H.A. A comparison of ride performance of hydro-pneumatic suspension system with those of rubber and leaf suspension systems. *IOP Conf. Ser. Mat. Sci. Eng.* **2020**, *914*, 012037. [CrossRef]
129. Badway, I.A.; Sokar, M.I.; Abd Raboo, S. Simulation and Control of a Hydro-pneumatic Suspension system. *Int. J. Sci. Eng. Res.* **2017**, *8*, 930–935.
130. Masoo, J.; Zoppi, M.; Molfino, R. Multi-terrain vehicle active suspension control modeling and design. In Proceedings of the 7th International ASME/IEEE Conference on Mechatronics & Embedded Systems and Applications (MESA2011), Washington, DC, USA, 28–31 August 2011.
131. Ghazalya, N.M.; Moaaz, A.O. Hydro-Pneumatic Passive Suspension System Performance Analysis using AMESim Software. *Int. J. Veh. Struct. Syst.* **2020**, *12*, 9–12. [CrossRef]
132. Hryciow, Z.; Rybaka, P.; Wojciechowski, M.; Wachowiak, P.; Kalicki, B. Hydropneumatic suspension testing of a wheeled armoured personnel carrier. *Eksploatacja i Niezawodność—Maint. Reliab.* **2023**, *25*, 1–10. [CrossRef]
133. Oscarsson, M. A Hydropneumatic Suspension Parameter Study on Heavy Multi-Axle Vehicle Handling. Master's Thesis, KTH Vehicle Dynamics, Stockholm, Sweden, 2015.
134. Lawniczak, S.; Siminski, P. Hydropneumatic suspension modelling for wheeled armoured fighting vehicle. *J. KONES Power Trans.* **2009**, *16*, 285–297.
135. Razenberg, J.A. Modelling of the Hydropneumatic Suspension System of a Rally Truck. Master's Thesis, Eindhoven University of Technology, Eindhoven, The Netherlands, 2009.
136. Koneczny, L.; Burdzik, R.; Wegrzyn, T. Analysis of structural and material aspects of selected elements of a hydropneumatic suspension system in a passenger car. *Arch. Metall. Mater.* **2016**, *61*, 79–84. [CrossRef]
137. Qiao, C.; Wen, H.; Liu, X.; Wang, G. Damping control and experiment on active hydro-pneumatic suspension of sprayer based on genetic algorithm optimization. *Front. Neurorobotics* **2021**, *15*, 707390. [CrossRef] [PubMed]
138. Qin, B.; Zeng, R.; Li, X.; Yang, J. Design and performance analysis of the hydropneumatic suspension system for a novel road-rail vehicle. *Appl. Sci.* **2021**, *11*, 2221. [CrossRef]
139. Wu, W.; Tang, H.; Zhang, S.; Hu, L.; Zhang, F. High-precision dynamics characteristic modeling method research considering the influence factors of hydropneumatic suspension. *Shock Vib.* **2020**, *21*, 8886631. [CrossRef]
140. Wu, Z.; Jiao, B.; Sun, C.; Zhang, Y.; Zhao, H. Design and optimization of hydropneumatic suspension simulation Test bench with electro-hydraulic proportional control. *Machines* **2023**, *11*, 907. [CrossRef]
141. Zhang, J.; Chen, S.; Zhao, Y.; Feng, J.; Liu, C.; Fan, Y. Research on modeling of hydropneumatic suspension based on fractional order. *Math. Prob. Eng.* **2015**, *11*, 920279. [CrossRef]

142. Yin, C.; Zhai, X.; Sun, X.; Wang, S.; Wong, P.K. Design and performance research of a hydro-pneumatic suspension with variable damping and stiffness characteristics. *J. Mech. Sci. Technol.* **2022**, *36*, 4913–4923. [CrossRef]
143. Vosloo, A.G. Hydropneumatic Semi-Active Suspension System with Continuously Variable Damping. Master's Thesis, University of Pretoria, Hatfield, South Africa, 2020.
144. Kang, S.; Kong, L.; Han, C.; Qiang, H.; Liu, K. Study on the impedance of active suspension drive unit under transverse slope condition based on track sensitivity. *J. Braz. Soc. Mech. Sci. Eng.* **2024**, *46*, 239. [CrossRef]
145. Li, C.-H.G. A novel suspension strut featuring constant resonance frequency. *Int. J. Heavy Veh. Syst.* **2015**, *22*, 293–310. [CrossRef]
146. Lin, D.; Yang, F.; Gong, D.; Rakheja, S. Design and experimental modeling of a compact hydro-pneumatic suspension strut. *Nonlinear Dyn.* **2020**, *100*, 3307–3320. [CrossRef]
147. Zhao, H.; Wang, G.; Lv, W.; Cao, Y.; Li, X. Optimization of hydropneumatics suspension for articulated wheel loader based on kriging model and particle swarm algorithm. *Adv. Mech. Eng.* **2018**, *10*, 1687814018810648. [CrossRef]
148. ASPlight. Tools for Optimal Calculation of the Hydraulic Accumulator. Available online: https://www.hydac.com/en/online-tools/asplight (accessed on 18 March 2023).
149. Rupprecht, K.-R. Hydrospeicher. Experimentelle und Analytische Untersuchungen zur Energiespeicherung. Ph.D. Thesis, Technische Hochschule Aachen, Aachen, Germany, 1988.
150. Dindorf, R.; Takosoglu, J.; Wos, P. Review of hydro-pneumatic accumulator models for the study of the energy efficiency of hydraulic systems. *Energies* **2023**, *16*, 6472. [CrossRef]
151. Dindorf, R.; Takosoglu, J.; Wos, P. Review of compressed air receiver tanks for improved energy efficiency of various pneumatic systems. *Energies* **2023**, *16*, 4153. [CrossRef]
152. HYDAC. *Diaphragm Accumulator*; Hydac International: Sulzbach, Germany, 2016.
153. HANSA. *Hydraulic Accumulators*; Hansa TMP: Modena, Italy, 2010.
154. Rotthäuser, S. Verfahren zur Berechnung and Untersuchung Hydropneumatischer Speicher. Ph.D. Thesis, Technische Hochschule Aachen, Aachen, Germany, 1993.
155. Korkmaz, F. *Hydrospeicher als Energiespeicher*; Springer: Berlin/Heidelberg, Germany, 1981.
156. Krus, P. *Transmission Line Modelling for System Simulation*; Linköping University: Linköping, Sweden, 2021.
157. *ISO 12185:2024*; Crude Petroleum, Petroleum Products and Related Products—Determination of Density—Laboratory Density Meter with an Oscillating U-Tube Sensor. ISO: Geneva, Switzerland, 2024. Available online: https://www.iso.org/standard/82592.html (accessed on 2 February 2024).
158. *DIN 53000-1*; Viscometry—Measurement of Kinematic Viscosity by Means of the Ubbelohde Viscometer—Part 1: Viscometer Specification and Measurement Procedure, Deutsches Institut für Normung, Berlin, Germany. 2023. Available online: https://www.din.de/en/getting-involved/standards-committees/nmp/publications/wdc-beuth:din21:330318702 (accessed on 4 July 2023).
159. Dindorf, R.; Wos, P. Energy efficiency of pressure shock damper in the hydraulic lifting and levelling module. *Energies* **2022**, *15*, 4097. [CrossRef]
160. Stosiak, M.; Karpenko, M. Dynamics of Machines and Hydraulic Systems. In *Mechanical Vibrations and Pressure Pulsations*; Springer: Cham, Switzerland, 2024.
161. Wang, Y.; Wu, T.; Ran, Z.; Lv, B.; Wang, S. Modeling analysis and experiments of a novel hydro-pneumatic suspension with piezoelectric energy harvester. *Smart Mater. Struct.* **2023**, *32*, 075005. [CrossRef]
162. Awad, M.M.; Sokar, M.I.; Rabbo, S.A.; El-Arabi, M.E. Performance evaluation and damping characteristics of hydro-pneumatic regenerative suspension system. *Int. J. Appl. Eng. Res.* **2018**, *13*, 5436–5442.
163. Lv, X.; Ji, Y.; Zhao, H.; Zhang, J.; Zhang, G.; Zhang, L. Research review of a vehicle energy-regenerative suspension system. *Energies* **2020**, *13*, 441. [CrossRef]
164. Kowal, J.; Pluta, J.; Konieczny, J.; Kot, A. Energy recovering in active vibration isolation system—Results of experimental research. *J. Vib. Control* **2008**, *14*, 1075–1088. [CrossRef]
165. Praznowski, K.; Brol, S.; Augustynowicz, A. Identification of static unbalance wheel of passenger car carried out on a road. *Solid State Phenom.* **2014**, *214*, 48–57. [CrossRef]
166. Smith, E.; Garcia, H. Wheel-Induced Vibrations in Heavy Vehicles. Bachelor Thesis, KTH, School of Engineering Sciences, Stockholm, Sweden, 2013.

167. Borutzky, W.; Barnard, B.; Thoma, J. An orifice flow model for laminar and turbulent conditions. *Simul. Model. Pract. Theory* **2002**, *10*, 141–152. [CrossRef]
168. Wu, D.; Burton, R.; Schoenau, G. An empirical discharge coefficient model for orifice flow. *Int. J. Fluid Power* **2002**, *3*, 13–18. [CrossRef]